The University of Manitoba

Measurement of Tensile Properties of Oil Sands

EdWard Buchan Wilson, P. Eng.

A Thesis submitted to the faculty of
Graduate Studies and Research
in partial fulfillment of the requirements
for the Degree of
Master of Science
in
Mechanical Engineering

Department of Mechanical Engineering
Winnipeg, Manitoba
October, 1988

ISBN 0-315-54920-3

MEASUREMENT OF TENSILE PROPERTIES OF OIL SANDS

BY

EDWARD BUCHAN WILSON

A thesis submitted to the Faculty of Graduate Studies of
the University of Manitoba in partial fulfillment of the requirements
of the degree of

MASTER OF SCIENCE

ABSTRACT

This thesis presents techniques for the measurement of the tensile properties of oil sands under a confining pressure.

All experimentation was carried out under an arbitrary confining pressure of 2 MPa.

Straight tensile testing was conducted at strain rates on the order of 150 με/sec. For an uncemented sand the tensile strength of 225 kPa found is vary significant. It was found that this material had a compressive to tensile Young's moduli ratio, $\varepsilon_c/\varepsilon_t$ ranging from 2.0 to 3.0 with a typical value of 2.5

Measurement of the fracture toughness led to an estimate on the order of 30 kPa$\sqrt{m}$ using the ASTM-E-399-CT compliance function.

A check of the applicability of the ASTM-E-399-CT compliance function for the evaluation of the fracture toughness of Wedge Loaded Compact Tensile (WLCT) specimens under confining pressures was performed using finite element method. It was found not to mimic the behavior of a material(s) under confining pressure.

The compliance function for WLCT specimens under confining pressure was found to vary with $\varepsilon_c/\varepsilon_t$ ratio.

ACKNOWLEDGMENTS

I wish to thank the people most important to this thesis first, Dr. Hsū, my supervisor, gets thanked for the freedom to carry out the work my way, and for his patience with me during the writing of my first thesis. Likewise I would like to thank Dr. Brian Stimpson first for saying I could and should, complete the thesis when I was having extensive difficulties with it. Thanks also go to the two technicians who helped me with the experemental equipment, Mr. Dave Kuss, and Mr. Al Lohse for their technical insight and encouragement.

I must also thank the Alberta Oil Sands Technology Research Authority paid for this research. I must also thank my current employer, the Department of Public Works and Highways of the Government of the North West Territories, who have supplied the duplication, and tolerated my many nights spent using their equipment, and days away from work completing this thesis.

I would also like to thank Drs. Ruth, Stimpson, and Hsü for reading this exhausting work, and giving (in the latter two cases repeatedly) valuable comments that have changed the work extensively. Dr. Ruth's request for a general overview of the work, after three years of total immersion in detail, was most refreshing.

Two of my undergraduate professors should be noted: Dr. Norm Wilson, and Dr. Doug Campbell, because they asked me to be their graduate students I responded to Dr. Hsü's ad for one.

I beg forgiveness, and thank my friends, and my cousin James Iredale for listening to me talk, endlessly, about this thesis druing the four years it has dominated my life.

I much thanks goes to Ms. Anne King and Mr. John MacPherson for their generous assistance with the most ornerous part of the thesis, correcting my spelling and grammer. Similar thanks belongs to Dr. Brian Stimpson's comments on the two occasions that he read major revisions of this thesis.

I could not have undertaken this course of studies without the support of my parents, and most of all, my Grandfather.

TABLE OF CONTENTS:

List of Figures

APPENDICES (Figures & Tables)

Chapter 1

INTRODUCTION

1.1) Introduction to Oil Sands

1.1.1) Importance of The Resource

Canada, and the rest of the world, will continue to need large quantities of oil for fuel, lubricants, and chemical feed stocks far beyond the foreseeable future. The requirements for oil will be met in Canada by a combination of conventional sources and the oil sands. The development of the oil sands as a new supply presents unique problems to engineers, geologists, businessmen, and politicians.

There is a great deal of oil in the oil sands of Alberta. It requires stable oil prices to permit its development on a commercial basis. It is estimated that there are 33 Gm^3 of oil in the Alberta oil sands.[1] Table 1.1 summarizes the state of Alberta's oil reserves in late 1985. From Table 1.1 it can be seen that approximately half of the conventional oil has been found and recovered. One percent of the mineable oil sand has been developed. Both of these are dwarfed by the huge "in-situ" reserves.

Table 1.1 Alberta Oil & Oil Sand Reserves M m^3

	Conventional	Mine	In-situ(1)	Totals
	M m^3	M m^3	M m^3	M m^3
Recoverable	2 970	7 000	39 000(2)	48 970
Recovered	1 566	97	7	1 670
Remaining	1 404	6 903	38 993	47 300

M m^3 = 6.3 x 10^6 barrel

Gm^3 = 10^3 M m^3

(1) Conventional is light and heavy crude oil, and natural gas liquids. Mineable Oil Sands are those under less than 50 m of overburden. In-situ oil sands are those under more than 50 m of over burden.

(2) Includes reserves not yet delineated of 38,940 M m^3 of in-situ oil and 1,700 M m^3 of mineable.

The oil sands themselves lie under 50,000 km² of northern Alberta, in four major formations. (See map, Figure 1.2). This thesis used oil sands samples' cored from the Sailine Creek area (a stream just north of Ft. McMurray, Alta.) of the McMurray Formation.

1.1.2 What are Oil Sands?

Oil sands are old (105 MY) silicate sands laid down in the lower Cretaceous period.[2] They are exceptionally dense (in-situ densities of 2 tonne/m³ or more)silica rich (81% by volume silica) [3] and fine (0.06mm dia.) to medium (0.2 mm dia.) sands. [4]

The "Oil" in oil sands is a solid at room temperature, and flows only when heated to 60° C [5] its in-situ, absolute viscosity is 6000 - 3,000,000+ poise (gram / cm * Sec).

The oil, and the small quantity of water adhering to the sand grains, have in solution a large quantity of N_2 and CO_2 [6]. This IS MUCH RUED as it leads to considerable difficulties in conducting experimentation on its in-place structural properties (See Section 1.6 Sampling & Handling Difficulties)

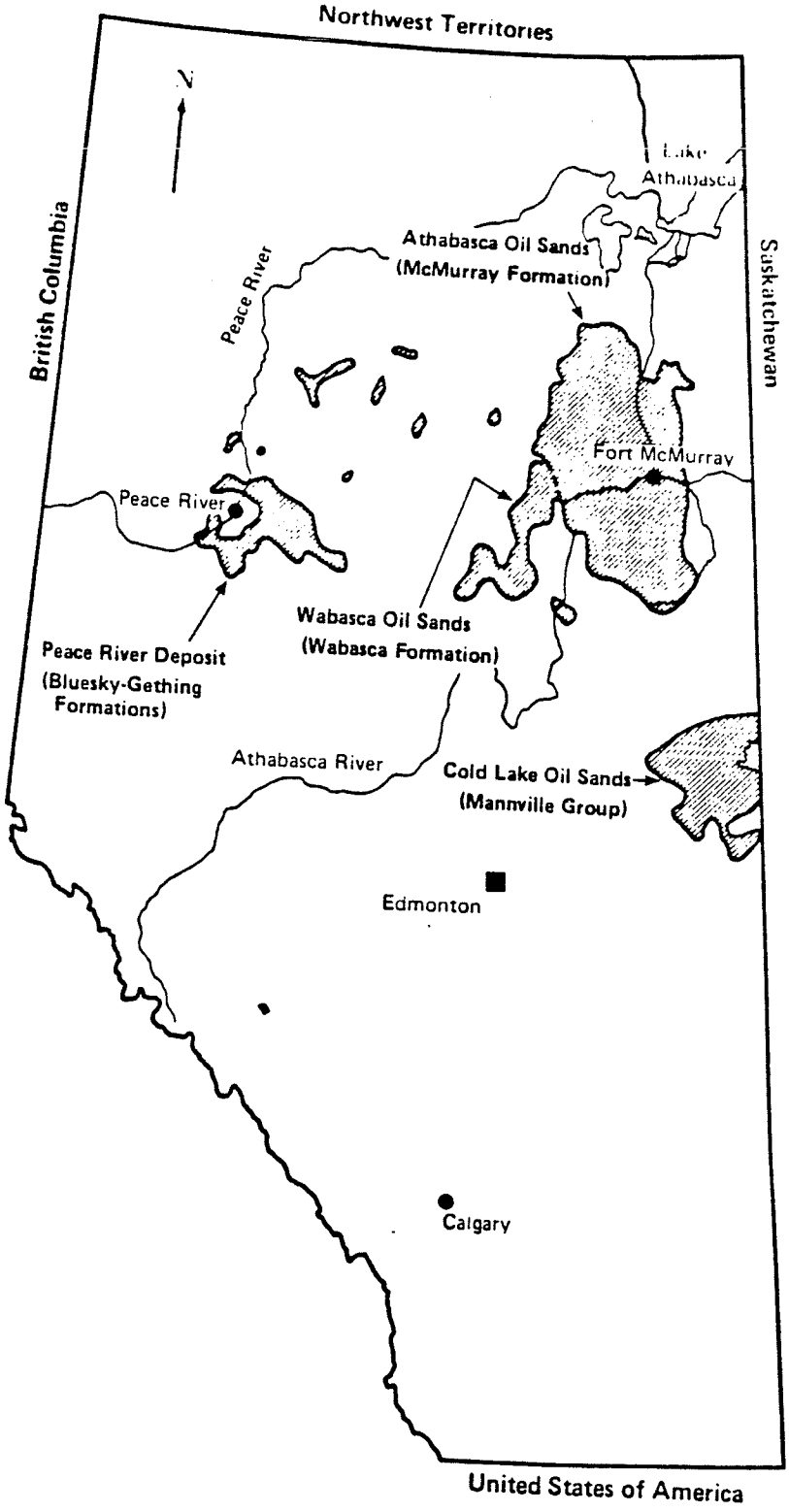

Fig. 1.2 Alberta Oil Sand Formations
After Dusseault.

Because of the high density of the sands and the stiffness of the oil, the oil sands themselves have a very low permeability [7]. This implies that flow of a fluid through an oil sand formation is very slow, and requires a substantial driving force to get any substantial flow rate.

1.2) In-situ Extraction & Fracture Assisted Steam-injection Technology [FAST]

The advantage of in-situ recovery schemes is that they require less capital, have a shorter lead time, cost less to operate, and cause less disruption to the environment than an open pit oil mining operation such as Syncrude operates. The disadvantage of any in-situ recovery method is that such schemes use very large portions of the recoverable energy in the recovery process.

The system portrayed on the right of the Figure 1.3 shows the FAST concept. This arrangement provides drainage through the introduced horizontal fractures in the formation. The fractures draw off the produced oil, together with the spent injected fluids. These fractures allow newly injected fluids ready access to the virgin formation, without recourse to expensive horizontal drilling techniques. The difficult part of this procedure is the control of the direction and extent of fracturing in the formation.

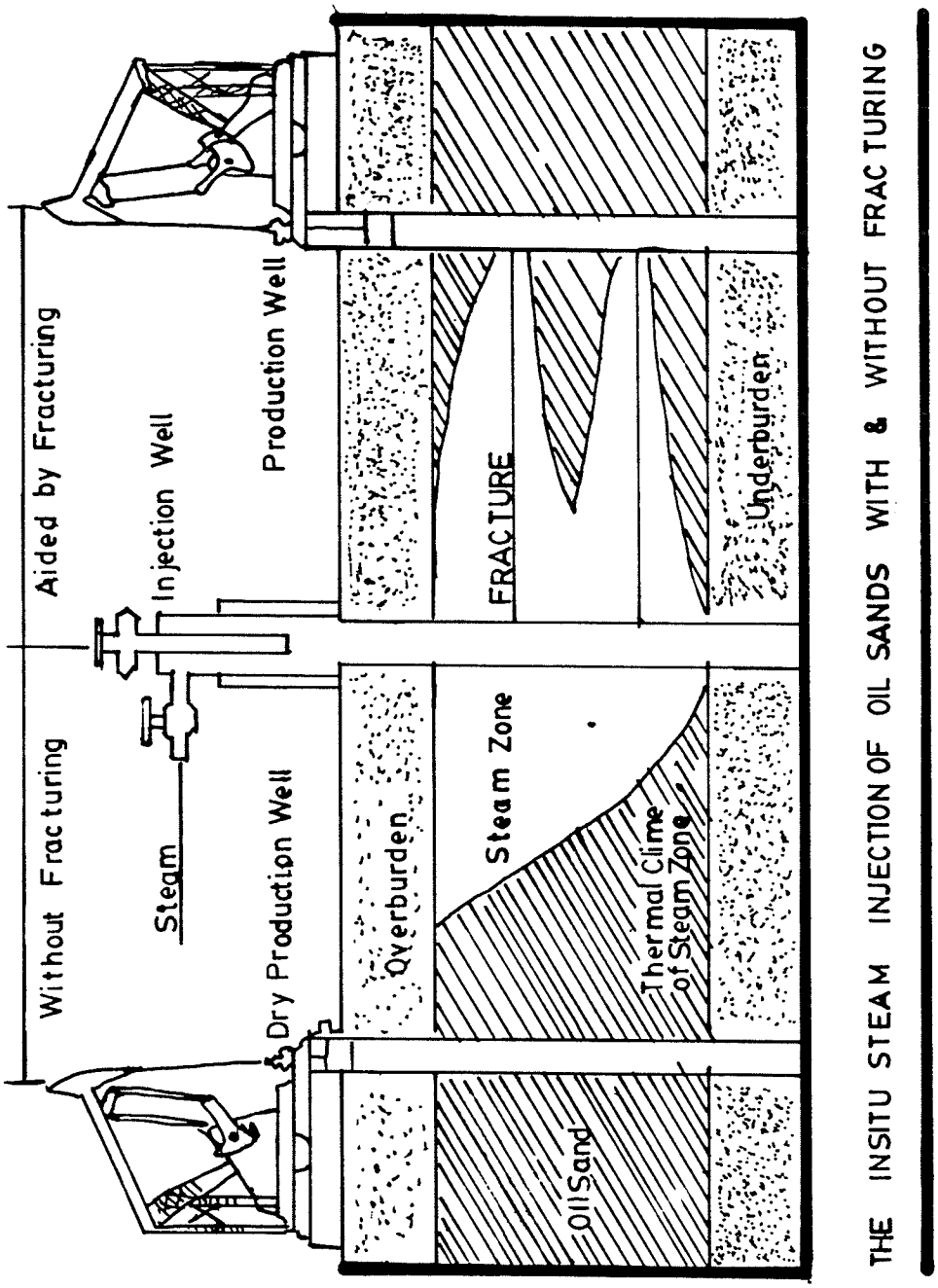

Fig. 1.3 Fracture Assisted Steam-injection Technology

The formation in Figure 1.3 left has not been fractured and the heated fluids are rising to the top of the formation and being drawn off along the boundary at the top of the formation. This can lead to a large amount of oil being left behind.

In 1983 Hsü [8-10], developed a finite element program to permit the modeling of the combined stress in, fracture of, and Darcy flow in a formation. In order to accurately simulate the mechanical behavior of oil sands and predict the extent of the fracture in the formation, the tensile properties of oil sand were needed. This thesis developed and applied methods for acquiring one set of values of tensile properties.

1.3 Engineering Investigations in Oil Sands.

1.3.1 Maurice Dusseault's Ph.D. Thesis

In the mid 1970's Maurice Dusseault investigated the geotechnical properties and geomorphology of oil sands' slopes. That work motivated and formed a basis for this thesis.

Dusseault defines the Alberta oil sands as a distinct engineering material, and refers to them as "Locked Sands". His definition is as follows:

1) Sand: an aggregate of dominantly sand-sized particles displaying little or no cohesion(less than 0.3 kg/cm²)in a saturated state, with an approximately linear peak strength envelope that is less than 10° to 12° steeper than the residual envelope.

2) Locked Sand: an aggregate of dominantly sand-sized particles displaying little or no cohesion in a fully saturated, stress-free state, characterized by a curved peak strength envelope that is more than 10° to 12° steeper than the residual envelope.

3) Sandstone: an aggregate of sand-sized particles having either inter-particle physical cementation, or a degree of interlock sufficient to impart an appreciable stress-independent cohesion in a saturated state. In the absence of true mineral cement, porosities are low, probably less than 20% in a well-sorted material. [11]

Using a number of micro-graphs of the sands and the work of Siever [12] & Dapples [13], Dusseault concluded that the inter granular fabric of locked sands was the result of the solution of silica away from the points of contact of the grains.

He suggested that this diagenesis may cause some tensile behavior. He stated:

> "The material may at this [with the development of interpenetrative fabric]* stage begin to display some true cohesion as the three-dimensional interlocked structure becomes better developed." [14]

* From Previous Sentence

He stated that only a small amount of diagenesis results in major changes in the engineering properties of a sand [15].

He used a finite element package to analyze slope stabilities in oil sand mines. One of the results of this exercise was the identification of a number of substantive zones of tension at the top edge of the cut face. He regarded the results that showed the oil sands sustaining a tensile load with great suspicion.

1.3.2 Research Since 1977 (Dusseault's Thesis)

In 1982 Dr. T.-R. Hsü was working on the dynamic properties of oil sands, with a view to using explosives to fracture the oil sands. He was encouraged in this by the extremely brittle behavior of oil sands at very high strain rates. [16]

The notion that oil sands have tensile properties arose in a definite form in a discussion between Dr. Hsü and Dr. J. D. Scott in 1982 [17]

Dr. Scott's student, H. Plewis, in his M.Sc. Thesis [18], performed a limited number of drained tensile tests on a "Bobbin" tensile specimen as illustrated in Figure 1.4

In a conversation between Plewis and the author in Feb. 1985, Plewis stated that he was getting around 70 kPa maximum total strength. In his thesis he concludes that there is no effective tensile strength (total stress less pore fluid pressure).

Most of Plewis' work, however, was devoted to determining the long term compressive strength at various strain rates up to .1 ε/sec. This work complemented the U.ofM. thermo-mechanics group's work in the range between 750 - 1800 ε/sec.

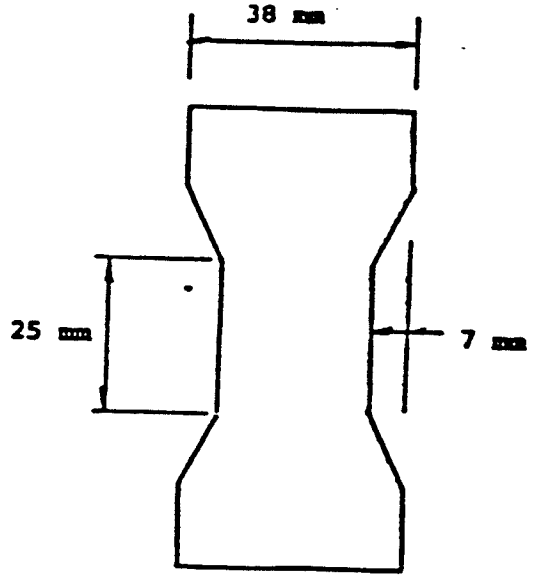

Fig. 1.4 Bobbin Specimen

These works show that the oil sands become increasingly strong and stiff in compression with increasing strain rates. (see Figure 1.5 ε & σ versus δε/δtime.) [19]

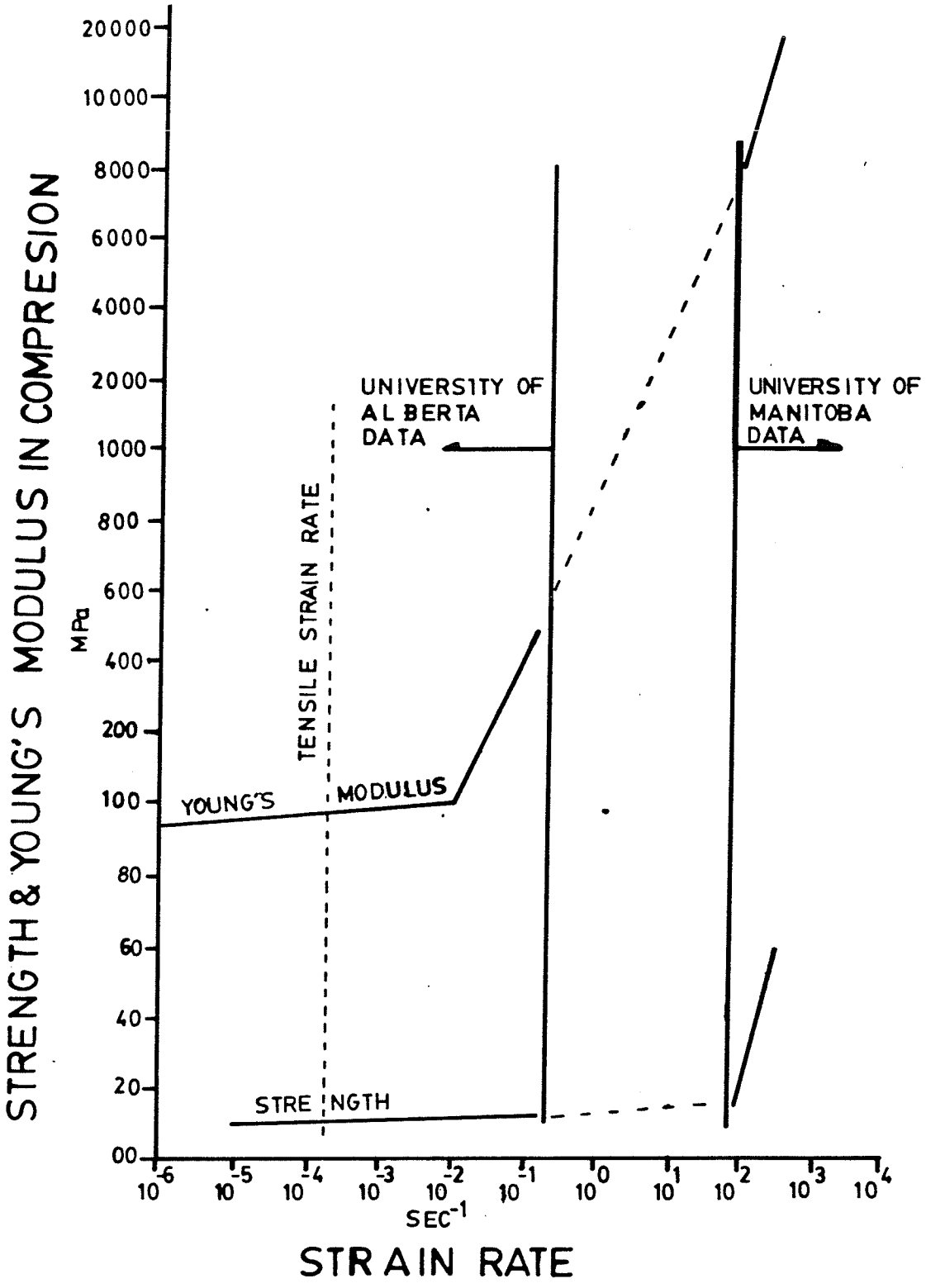

Fig. 1.5 Strength & Young's Modulus Versus Strain Rate

1.4) Sampling & Handling Difficulties

These sands' unique properties are a function of their interpenetrative nature. Because sands are a structure with a system of weak, lose mechanical joints between rigid sand grains the bulk properties then are therefore the cumulative effect of the sand grains themselves and the unique natural mechanical joints between them.

Oil sands unfortunately contain a pressurized liquid in their pore spaces with a large quantity of gas in solution. When the pressure is removed the gas comes out of solution and disrupts the interpenetrative fabric of the sands. This destroys their unique structural characteristics.

In order to overcome this problem it is necessary to take the samples in the winter. The sample is extracted from the coring device and placed in a heavy walled container under a gas cap. The pressure of the gas cap is slowly lowered to minimize sample disturbance.

All work, in particular specimen preparation, on oil sands must be done in a frozen condition to minimize any further disturbance. Freezing increases the solubility of the dissolved gases in the oil phase (which does not crystallize). Freezing reduces the volume of both the oil and sand phase. The reduction in the volume in the sand and oil allows the water (3-8% by weight) which expands during crystallization to do so without destroying the structure of the oil sands. The ice then acts as a continuous cement during cutting operations, provided it does not melt.

1.5) Tensile Properties Measurement

There are three properties that the author was interested in determining, a fourth Poissons ratio was omitted. They are the tensile strength, tensile Young's Modulus, and the fracture toughness in opening (Mode I).

In order to evaluate these three properties under in-situ conditions two experiments were needed. The first is referred to as the tensile measurement, the other the fracture toughness measurement.

To evaluate the strength and Young's modulus it is necessary to pull a straight length of oil sand and record its load and displacement record until it breaks. From this it is possible to measure the strength and stiffness of the specimen.

To evaluate the fracture toughness a wedge is driven into a notched oil sand specimen. The record of load and the wedges vertical displacement is inspected for the highest load before a drop as the load is applied. This load is taken as the critical load.

There is a less than direct relationship between the "critical load" and a true material property. The cause of this is the extreme sensitivity of the material to the exact specimen geometry. To remove the effects of specimen geometry the geometry is rigorously defined, and there is a relationship (Compliance Function) defined for each specimen geometry that absorbs the effect of the uncontrollable variation in the length of the crack.

1.6) Fracture and the Compliance Function

The measurement of fracture toughness of engineering materials only began after the World War I. Current texts are those by Broek [20] and Dawes [21].

In general the value of fracture toughness is of the form:

$$K_{Ic} = \frac{P_c * F(a/w)}{b * \sqrt{w}} \qquad (1.1)$$

Were

K_{Ic}	=	Apparent fracture toughness in opening
P_c	=	Load at onset of crack advance
F(a/w)	=	Compliance function
b	=	Specimen thickness
w	=	Specimen height
a	=	Crack length

Where b, a, and w for a compact tension specimen are illustrated Figure 1.6

The important feature in the determination of K_{Ic} is the length of the crack relative to the total height of the specimen (a/w) and the thickness of material, both of which must must be certain proportions to ensure a plane strain state at the crack tip.

In developing an experimental protocol the ASTM [22] defines a number of specimen geometries that are reasonably typical of engineering applications for metals. In procedure E-399, each specimen geometry has a defined function that compensates for the effects of crack length. This compensating function is called the compliance function.

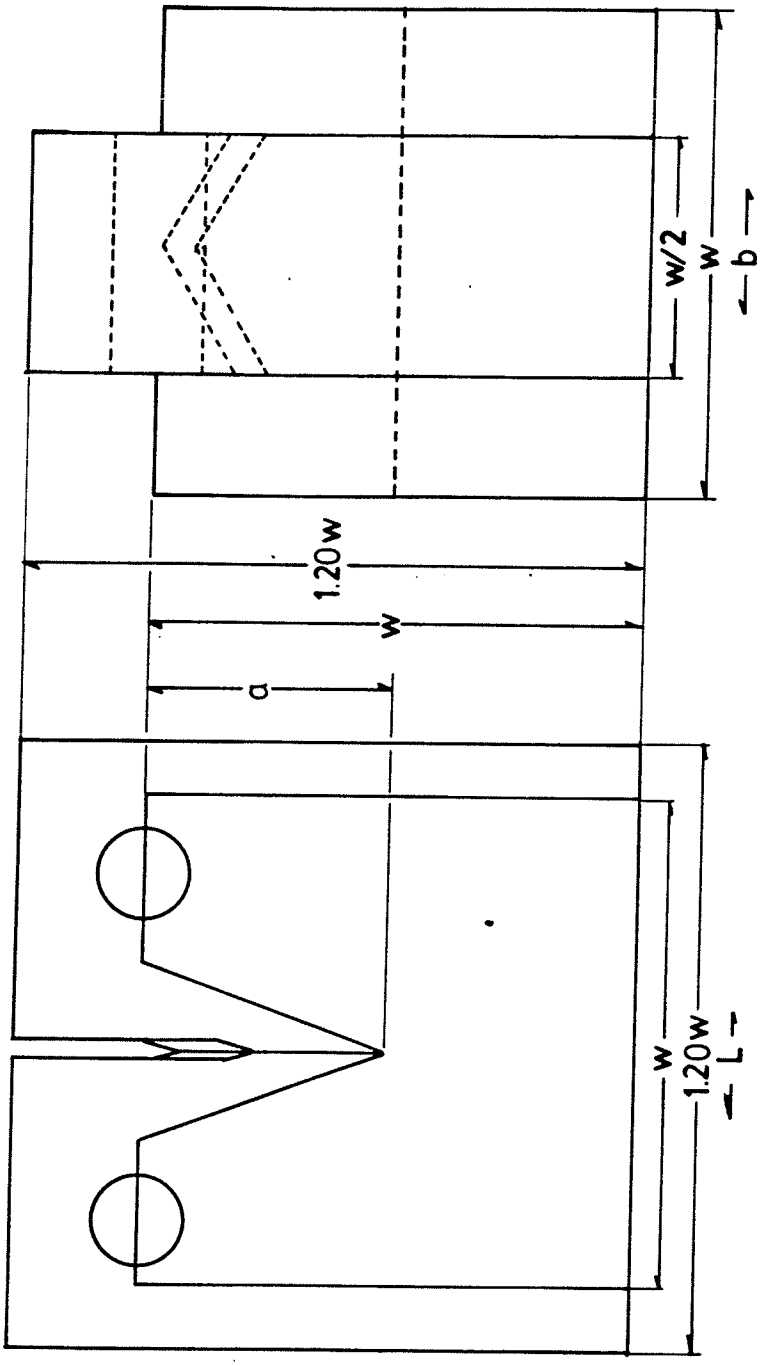

Fig. 1.6 Orthographic views of ASTM-E-399-CT Specimen, and WLCT Specimen

The larger ASTM-E-399-CT specimen with two holes, and the thicker WLCT Specimen with the broader notch. Drawn with a common crack tip, and center. See Figure 4.2

A typical compliance function is given below for the compact tension specimen.

$$F(a/w)=\frac{(2+[a/w])\,(0.886+4.64[a/w]-13.32[a/w]^2+14.72[a/w]^3-5.6[a/w]^4)}{(1-[a/w])^{3/2}} \qquad (1.2)$$

A second concern is that the crack tip be as "sharp" as possible. This is ensured in metals by using a fatigue fracture. This fracture is advanced until a/w becomes approximately ½.

In developing the experimental protocol for the fracture toughness measurement, it was suggested to the author that the ASTM-E-399-compact tension specimen compliance function satisfactorily mimicked the variation in P_c with a/w.

In reviewing the origins of the compliance function [23-26] in metals in the 1950's & 60's, it was apparent that the experimental protocol was significantly different to that used in developing Equation (1.2).

These differences are:

1) The presence of a confining pressure on the outside of the specimen.
2) The material's $\varepsilon_c/\varepsilon_T$ ratio was not 1.00.
3) A specimen geometry substantially different to the ASTM Compact tension specimen.
4) The load imposed by the friction of the wedge on the shims that apply the load to the specimen.
5) Variation of material properties with confining pressure.
6) Effects of the friction between the specimen and the bottom platen.

It was the development of this list of uncertainties that led the author to perform the simple check of the validity of the E-399-CT compliance function that became the sixth chapter.

1.7) Organization of This Thesis.

The first chapter introduces the oil sands, outlines the problem addressed by the thesis, and concludes with a formal statement of the hypothesis and scope of the thesis.

The second chapter describes the common experimental laboratory set up for each of the two experiments necessary to fully describe this material's tensile properties.

The next two chapters (3 & 4) discuss the experimental methodology for finding the strength and stiffness in Measuring Tensile Properties, Chapter 3, and the methodology for finding the fracture toughness (K_{Ic}) in Measurement of Fracture Toughness, Chapter 4.

The discussion of results occupies the fifth (Discussion I) and sixth (Discussion II) chapters. The former discusses the results of the experiments; the latter examines the validity of using the ASTM-E-399 Compact Tension specimen compliance function in this application, and develops a proposed compliance function suitable for the present investigation.

The conclusions and recommendations (Chapter 7) recall the findings developed, and outline what further steps are needed.

The References follow with each citation shown in the text as [Citation Number]. The first appendix (A.I) contains the procedures for the manufacture of the membranes for the fracture toughness tests. The second appendix (A.II) contains experimental data.

1.8) Statement of Hypothesis & Scope.

Hypothesis: As a result of their interpenetrative micro-structure, oil sands can be described as a "locked sand" and as such have a tensile strength, a tensile Young's modulus, and a non-zero K_{Ic}. Further, the Young's Modulus in tension is not equal to that in compression.

Experimentation was carried out to establish the values of the following physical properties

1) Tensile strength;
2) Compressive & tensile Young's moduli;
3) P_{Ic} & K_{Ic} of a wedge loaded compact tension specimen (WLCT).

As the strength, and other properties of oil sands are strongly affected by confining pressure, and as the results are intended for in-situ conditions, it is necessary to ensure that the oil sands in the test were under a confining pressure similar to those encountered in the field. A 2 MPa confining pressure was used in all tests. This value was used because the new Alberta Oil Sands Technology Research Authority (AOSTRA) tunnel test site is subject to this pressure

The analysis of the data include:

1) Ratio of compressive / tensile Young's moduli.
2) A summary of the average total tensile strength observed at one strain rate.
3) Calculation of the apparent fracture toughness (K_{Ic}) using the ASTM-E-399-CT compliance function.
4) A first order validity check of the ASTM-E-399-CT compliance function using a modified finite element procedure.

CHAPTER 2

Laboratory Set Up

The apparatus used in these experiments was designed principally to facilitate the fracture toughness measurements. When tensile testing was added to the experimental program, the load cell system was modified to accommodate it.

The entire testing facility is shown in Figure 2.1. There are three principal common systems used in both tests. The data gathering system, the operational support systems supplying the confining pressure, and the load application and displacement control. Most of the load cell is part of the last common system; it is discussed in section 2.3

Both tensile and K_{Ic} experiments had some special equipment associated with them. This equipment is discussed at the beginning of each experiment's chapter. The load cell, and its calibration for both the tensile and fracture toughness measurements form the final section of this chapter.

2.1) Data Acquisition Systems

There were four variables of concern; load, displacement, confining pressure and time. Three of these variables were rendered as an electrical (voltage) signal. The time signal was generated by an LED clock radio positioned on top of the three voltmeters.

The electrical signals, and the time signal, were recorded as images of light-emitting volt meters on the video tape. The load and displacement signals were sent to an X-Y pen plotter.

The LED voltmeters had a 7/30th of a second cycle period. This arrangement proved reliable, and yet very simple to set up and use.

The dual system is the result of an early series of experiments in which pen plots became indecipherable. The video tape record gave both accurate and easily decipherable results. The data was transcribed by hand. It could then be replotted, or used to precisely identify a result from the pen plotter.

The overall arrangement is shown on the data and support system diagram. (Figure 2.1)

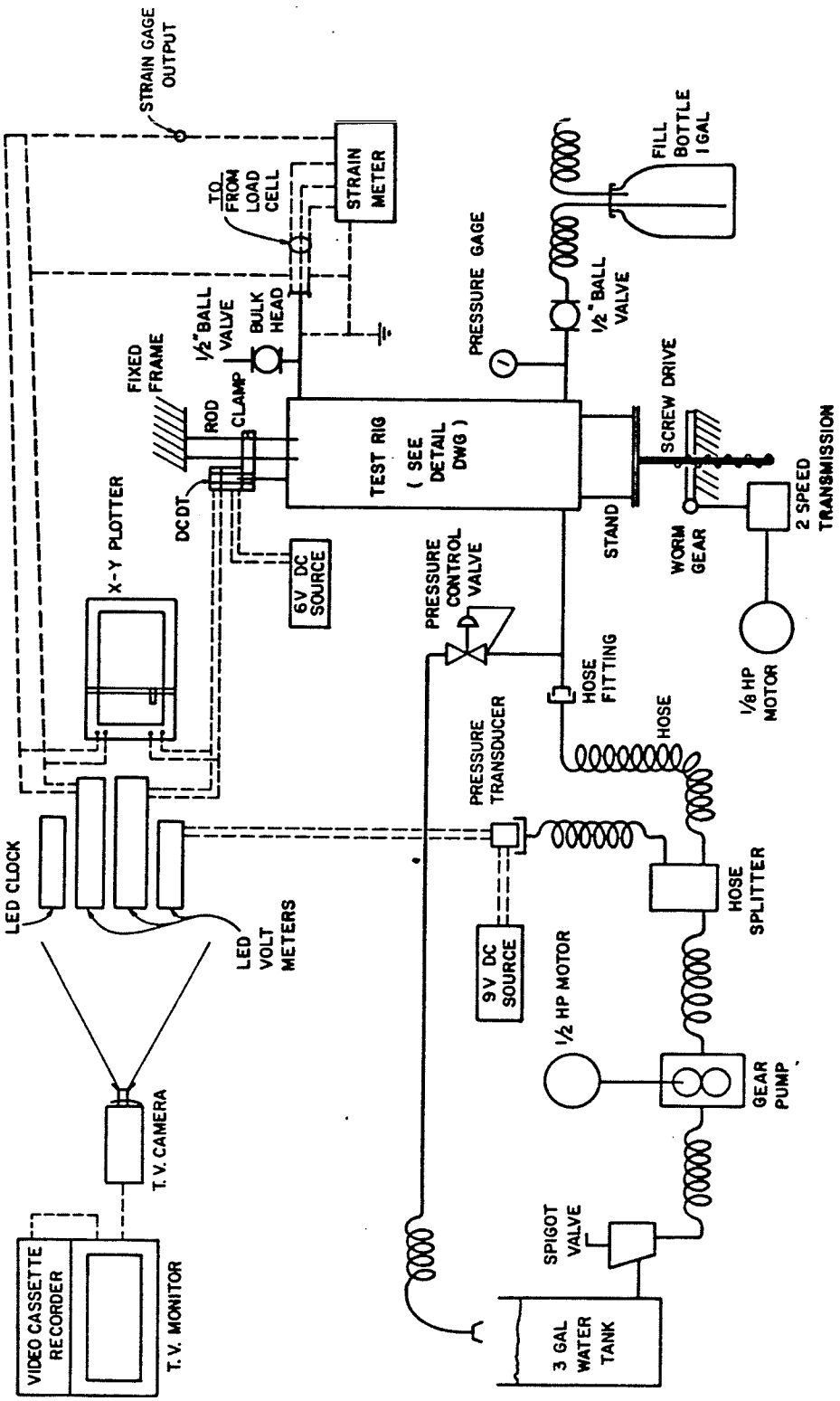

Fig. 2.1 Data & Operational Support Systems Arrangement

Load was measured by a hand made load cell which is discussed in detail in Section 2.3. The transducer itself was a half-bridge resistance circuit. This was connected to a strain gauge box that gave a voltage output. (See sections 2.3, 3.1 & 4.1)

Displacement was measured using a Direct Current Displacement Transducer (DCDT). The DCDT was mounted in a brass case screwed into an aluminum arm attached to the mobile hydraulic cylinder piston rod. The core of the DCDT was attached by a #80 thread to a 3/64th" brass rod mounted on a bracket held in place by two of the four 1/2" rods that held the top of the hydraulic cylinder down.(For details see Section 2.2)

The only problem encountered with this arrangement was that the brass rod was mounted in a puddle of cyano-acrylic glue that was more fatigue resistant than the brass rod! The result was that the rod had to be replaced, such replacements were often preceeded by a desperate hunt for the core of the DCDT.

The calibration (Figure 2.2) of the DCDT indicated that it was insensitive to input voltage, and had a linear zone in the ± 4 volts range at 1.20 V/mm. The output voltage from the DCDT was fed to both an X-Y pen plotter and an LED Volt Meter. The calibration curve is shown in Figure 2.2

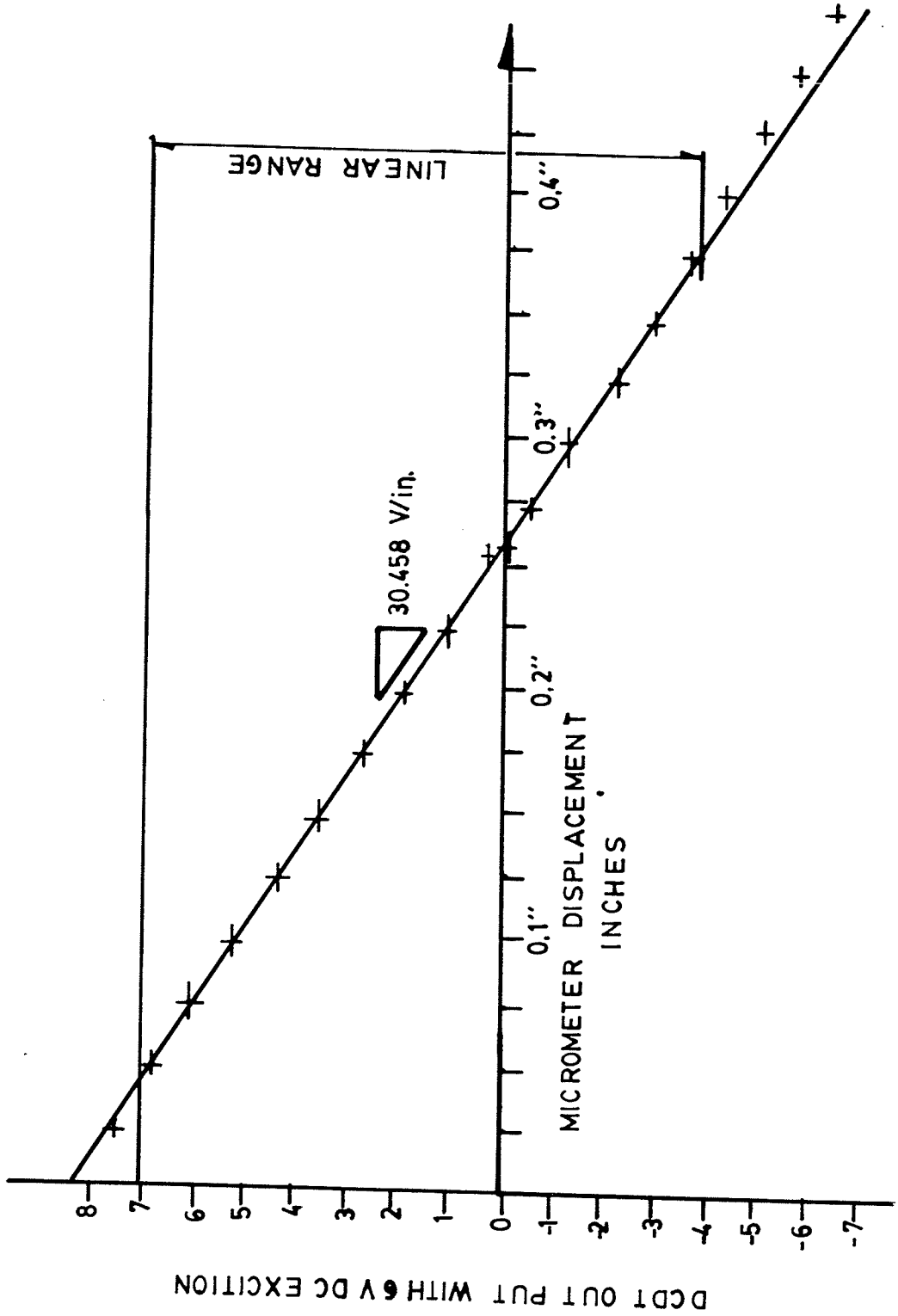

Fig. 2.2 DCDT Calibration Curve

The pressure transducer was of the foil type, with a full bridge circuit. It was mounted in a quick disconnect plug and attached to the fluid supply hose system. It supplied assurance data only and did not control the confining pressure.(See Section 2.2)

The pressure transducer was calibrated at 9.000 V and found to have the response shown in Figure 2.3 It was fairly sensitive to input voltage and so care was taken to insure that a 9.000 V was fed to it by a second rectifier.

2.2) Operational Support Systems

There were three major support systems; the pressure vessel, the pressurized fluid supply system and the displacement control system.

2.2.1) Test Chamber

A reworked hydraulic cylinder, 4" dia. x 10" stroke, was used as a test chamber, see Figure 2.4. This cylinder could be pressurized to a maximum pressure of 41.25 MPa MPa with two 1/2" NPT pressure ports on the bottom end and one on the top.

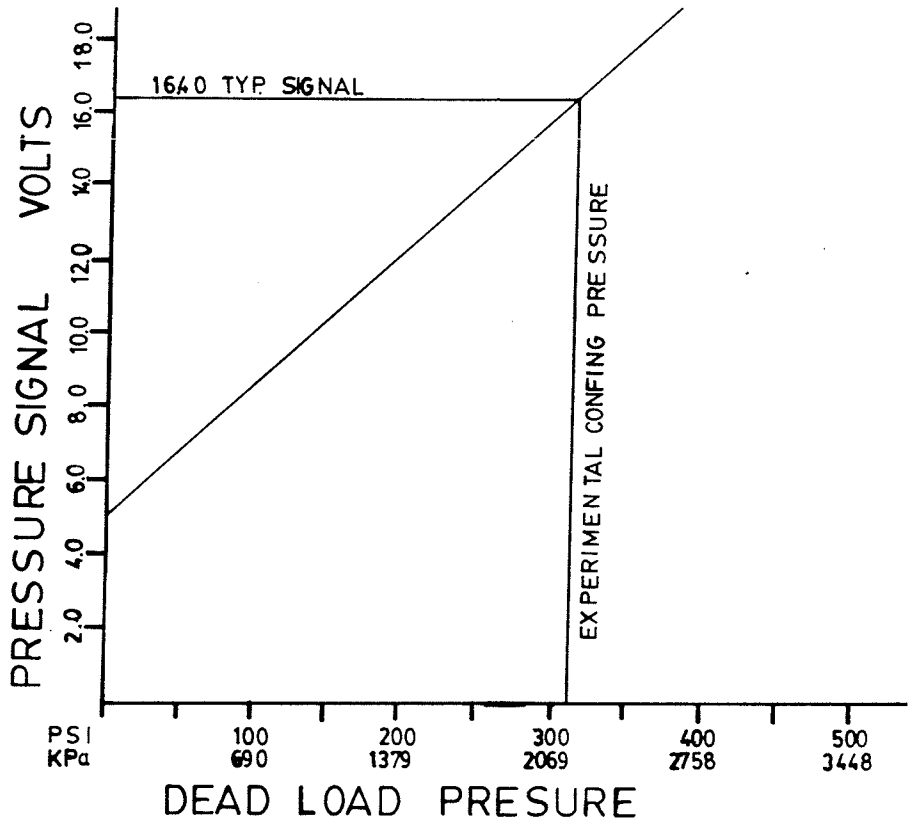

Fig. 2.3 a Pressure Transducer Calibration Plot

Table 2.3 b Pressure Transducer Calibration Data Taken July 1985 using a dead weight pressure testing machine capable of testing in 25 psig increments to 1000 psig. Input voltage tolerance was ± 0.03 V.

Pressure PSI	kPa	Voltage Volts	Pressure PSI	kPa	Voltage Volts	Pressure PSI	kPa	Voltage Volts
0	0	4.98						
25	172	5.90	325	2241	16.90	625	4309	28.01
50	345	6.805	350	2413	17.82	650	4482	28.93
75	517	7.73	375	2586	18.74	675	4654	29.86
100	690	8.65	400	2758	19.67	700	4827	30.80
125	862	9.57	425	2930	20.59	725	4999	31.73
150	1034	10.48	450	3103	21.53	750	5171	32.66
175	1207	11.40	475	3275	22.45	775	5344	33.59
200	1379	12.33	500	3448	23.37	800	5516	34.53
225	1551	13.245	525	3620	24.30	825	5688	35.46
250	1742	14.16	550	3792	25.22	850	5861	36.39
275	1896	15.07	575	3965	26.15	875	6033	37.325
300	2069	15.98	600	4137	27.08	900	6206	38.255

Step: Average = 0.92347 Volts/25 psig

Slope: Average = 0.03694 Volts/Psig = 0.254693 Volts/kPa

One of the two bottom ports (Figure 2.4, Part #23) was used to fill the chamber with fluid prior to applying the confining pressure. This line had a dial pressure gauge, and a ball valve. The fill bottle was attached using plastic tube (1/2" Tygon) and worked on a siphon system. The other port was connected to the pressurization system.

The bottom of the hydraulic cylinder rested on a stand. In addition to accommodating the 3" diameter tractor attachment that was cast into the bottom of the cylinder, the stand also held the 4 x 1/2" - 13 hex head bolts, welded onto it, that supported the four 1/2" rods that secured the top of the vessel against the confining pressure.

The top port had a T installed with a ball valve hard piped to allow venting during filling. This was done through a length of large diameter (3/4" Tygon) tubing to prevent overflows. The other end of the T accommodated a bulkhead port that passed the wires for the load cell into the pressure vessel. (See Figure 2.1)

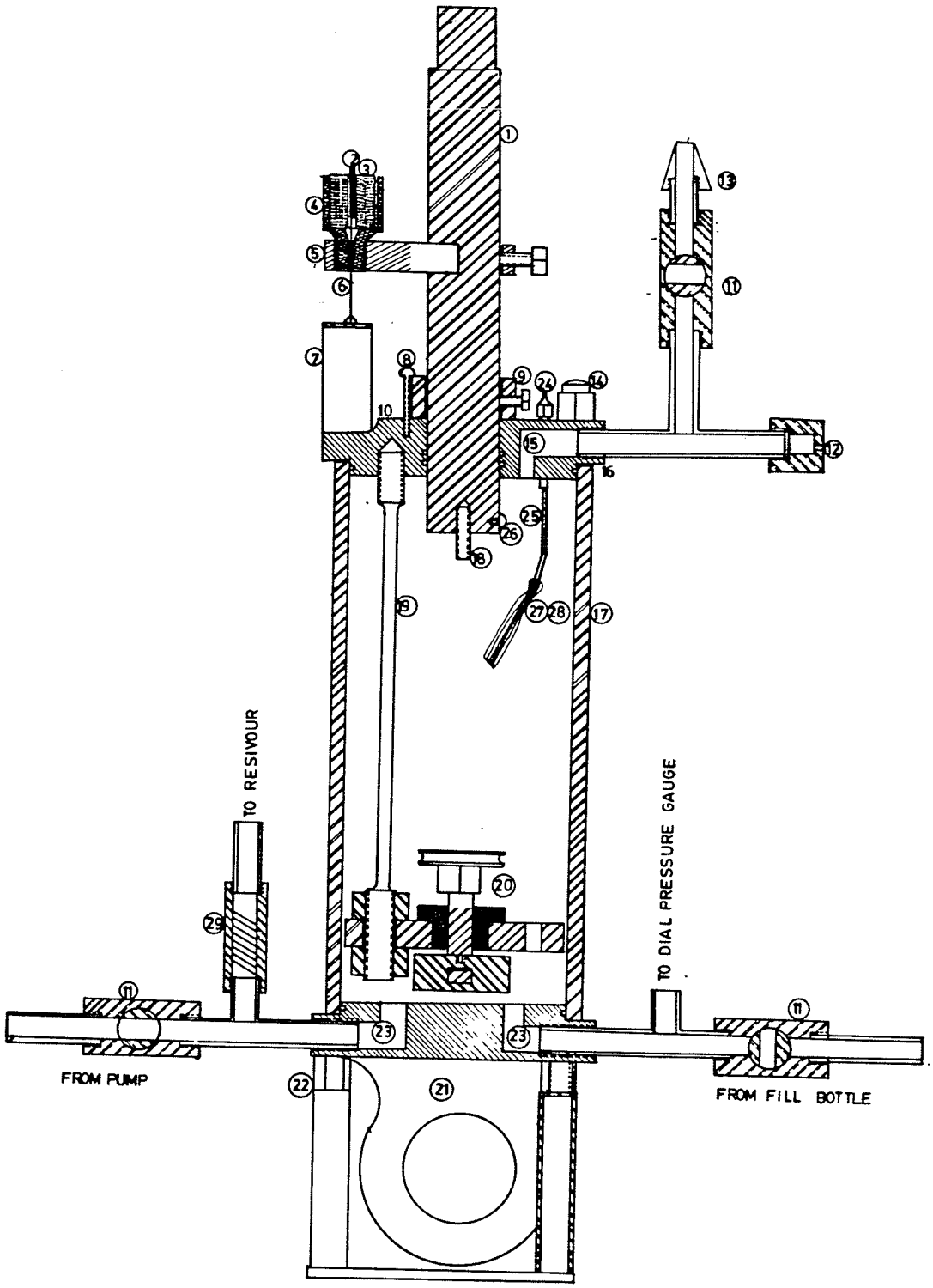

Fig. 2.4 a Test Chamber
Approximate Scale 1:3

Upper Assembly

1	Rod,	Steel
8	Ret. Collar Hold down Screw	
9	Retaining collar	Steel
14	Threaded Rod	1/2"-13 Long Bolt Cylinder
19	Load Cell Support Rods	1/2"-13 UNC Ready Rod
20	Load cell	See Figure 2.6
18	1/4-20 UNC 1"	ex 1/4"-20 x 1" bolt
26	Retaining screw	1/8"-32 x 1/4 Dome

DCDT Assembly

2	Core
3	DCDT
4	DCDT mounting
5	DCDT Mounting Bracket
6	Core Wire
7	Core bracket

Cylinder Top Assembly

10	Top of Cylinder	Cast Iron
15	Top Port	
16	O-Ring	
17	Cylinder Wall	6" Steel Pipe

Specimen Vent System

24	Vent port fitting	3/16" SS
25	Vent stack	1/8" SS
27	Tygon Tube (Outside)	0.010" ID
28	Spaghetti Tube (inside)	0.005" ID

Miscellaneous Piping

11	1/2 Ball Valve
12	Bulkhead Fitting
13	Overflow Tube Connection

Bottom Assembly

21	Bottom of Cylinder	Cast Iron
22	Base	Welded Steel
23	Bottom Port	
29	Pressure Relief / Control Valve	

Fig. 2.4 b Test Chamber Key

The top of the cylinder was removed as were the original internals. The end of the rod had a 1/4-20 UNC hole drilled in the bottom center. The top cap (for tensile testing) and the loading wedge were designed to attach using this thread.

A 1/8-UNC hole was drilled and taped 1/4" from the bottom of the piston rod. This hole was fitted with a 1/8" domed screw to act as a safety stop on the rod.

Two concentric plastic tubes(Figure 2.4, Item # 27 & 28) were run between the breather vent on the specimen assembly and the vent stack (Figure 2.4, Item # 25). The smaller (Spaghetti tubing) penetrated the 0.020" diameter tube mounted on the specimen assembly , and the outer covered the connection (Tygon) providing a water tight seal. The tubes were laid so that there was some slack in them. These allowed fluid to be vented from the specimen to atmosphere.

The double tube arrangement was necessary because the outer tube would seal but also collapsed under confining pressure. The spaghetti tube would not seal but would remain open under the 2.1 MPa confining pressure.

Four 1/2" - 13 UNC x 5/8" deep holes were drilled and tapped into the top cylinder head (Figure 2.4, Item # 10) to hold the rods which supported the load cell. A 1/4" through drilled hole was used to install a fitting which provided venting from the sample (Figure 2.4, Item # 24). Externally a 1/4" - 20 UNC bolt hole was installed 1/2" (Figure 2.4, Item # 8) away from the rod exit to hold the restraining collar (Figure 2.4, Item # 9) in place. (for use see sections 3.5 and 4.2)

Three 1/2" threaded rods, 10" long, were trimmed down to 3/8" along most of their length, leaving 1 1/2" of thread at either end. These rods supported the load cell.

2.2.2) Pressurization System

A variety of water/glycol mixtures provided confining pressure during the course of experimentation. These were stored in a 3 gallon open top water tank. The spigot valve on this tank was connected to a pump by a short length of 3/4" Tygon tubing.

The pump was a positive displacement type, two piston, belt drive, driven by a 3/4 horse power motor. The whole pump & motor arrangement was mounted on a 1/4" piece of plywood. This piece of plywood acted as a sound resonator during experimentation.

Fluid pressure was controlled by a pressure relief/control valve set just upstream of the entrance to the test chamber (Figure 2.4, Item # 29). The procedure for setting the pressure was: close up the test chamber and pressurize, note the pressure on the dial gauge, stop the pump, remove the fluid return hose (Figure 2.1), adjust the set screw of the pressure relief / control valve , re-attach the fluid return hose.

This procedure was repeated as necessary until the dial gauge read 2.0 MPa. In reviewing the data from the electronic pressure transducer (Figure 2.1). It appears that the dial gauge was a little hard and the actual pressure was 2.1 MPa.

Pressurized fluid was conveyed to the test chamber by high pressure hose. There was also a length of hose that led to a pressure transducer. This hose acted as a small hydraulic capacitor, smoothing out the pumping action of the reciprocating pump. It did not however remove the slow fluctuation that was the result of the oscillation in the pressure relief/ control valve's spring vibration interacting with the pump and hose systems. This instability amounted to 70-80 kPa in maximum shift brought about by fluid heating, and a sinusoidal variance of 10 - 20 kPa with a 10-15 second period.

Most of the fluid pumped did not go to the pressure vessel; the vast majority was allowed to flow through the pressure relief / control valve and was returned to the reservoir by garden hose wrapped around a convenient pipe. After circulating for some time (20 min - 2 hours) the 3 gallons of pressurizing fluid would heat up noticeably due to the fluid friction in the pump, valves, and hoses. As little or no circulating fluid would enter the test chamber this heating would have no significant effect on the experimental results, or on the test chamber temperature (approximately 20°C)

2.2.3) Load Application and Displacement Control System

The test chamber assembly was supported in a loading frame equipped with a screw driven bottom platform and a rigidly fixed top as shown in the photograph Figure 2.5

The 1" diameter Acme Slotted screw was attached to the platform that supported the test chamber. It was driven by a worm that drove the 12" diameter nut. The worm was driven by either a belt off of the end shaft of a 1/8 horse power reduction motor, or by a chain drive off of a shaft that was driven by a bevel gear from the reduced speed of the same motor.

The speed of the worm, and hence the speed of the linear movement of the bottom platform, was controlled by positioning the motor so that either there was a tension on the belt drive, or the chain drive was engaged. This gave a fast(belt drive) for the set up, or a slow speed (chain drive) for the experimentation.

The motor start control was able to give forward and reverse motions.

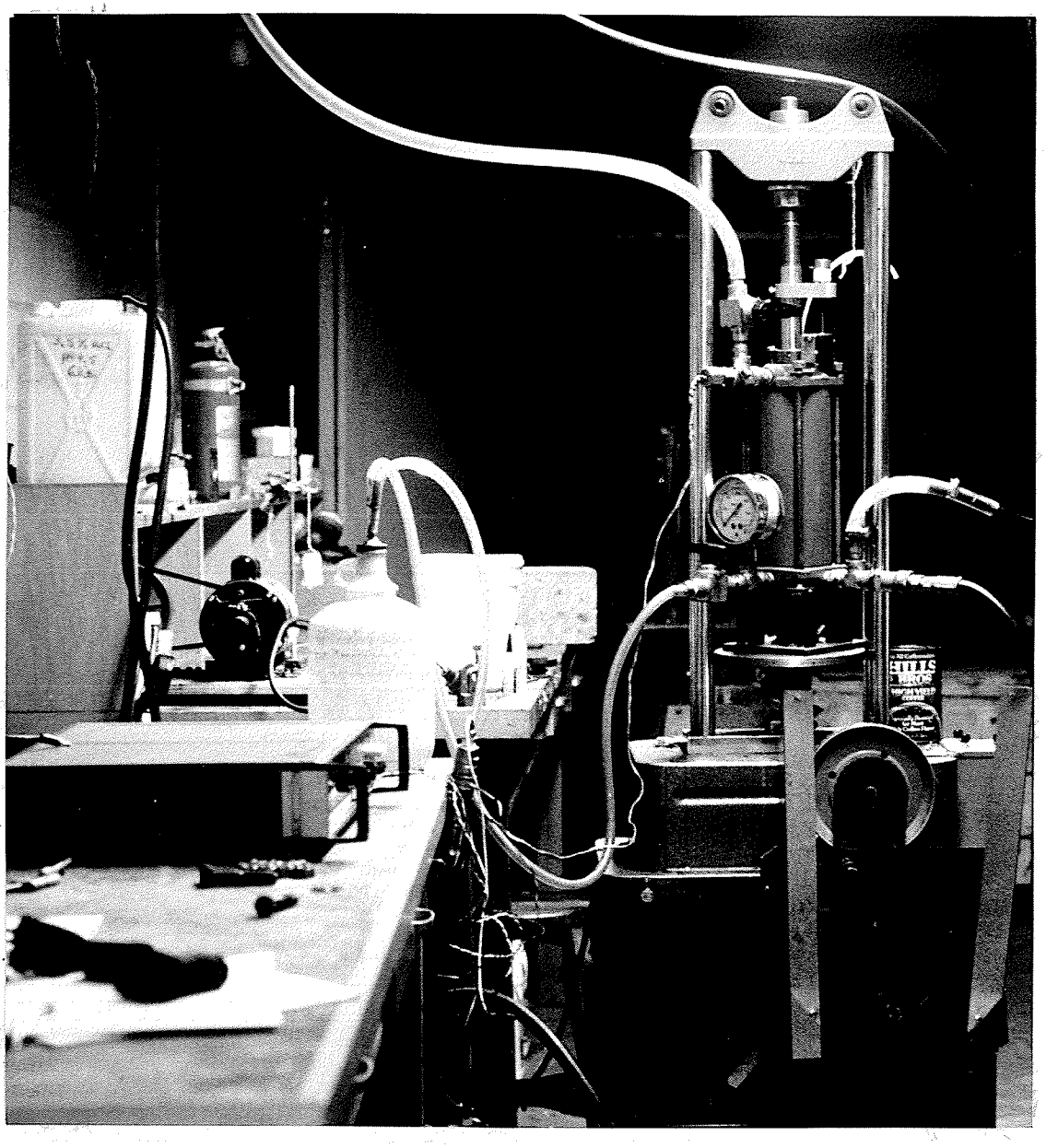

Fig. 2.5 Photo of Load Frame
Photographed by D. Kuss

2.3) The Load Cell

2.3.1) Load Cell Design Requirements

It was anticipated that the loads from the fracture toughness experiment would be very small, on the order of several tens of Newtons at the very most. Any externally mounted load cell would have faced a load of 1700 N. or more as a result of confining pressure. Further, that load would have been highly variable as a result of the positive displacement pump and the instability of the pressure control valve.

It was therefore necessary to devise a load cell that was sensitive enough for the measurement of the expected fracture toughness P_c loads, and could be used inside the cylinder.

Even in the tensile property measurements with loads of approximately 1700 N., an external load cell would have presented serious problems. The hydraulic cylinder rod acted through a two O-ring seal, which produced a major friction force. The load required to overcome this friction would have been registered on an external load cell.

2.3.2) Load Cell Construction

The load cell was built around a base plate, 1/2" thick, which supported the other components. The load cell consisted of two fixed supports supporting a "simply supported" load beam. The load was delivered to the beam by a loading wedge attached to the platen and the support shaft (made from a 1/2-13 x 2 bolt) by a 3/32" UNF thread. The platen was held 'vertical' by a brass bushing mounted in the base plate. The clearance was a loose sliding fit and generously greased.

The stationary supports were originally 30° knife edges set at the ends of the load beam. For the first two tensile tests and the fracture toughness measurements they were welded structures.

As a result of a misplaced welding rod, while remodeling to conduct the last four tensile tests, one of the supports was rendered useless. New supports were fabricated. These were made with mounting roundels and a piece of 1/4" doweling held in place by #6 - 32 UNC Screws.

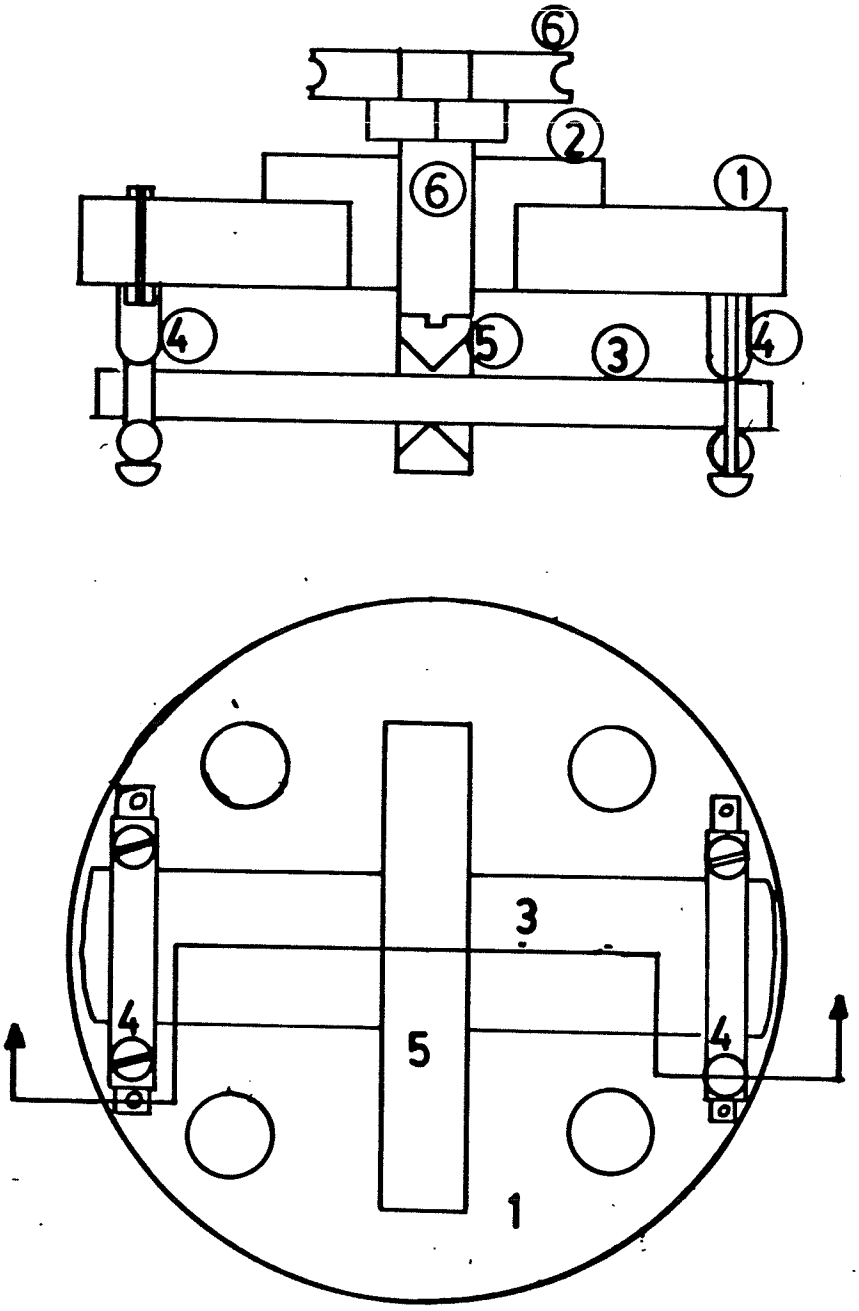

Fig. 2.6 Load Cell Detail

Parts:
1 Base Plate (1/2" steel plate)
2 Bushing (2" brass rod)
3 Load Beam (Ø.ØØ2Ø" galvanized 1/4" mild and Stainless Steel) Strain gauges attached Top and Bottom at this point.
4 Fixed Supports (1/4" steel rod, #6 Screws)
5 Loading Wedge (Mild steel)
6 Platen (2" x 1/4 brass)

Fig. 2.7 Load Cell Detail (viewed from bottom)
Photographed by D. Kuss

The load beam used for tensile property tests was initially made of approximately ¼" thick mild steel to which were attached two electric resistance strain gauges. These were covered in a polyurethane coating and then a thick layer of either liquid latex or silicon caulking compound was applied to "keep the water out" and ensure that the gauges were electronically intact.

The net result of this arrangement was the trapping of water on the steel, and corrosion-induced separation of the strain gauges, below the adhesive. This led to the sudden, and at the time mysterious, loss of calibration of the load cell. For the last four tensile tests a stainless steel load beam was used.

2.3.3) Calibration

Load Cell calibration was first accomplished using a number of weights. Care was taken to ensure that the relative position of the beam was maintained.

Initially this meant that the ends of the load beam (Figure 2.6, Item # 3) were glued in place onto the outside(s) of the stationary supports and then calibrated. With the roundel support system the doweling was tightened until it formed a tight friction fit. As there was no significant traverse loads on the beam. This friction was sufficient to ensure the beam remained stationary.

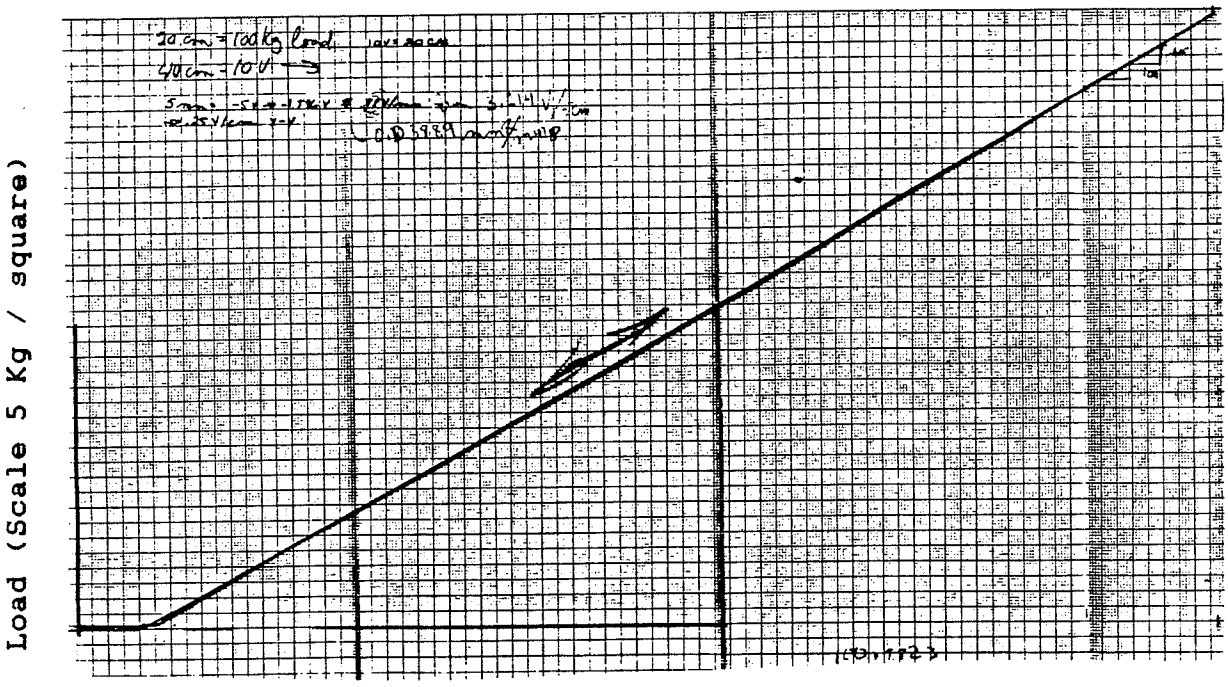

Fig. 2.8 Load displacement record from the Instron Testing Machine of the spring used in the Calibration of the load cell for tensile experiments.

Spring Constant from this plot is 93.72 nt/mm

The calibration of the lighter load cell system used for fracture testing was done using dead weight loading exclusively throughout the entire range of loads encountered.

There were major problems with the calibration of the load cell for tensile testing. To accommodate loads up to 2000 N. the load cell could not be calibrated by dead loading. To get around this problem a spring was acquired and its load-displacement characteristics found in the Instron machine. The load displacement record of the measurement of the spring's stiffness is shown in Figure 2.8

The procedure in this test was to set the spring in the machine and apply load through its active length from full expansion (no load) until there was no space between the coils and the load displacement curve flattened (this part of the curve was removed from Figure 2.8). It was then unloaded with the displacement record going in reverse. Note the tiny area of hysteresis that shows on this diagram as a gap between the two lines.

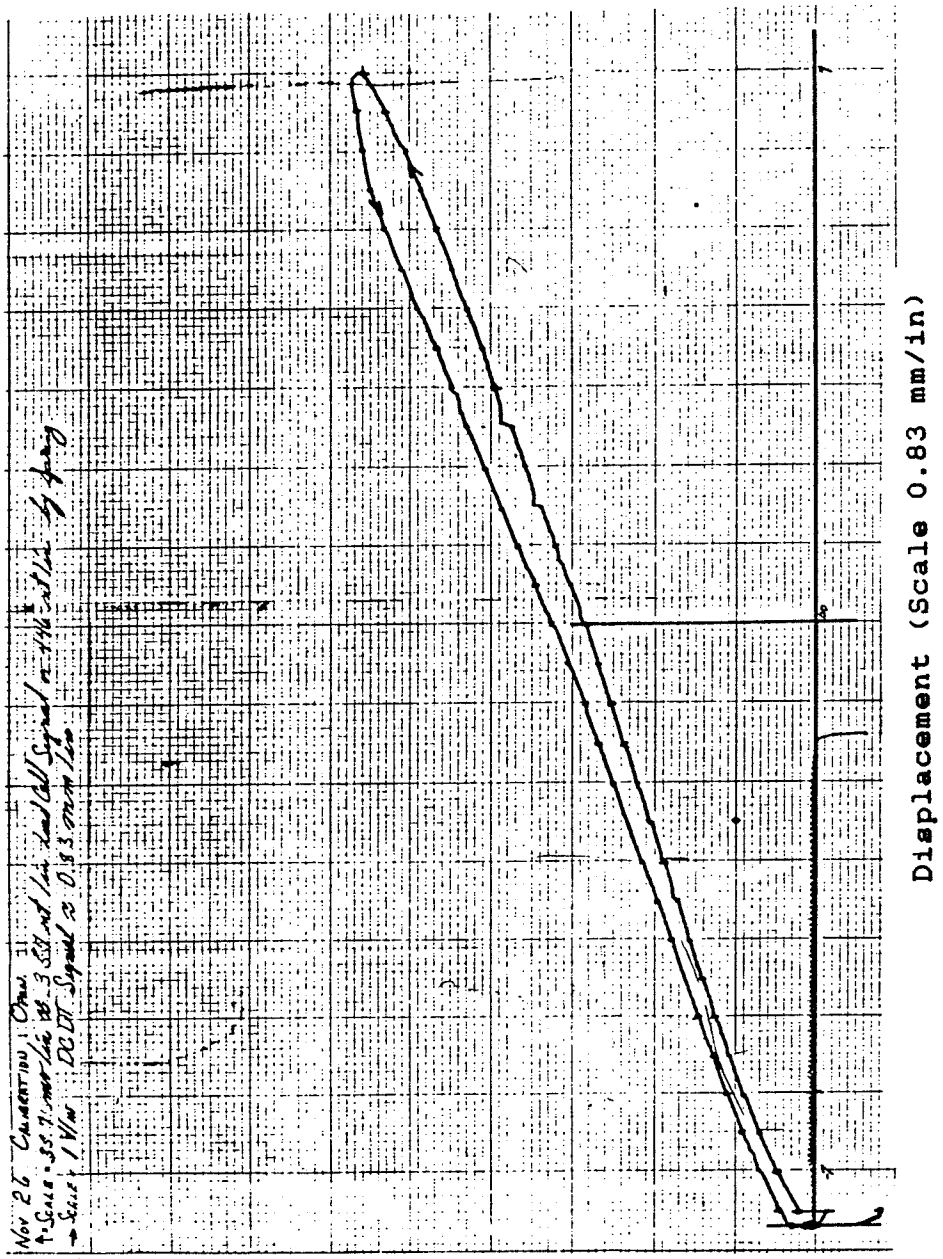

Fig. 2.9 The load versus displacement record produced on the experimental load cell tested against the spring calibrated above.

Note: The dots on the plot are where the displacement was stopped to allow the direct measurement of the spring using a pair of calipers (calibrated in inches/1000).

The spring (calibrated in Figure 2.8) was then placed in the upper assembly in the load frame and slowly compressed. About every 50 N on the load cell the motion was stopped and the 'length' of the spring measured using a dial caliper. The load and the spring displacement (in inches/1000) were recorded. The load vs displacement record from the X-Y plotter of this operation appears in Figure 2.9

The record was then analyzed using a spread sheet. This report, reproduced as Figure 2.10, showed that the load cell readings were acceptably consistent throughout the entire range and about 20% less than the calculated spring load.

The strange behavior when the spring was fully loaded, at the beginning of the unloading phase of the calibration experiment (where measurements were taken as the spring was unloaded) suggests that there was some residual (friction) force in the bush, or the rod seal.

Some 450 N. were required to seat the spring on the rod and load cell. This is the cause of the non-uniformity in the lower part of the range discussed on table 2.10. Noted as area 2 on Figure 2.9.

The results, in Chapter 5, do not include the 20% additional load that this procedure suggests should be applied.

LOAD CELL CALIBRATION REPORT

NOMINAL LOAD NEWTONS	REPORTED LOAD NEWTONS	SPRING LENGTH INCHES	SPRING DEFLECTION MM	SPRING LOAD NEWTONS	SPRING LOAD /REPORTED LOAD
0	0.25	3664.0	0.0000	0.00	0.0000
50	53.75	3621.0	1.0922	102.36	1.9044
100	103.50	3583.0	2.0574	192.82	1.8630
150	153.75	3552.0	2.8448	266.61	1.7341
200	204.25	3528.0	3.4544	323.75	1.5850
250	253.50	3506.0	4.0132	376.12	1.4837
300	305.25	3481.0	4.6482	435.63	1.4271
350	353.50	3458.5	5.2197	489.19	1.3838
400	403.25	3433.5	5.8547	548.70	1.3607
450	453.75	3411.0	6.4262	602.26	1.3273
500	505.50	3388.5	6.9977	655.82	1.2974
550	554.00	3362.0	7.6708	718.91	1.2977
600	607.00	3338.0	8.2804	776.04	1.2785
650	652.75	3314.0	8.8900	833.17	1.2764
700	700.25	3291.5	9.4615	886.73	1.2663
750	756.00	3264.0	10.1600	952.20	1.2595
800	801.25	3239.0	10.7950	1011.71	1.2627
850	855.00	3216.0	11.3792	1066.46	1.2473
900	903.50	3190.0	12.0396	1128.35	1.2489
950	950.25	3164.0	12.7000	1190.24	1.2526
1000	1003.50	3133.0	13.4874	1264.04	1.2596
1050	1059.75	3107.0	14.1478	1325.93	1.2512
1100	1099.50	3086.0	14.6812	1375.92	1.2514
1150	1152.50	3061.0	15.3162	1435.43	1.2455
1200	1201.25	3033.0	16.0274	1502.09	1.2504
1250	1250.00	3008.5	16.6497	1560.41	1.2483
1300	1300.00	2983.0	17.2974	1621.11	1.2470
1350	1345.00	2959.0	17.9070	1678.24	1.2478
1400	1400.00	2930.5	18.6309	1746.09	1.2472
1450	1446.00	2909.0	19.1770	1797.27	1.2429
1500	1497.50	2878.0	19.9644	1871.06	1.2495
1550	1548.00	2851.0	20.6502	1935.34	1.2502
1600	1608.00	2817.0	21.5138	2016.27	1.2539
1650	1650.75	2788.0	22.2504	2085.31	1.2632
1700	1694.25	2764.0	22.8600	2142.44	1.2645
1750	1751.00	2735.0	23.5966	2211.47	1.2630
1800	1800.50	2709.0	24.2570	2273.37	1.2626
1850	1852.00	2686.0	24.8412	2328.12	1.2571
1900	1900.00	2659.0	25.5270	2392.39	1.2592
1950	1952.00	2639.0	26.0350	2440.00	1.2500
2000	2001.50	2614.0	26.6700	2499.51	1.2488
SPRING/REPORTED LOAD AVERAGE					1.2944
SPRING / REPORTED LOAD FOR LOADS OVER 500 NEWTONS					1.2581

Table 2.10 Load Cell vs. Spring Load Summary Report

CHAPTER 3

MEASURING THE TENSILE PROPERTIES OF OIL SANDS

3.1) The Rationale and Specimen Gripping

Of principal concern in this investigation was the evaluation of the Young's modulus (E_t)of oil sands in tension, and of decidedly secondary importance was an evaluation of the tensile (or parting) strength ($\sigma_{t,\ max}$) of this material. Therefore it was of the utmost importance that the cross section of the specimen be kept uniform along its entire (gauge) length. Given the equipment design there was no alternative to keeping the specimen diameter constant.

It was therefore necessary to attach the specimen to the platens using an adhesive that was much stronger and very much stiffer than oil sands. A two-component epoxy glue proved acceptable. Hence the specimen was glued to the platens at both ends, with an arrangement provided to vent the top end of the specimen through the top cap and into the atmosphere.

As the test kit was designed to give accurate relative displacement only, it was necessary that the expression of the values of Young's moduli (£) be as machine independent as possible. The simplest method of achieving machine independence was to use the ratio of a known quantity, as measured by the machine at the same time that the unknown quantity was measured. To this end the ratio of Young's moduli in tension ($£_t$) and compression ($£_c$) was used. This measure is independent of any error in the testing machine.

Provided adequate care was taken of the load cell, the measured load values were found to be acceptably accurate and consistent.

3.2) Special Equipment

Figure 3.1 shows the arrangement of the specimen.

For tensile testing, a ¼ thick beam was used in the load cell. Both of the two beams manufactured for this application were calibrated to give 10 N/v from the attached strain gauges.

To allow an easy check of load cell calibration, a washer was glued to the bottom of the specimen, rather than the platen. The top washer, top cap, and linkage assembly were glued to the top of the specimen (see Figure 3.1) and attached to the original piston rod of the hydraulic cylinder by a 1/4"-20 thread.

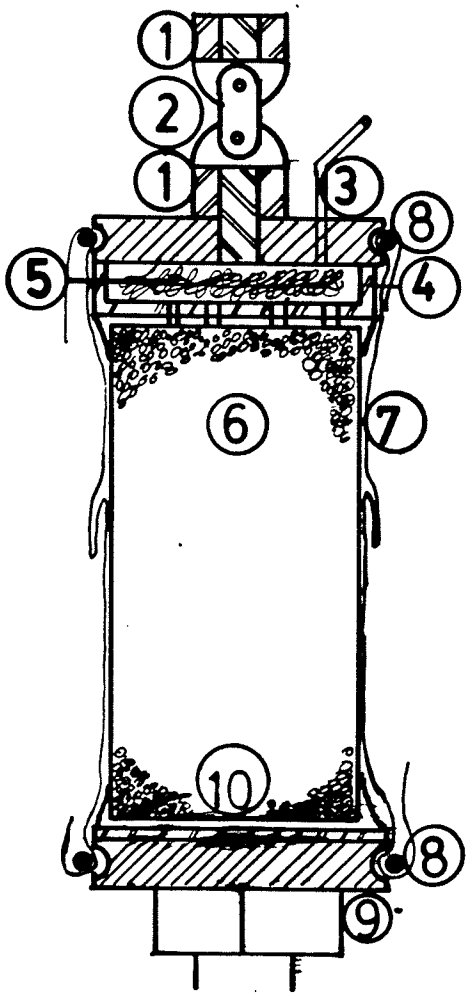

Fig.:3.1 Tensile Test Specimen Arrangement
Approximate Scale 1:1

Link Assembly:

1 2 Female Link- 1/4"-20 threaded
2 Male Link

Top Assembly:

3 Top Cap (/w 1/4-20 UNC screw) c/w Breather Tube
4 Top Washer (Aluminum)
5 Steel Wool Filter

6 Specimen
7 Membrane
8 O-Rings (2 of)
9 Platen
10 Bottom Washer (Aluminum)

Because the link assembly had only one link with circular pins, the link was essentially a fixed length. This meant that it could transmit both tensile and compressive loads (With only a small dead spot between). More links would have prevented the transmission of compressive loads. They would also have made set up operations easier.

3.3) Specimen Preparation

Oil sand samples were supplied to the University of Manitoba by the University of Alberta. They were cored from a variety of sources within the McMurray formation in northern Alberta. The principal source was the Saline Creek outcrop in the winter of 1984/85. Others were the new Alberta Oil Sands Technology Research Authority (AOSTRA) underground mine site. They were cored in the 1983/1984 season.

The samples had been de-gassed. This process allowed most of the dissolved gases lighter than CH_4 in the pore fluid mixture to escape without extensively disrupting the structure of the sands. At the UA they were packed into freezer chests along with dry ice chips, and air-freighted to the University of Manitoba where they were stored in a freezer.

Preparation of specimens for tensile testing was carried out in a cold room maintained at -15 °C at all times.

Specimens were first cut roughly to the intended length by a lapidiary saw. In instances where a core was large, (3" or 4" dia.) it was cut lengthwise into pieces to give a better yield of specimens. The pieces were then put into a lathe where they were held in place directly with the normal jaws on a three-jaw self-centering chuck. Care had to be taken to clean the jaws when they had been in contact with the outside of a core, or a saw cut surface, as these became very sticky, even at a cold room temperature of -15°C. All work on the lathe was done using a diamond tool. Non-circular sections were turned using shallow cuts of from .010 - .025 in.

Initially, there was concern over the effects of vibrations caused by non-continuous cutting. The most serious of these was the movement of the specimen in the jaws of the lathe. When this happened, the tool dug into the specimen and destroyed the whole work piece.

Once cut to round, the end was cut square and the specimen turned end for end. The remaining material was then removed.

The feed rate during cutting was 0.025" when cutting noncylindrical sections; and 0.050" when cutting cylindrical sections nearing the final cut. When cutting round sections well away from the final cut, in 'good' oil sands, cuts of up to 0.100" were possible. (And with the experimenter in that extreme cold (-15°C) for hours the experimenter took them!)

Specimens were fabricated in batches. The first specimen would be machined to its final size, using very small cuts to get the last bit of material off. The remainder were cut to the same tool position indicator values as the first specimen used.

The quality of the material being cut became rapidly apparent. Good material when cut was a light gray, and gave a uniform grinding sound during cutting. Poor material would not hold together throughout the machining process. Samples made of poor material were either streaked with red or gray clay(s), or were black from thawing. Poor material cut much more quietly than good material. One specimen had only a thin lens of clay, which parted during the specimen assembly process.

Every effort was made to remove all disturbed material from the specimens. Disturbed material left a black, reflective surface after cutting, whereas undisturbed material left a flat gray surface.

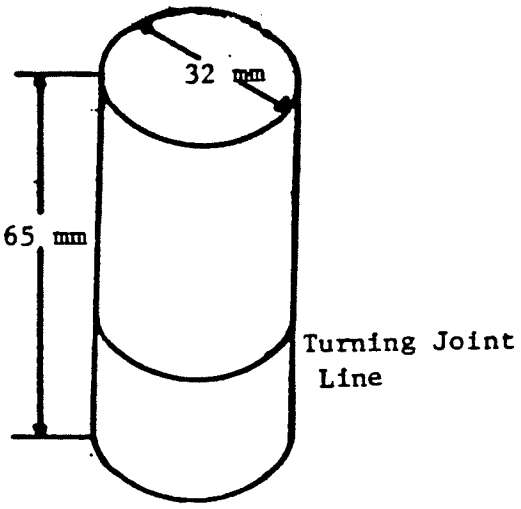

Fig. 3.2 Tensile Specimen

In cutting the many specimens used in this thesis only one other object was encountered. There was a small pebble in one of the tensile specimens.

Upon completing the initial cut, the specimen was turned end for end and the back end was turned down. This was done using hand feed and the cuts were larger during the initial cut down. The final cut was made using the machine feed, and was normally 0.020" or thinner.

This end was then faced down to produce specimens that were 32 mm in diameter and 65 mm long. Many specimens had a noticeable mark near one end where the end cut in the first turning joined the area cut in the second turning as shown in Figure 3.2. An examination of these marks indicated a small eccentricity of less than 0.5 mm. This eccentricity was always placed in the lower portion of the specimen when assembled. Since no specimen broke near any of these marks it is concluded that they had a negligible effect on experimentation.

The specimens were then transferred to the freezer in the laboratory. This freezer was set to run continuously to ensure the complete freezing, with a significant subcooling of the material. On occasions where the freezer failed the specimens thawed and gave maximum loads of 35 nt. All such results were discarded.

3.4) Assembly of the Specimen to the Platens

Before assembly each specimen had its diameter measured at each end and in the middle. The length was measured with the caliper arms placed on three different diameters. All measurements were made using a vernier caliper with an accuracy of 0.001" (0.025 mm).

The specimen was removed from the freezer, its dimensions measured, and it was returned to the freezer. There may have been some slight damage to the outer surface of the specimen by this heating at room temperature. Indeed, as the process took only a minute or so the frost was still forming on the specimen when it was returned to the freezer.

A small quantity of 5-minute epoxy glue was mixed. It was applied to the specimen side of the top (Figure 3.4 Item # 4) and bottom washers (Figure 3.4 Item # 10) and allowed to stand for four (4) minutes. The specimen was then recovered from the freezer. It was inserted into the glue puddle on the bottom washer, and the top washer was then flipped and pressed onto it. Both washers were firmly pressed onto the specimen. Excess glue flowed out the sides and through the breather holes in the top washer. The excess glue that flowed through the breather tubes was removed using a small palette knife and spread down the side of the specimen.

The partial assembly was returned to the freezer after the glue stopped flowing. This cooling prevented the glue from completing its curing. The chilling caused by the presence of the cold oil sands further slowed the curing process. As the epoxy will only cure above 0°C, and takes 30 hours to cure at that temperature, and because it was attached to an oil sand specimen that may undergo some thawing at that temperature, it was not possible to cure it at a warm temperature. This would have greatly slowed experimentation, due to both the 30 hour delay between experiments and the highly probable increase in specimens which failed to give a load reading.

After the assembly had again chilled in the freezer it was removed. Holding it firmly by hand the excess glue was removed from the breather holes in the top cap. This was usually done using the flat tip of a pair of tweezers as a drill. Other techniques proved unsatisfactory or unsafe.

The specimen was much larger (more massive) than the volume of glue, and was partly (on the ends) insulated by it. The glue layer was both thin and in contact with a good conductor, i.e.: the aluminum washers. Thus the glue would warm very rapidly while the core of the specimen would not. So the repeated warmings that accompanied each step in the assembly process allowed the glue enough time at a warm enough temperature to cure, while at the same time not damaging the specimen too extensively. The specimen was then allowed to thoroughly refreeze.

A coating of cyano-acrylic catalyst (type: M-Bond 200) was applied to the top cap (Figure 3.4, Item # 73). The specimen was removed from the freezer and the bottom of the bottom washer (Figure 3.4, Item #.9) was similarly treated. A drop of cyano-acrylic was placed on the platen. The sample was then placed onto the platen and pressed down. It was centered, hurriedly, as the glue set up very quickly.

A piece of steel wool (Figure 3.4 Item #5) was inserted into the cavity of the top washer (Figure 3.4 Item #4) to prevent any oil sand that came through the top washer getting drawn into the breather tube of the top cap. A bead of cyano-acrylic glue run around the top of the washer. The top cap, which had been coated with catalyst, was placed on top. Care was taken to insure that the top cap was located so that its edge was parallel with the top of the top washer adjacent to the breather tube. This ensured that no glue got into the breather tube. (With no cyano-acrylic glue solvent available this would have been a disaster!)

The entire assembly was returned to the freezer. Once the specimen was thoroughly frozen (again!). It was taken from the freezer, and then removed from the mounting stand (a rack with a 1/2" dia. hole in it). A commercial membrane cut to length 1 1/2" dia. x Ø.ØØØ in. thick was slid over the entire assembly (Figure 3.4 Item # 7).

Two O-rings (Figure 3.4 Item # 8) were positioned on the top assembly (on the notch cut in the top cap) and the platen. Great care had to be exercised to ensure that minimal shear forces were developed in this operation. The top O-ring was put on while holding the body of the specimen close to the top assembly.

The bottom O-ring was positioned with the assembly in the mounting stand and the O-ring brought into position from below. In doing this it was also necessary to be sure that there were no irregularities in the membrane below the O-ring. Excess membrane was folded back down onto the specimen. And the specimen was again returned to the freezer, ready for test.

3.5) Test Procedure

The test cell was first disassembled, and the pressure vessel was set beside the loading frame. An interim support (a concrete block) was placed under the load cell for support (see Figure 4.4).

The specimen assembly was removed from the freezer. It was then screwed into the loading knife of the load cell until finger tight, and then backed off by a full turn. This allowed the specimen to revolve in either direction when the rod was connected.

The load cell was then turned on and set to zero. The displacement control motor was started and the load cell assembly raised until the bottom of the flexible link (Figure 3.4 Item # 1 Lower) was engaged. The top assembly, the specimen, and the link on the rod could then be rotated to facilitate the insertion of the male link (Figure 3.1 Item # 2) into the upper female link. Once assembled the entire assembly could be rotated to allow for some additional misalignment or eccentricity of the loading of the specimen to be taken up, reducing parasite stresses.

When the male link was positioned in the upper female link a # 632 screw was passed through it. A nut was then put onto the screw and tightened finger tight.

The lock bolt on the collar was tightened to prevent motion of the assembly (Figure 2.4 Item # 9). This prevented the accidental application of load between this point in the procedure and its release immediately prior to testing.

The two concentric plastic tubes were attached to the top cap breather tube (Figure 3.1 Item # 3). The loading platform was lowered and the interim support block was removed. The upper part of the test chamber was removed from the test frame and lifted into place in the base of the pressure chamber. Care had to be taken not to let the breather tubes or the load cell wires (or fingers) get pinched in the pressure vessel seal.

The four threaded rods (Figure 2.1, Item # 14) that held the top of the hydraulic cylinder down were then guided into their respective holes and the vessel seal set. The DCDT core wire, core bracket (Figure 2.1, Item #'s 2,6,7) mount and core were usually left in place during mounting, however, it was at this time they would be reset if they had fallen off or been removed. The DCDT core bracket fitted over the two rods adjacent to the main pressure inlet.

The nuts were put on the threaded rods (Figure 2.1, Item # 14)and tightened in a star pattern. The whole assembly was then lifted back onto the loading frame platform. The platform was lowered, if needed, until the rod could be attached to the top of the loading frame. This attachment was secured by a nut in the top of a bolt arrangement. The loading platform was then raised until the washer on the bolt would only just turn. The nut on the bolt was then tightened down.

A short length of Tygon tube was attached to the Vent port fitting (Figure 2.1 Item # 24) to allow the easy determination of leakage and the out gassing rate. This length of tube was filled with clear water, the confining fluid was green.

An overflow reservoir made of a large Tygon tube was attached to the overflow tube connection (See Figure 2.1 Item # 13) and the pressure vessel was filled from the fill bottle with the liquid medium that would provide the pressure on the membrane. This was done through the bottom port Figure 2.1 Item # 23 Right.

A final check was made of all instrumentation. In particular:

the feed voltage for the pressure sensor,

the location of the pen on the XY plotter,

the DCDT voltage (output),

the load reading (Ø),

the Pressure reading was recorded.

The Video recorder was started. A moment later the confining pressure pump was turned on.

It is important at this point to note that all the forces necessary were generated by the confining pressure in the cylinder acting on the 1.25Ø" rod diameter imbalance between the top of the cylinder and the bottom. The load applied to the 32 mm specimen was less, often substantially less, than the load developed by the hydraulic forces. The base of the the test chamber (Figure 2.4, Item # 22) was at no time clamped to the testing machine. At all times when there was confining pressure on the system the loading frame was in tension.

On a number of occasions a definite twitch was noted as the confining pressure was applied to the system. This twitch was attributed to the threaded shaft that the assemblies sat on. As this shaft is only 1" diameter when a compressive load of about 1300 N. (300 Lbs.) was suddenly applied to the shaft it flexed. Ideally this happened when the retaining bolt (Figure 2.1 Item # 9) was released. This suddenly applied eccentric load was suddenly applied to the shaft (Figure 2.1). caused the entire structure to 'twitch'.

The restraining bolt was necessary to ensure that the specimen was not placed under a compressive load in an unconfined condition as the test assembly was lifted into the load frame.

When the confining pressure was applied, a significant load was carried by the restraining bolt. With the release of the restraining bolt was there was usually some, and often significant, motion of the top assembly as a result of a less than tight assembly at the junction between the load frame and the test chamber. This frequently resulted in the application of considerable strain and the removal of a significant fraction of the confining load in the direction of testing.

In Tests # 1 & 2 (Figure A.II.1 & 2) the specimens were "heat soaked" for 1 hour to ensure a complete thawing of the specimen (and curing of the glue). The other 4 tests were "Heat Soaked" for 10 to 20 minutes in the room temperature fluid (With a specific heat estimated to be about 80% that of water) before starting the test.

The loading frame motor was then started and engaged until a number of things happened:

1) the DCDT voltage deviated from the linear range
2) the bleeder valve started spouting confining fluid as a result of specimen failure which caused a membrane failure,
3) the load dropped indicating specimen failure,
4) the travel of the DCDT used up its liner range, and a maximum load of 20 nt. was developed (failed test).

When it was apparent that the test was over the following operations were performed. The loading frame motor was turned off. The fill bottle breather tube was inserted into an empty tub. The pump was turned off, as well as the video tape recorder. The two valves were opened and the pressure chamber emptied, also the feeder valve to the pump was closed. The system was disassembled. The specimen was removed and the end geometry observed. The broken specimen was then either refrozen for record or had its specific gravity measured.

When the platen was cleaned the load cell was reactivated and a 30 N load was applied to check the calibration of the system.

CHAPTER 4

MEASUREMENT OF FRACTURE TOUGHNESS

4.1) Intent of Fracture Testing

Because of the difficulty in producing compact tension specimens in oil sands the wedge loaded compact tension (WLCT) specimens were used for fracture toughness testing [28]. The WLCT and the ASTM-E-399-CT specimens are shown in Figure. 4.2 below.

4.2) Special Equipment

The load cell was adjusted to the sensitivity of 1.Ø N/v Figure 4.1 shows the experimental arrangement for fracture toughness testing. The platen mount (Figure 4.1 Item # 5) permitted easy assembly and drainage for the pore fluid in the specimen. It was attached to the platen (Figure 4.1 Item # 6) by a bead of Cyano-acrylic glue. Cyano-acrylic was also used to secure the tube that connected with the specimen breather tube
Figure 4.1 Item # 7.

No membrane that would fit the shape of the WLCT specimens were available commercially. Fabrication of such membranes in the laboratory became an important activity and is described in detail in Appendix I.

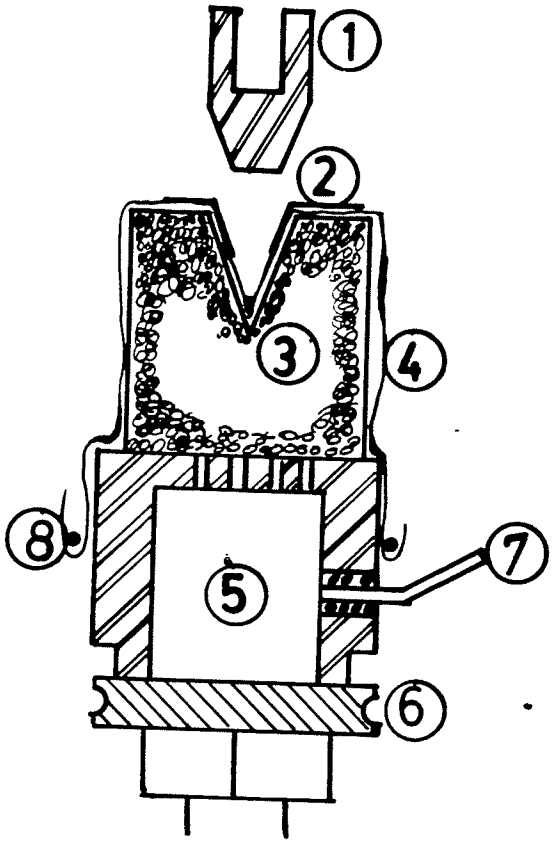

Fig. 4.1 Fracture Toughness Specimen Arrangement

1	Braille	Aluminum
2	Metal Shims	Steel
3	Specimen	
4	Membrane	See Appendix I
5	Platen Mount	Steel
6	Platen	
7	Breather Tube	Ø.Ø2Ø"
8	O-Ring	

The membranes, like those used in the previous experiment, were necessary for separating the oil sand specimen and its pore fluids from the confining pressure fluid. The geometry of the specimen and the platen mount are very complex as can be seen from the mandrel. (See photo Figure. A I.1)

When complete the membranes fabricated by the procedure described in Appendix I were coated in detergent to prevent self adhesion while awaiting use. When entering service each membrane had two heavy gauge shims made from sheet steel applied to the working surfaces Figure 4.1 Item # 2. These shims were attached by a bead of cyano-acrylic glue to the membrane

4.3) Specimen Fabrication

The WLCT specimen consists of a cube of material with a notch cut on one side as shown in Figure. 4.2(c). Fabricating this geometry in oil sands proved to be one of the more unpleasant tasks in this research project. This was due to the extremely cold temperatures used in the cold room when manufacturing fracture toughness specimens (-25°C). This extreme cold was necessary to ensure a solid, easy cutting oil sand block and a rapid cooling of saw blades between successive cuts. The saw would be grabbed by the oil sands if either became too warm.

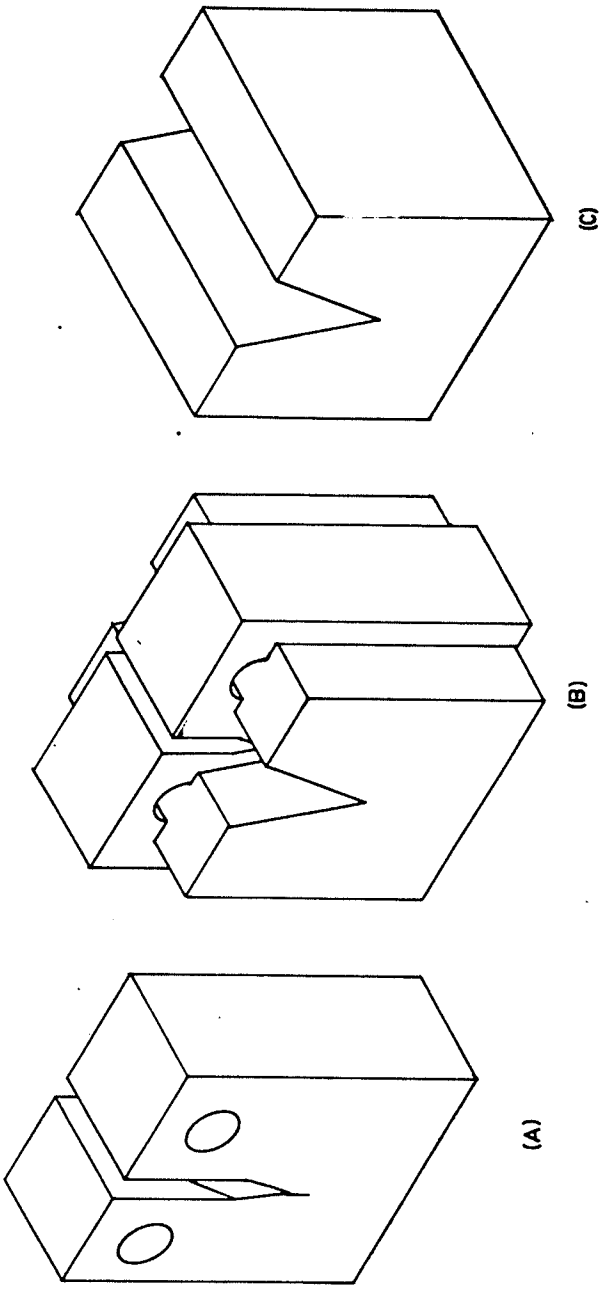

Fig.: 4.2 Isometric views of a: Wedge Loaded Compact Tension ASTM-E-399-CT

A) ASTM-E-399-Compact Tension specimen.
B) WLCT & ASTM specimen drawn with common crack tip center.
C) Wedge Loaded Compact Tension Specimen

A radial arm saw was used. The guards were removed and the thickest available diamond saw was attached. It was then possible to cut cubes with as few as six strokes of the saw blade.

These oil sand cubes were covered in a thin layer of disturbed material as a result of blade heating during the cutting operation. However, this would not have penetrated very far into the specimen because of the initial cold state of the oil sands and the long periods allowed between cuts that prevented the blade from heating up to an unacceptable degree.

The notches of several cubes were cut in a group by turning the saw blade to 20° and raising it until it cleared the guard bar. On one occasion a bar of oil sand was prepared and a long notch cut out of it and then sections cut off in appropriate lengths. However, the dimensions of the notches varied unacceptably. In later batches the cubes were cut first, then the notch in each cube was cut individually.

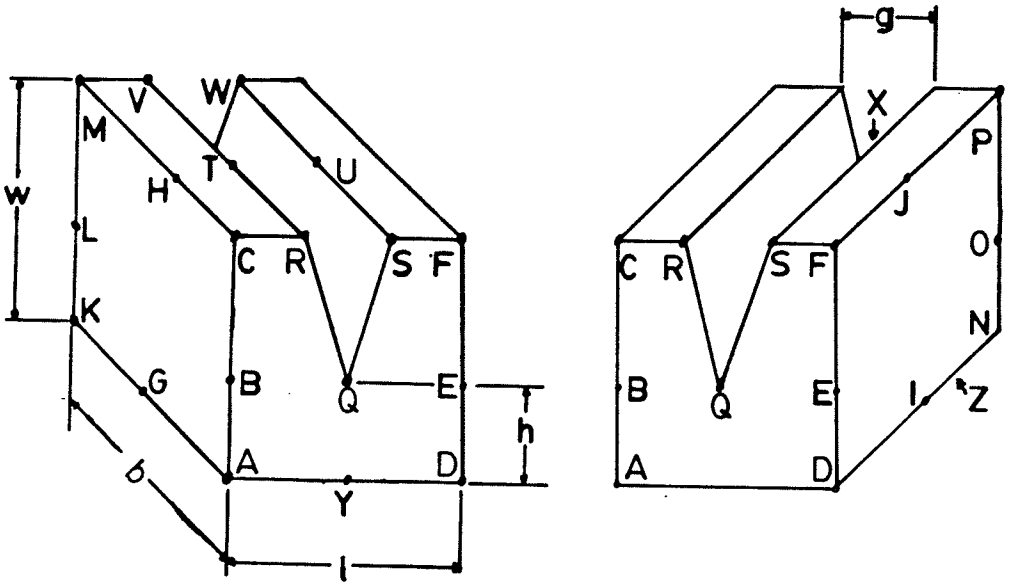

w = Average (AC,GH,KM,DF,IJ,PN)/6
  = Height of Cube ≈ 28 mm typically

b = Average (AB&DN,BL&EO,CM&FP)/3
  = Depth of Cube ≈ 28 mm

l = Average (AD&KN,BE&LO,CF&MP)/3
  = Width of Cube ≈ 28 mm

h = Average (QY,XZ)/2
  = Remaining material below Notch ≈ 12 mm

a = Average (RS,TU,VW)/3
  = Notch Opening ≈ 13 mm

$\theta = 2 \cdot \arctan[(a/2)/(w-h)]$
  = Notch Opening Angle ≈ 22°

a = w - h

Fig. 4.3 Wedge Loaded Compact Tension Specimen Measurements

4.4) Test Procedure

The membrane was prepared for service by having two shims glued to the top surfaces, adjacent to the notch. These shims provided metal to metal sliding friction surfaces for the wedge loading arrangement, thus minimizing frictional loadings. The membrane and shim assembly was then tested for water tightness. The shims were then covered in molybdenum sulfite lubricant.

The specimen was removed from the freezer and precise dimensions were measured as illustrated in Figure 4.3 This specimen was returned to the freezer for a short period.

The measured specimen was removed again from the freezer and placed in the membrane. The membrane with the specimen in it was then put onto the platen mount and an 'O-ring' lifted up over the breather tube and placed around the bottom skirt of the membrane.

The whole assembly was then filled with water, care was taken to drive out as much of the air as possible. The spaghetti tube was inserted into the full outer tube and the platen was screwed into the load cell. The breather tube was connected to the pressure vessel vent stack (Figure 2.1 Item # 25).

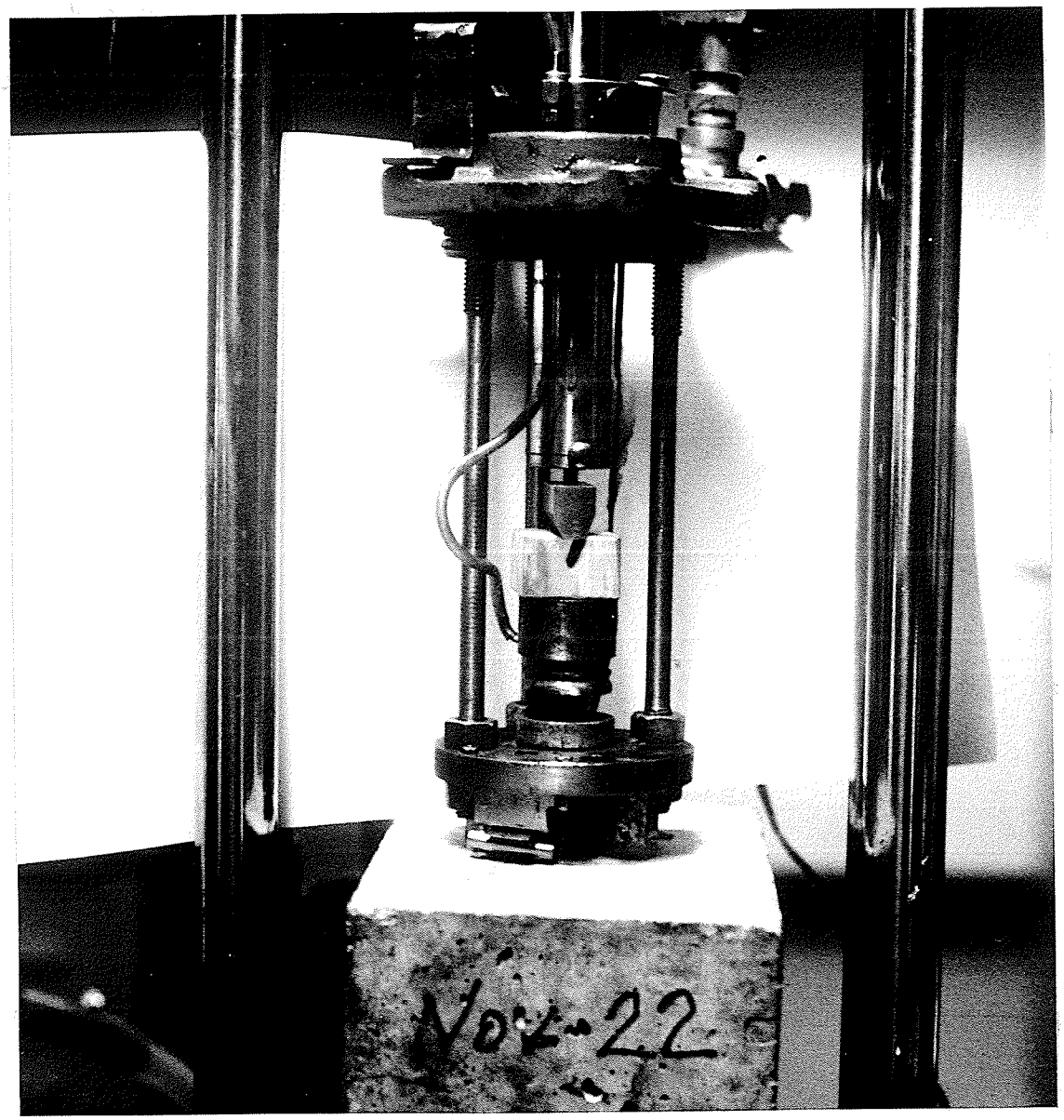

A Dummy Specimen is shown.
No Membrane was used.

Fig. 4.4 Fracture Toughness Tests Set Up Photograph
Photographed by D. Kuss

The braille/wedge was adjusted until it was just touching the metal shims on the top of the specimen assembly. The rod position was then secured using the bolt in the collar.

The load cell and rod assembly were then lifted into the confining pressure vessel. The vessel was then bolted shut and lifted onto the testing machine.

The recording devices were turned on. The machine was adjusted so that there was as little slack in the system as possible, and the DCDT was set to go. The confining pressure pump was switched on.

The braille was then forced downward relative to the specimen. The resulting load and displacement signals were recorded on an X-Y recorder. These signals as well as pressure and time signals were recorded on the video tape. When the signal output indicated that the specimen had crushed, or the braille had reached the platen, the experiment was terminated.

The pump was turned off and the kit disassembled. Notes were taken of the configuration of the crack and the general condition of the specimen.

In cases where there had been no response to loading the specimen came out of the membrane as an almost liquid pulp. This outcome was attributed to the fact that the specimen had thawed out.

Where there had been a significant load the specimen was recovered either in two halves, or split almost through.

The specimens were then tested for density either by cutting a rectangular solid or by measuring the amount of water that the specimen's remains displaced and weighing. This was done after testing because either of these measurement techniques performed prior to testing would have caused structural damage to the specimen and would have made the subsequent test invalid.

Chapter 5

Results and Discussion I

5.1) Results of the Tensile Strength Measurements

The measurements were conducted with the top of the breather tube connected to a length of Tygon tubing. In all cases where there was no leakage a stream of small bubbles could be seen going up the water column in this tube. Leakage, shown by green confining fluid, was tolerated, provided that the flow did not separate from the horizontal end of the tube.

Each test yielded an X-Y plot and a video record of the LED voltmeters.

Measured data were recorded and plotted. The records of the successful tests are shown in figures that form section A.II.1.

At the beginning of each test the specimen was under a uniform 2.1 MPa compressive stress in all directions. The value of Young's modulus in compression (E_c) was determined during the unloading of the specimen to a stress free state.

As can be seen in Figure A.II.4 readings collected at no applied load represent an initial stress of -2.1 MPa, as the load reached a state in which the initial compressive stress imposed on the specimen by the confining pressure was reduced to zero. A distinct bi-linear stress variation was observed (and is shown to be the Ø stress, Ø strain point). Tensile stress in the specimen then increased with further increases in tensile load.

The evaluation of the ratio of compressive to tensile Young's moduli of oil sands, i.e. E_C/E_T was done by extrapolating both of the two lines from the point of bi-linearity and forming two right triangles with one common side, and then measuring the relative height of the side opposite the two angles.

The tensile strength was found by measuring the value of the applied load value at the highest point relative to the point of bi-linearity and dividing by the cross-sectional area of the specimen. The results are summarized in Table 5.1 below.

Table 5.1 Tensile Properties Summary Table

Test #	Date	£ (Compression) / £ (Tension)	σ(Ultimate Tension) kPa
1	30/8/85	2.6	200
2	19/9/85	2.4	266
3	10/3/86	3.0	177
4	13/3/86*	2.7	227
5	14/3/86*	2.5	220
6	15/3/86	2.1	192
Arithmetic Mean		2.55	214
Engineering Values		2.5	225 2 ¼ x 10^5 Pa

* Graphic Results Only.

The specimens tended to break near the top, and not far from the glued surface. One exception was specimen Number 6 which had a small stone in it. This specimen broke near the upper surface of the stone.

Of the six tests conducted two showed the 'classic' cap and cone failure pattern that was found at the failure plane. Such failure of a tensile specimen is common in brittle material like cast iron. Two others showed evidence of eccentricity in their failure surfaces. One failed on the small stone and the last failed in part because of an excessively deep breather hole. It was the one specimen on which a drill was used to clear the breather holes. In both tests showing cap and cone failure surfaces, the failure touched the end cap near at least one breather hole.

5.2) Discussion of Results of the Tensile Measurements

As can be seen from Table 5.1 the $\varepsilon_c/\varepsilon_t$ ratio varies between 2.0 and 3.0 with an average around 2.5. This indicates that there were two distinct phenomena being observed.

The failed specimens did not show significant necking. Only about a 1% decrease in diameter was found by measurement. There is adequate data in all cases to establish the ratio of Young's Moduli, (E_c/E_T) before failure takes place. The value of 225 kPa (2 ¼ x 10^5 Pa) tensile strength was chosen as a value suitable for engineering purposes.

All of the failures were close to the top end or other fracture starters. The causes for these failure patterns are: 1) the small amount of damage caused by the clearing of the breather tubes in the top washer (Figure 2.1, Item # 4), 2) the effect of the weight of the specimen (which represents a significant fraction of the total tensile strength), 3) the strain rate was such that only the upper part of the specimen was fully drained, thus in the lower part of the specimen the pore fluid added to the structural strength of the sand, 4) there may have been some eccentric loading that concentrated stress on one side resulting in a tearing of the specimen.The tensile strength measured by the author is higher than the 90 kPa measured by the group at the University of Alberta

The discrepancy between the University of Manitoba results and the University of Alberta [28] results may be attributed to: (i) the higher strain rates at the University of Manitoba (150 με/second vs. 10 με/second),(ii) the greater confining pressures at University of Manitoba (2100 versus 70 kPa), (iii) the effect of the different specimen geometry and volume (Bobbin vs. Strength), and (iv) the differences in the design of the load cells.

The much higher strain rates used in this research may also have significantly raised both tensile and compressive strength, as well as both Young's Moduli. While the tests conducted at the University of Alberta took around 4 hours to failure, the tests in this research took between two and five minutes. In discussions during the defense of this thesis it was concluded that interlocks between particles tend to come apart less easily when strained quickly. A higher degree of jamming up obviously would result in higher strengths. Au [29] suggests that the properties of oil sands found in the laboratory are consistently below those encountered in-situ.

The stress state found in a typical specimen at the University of Manitoba at failure is shown in Figure 5.2

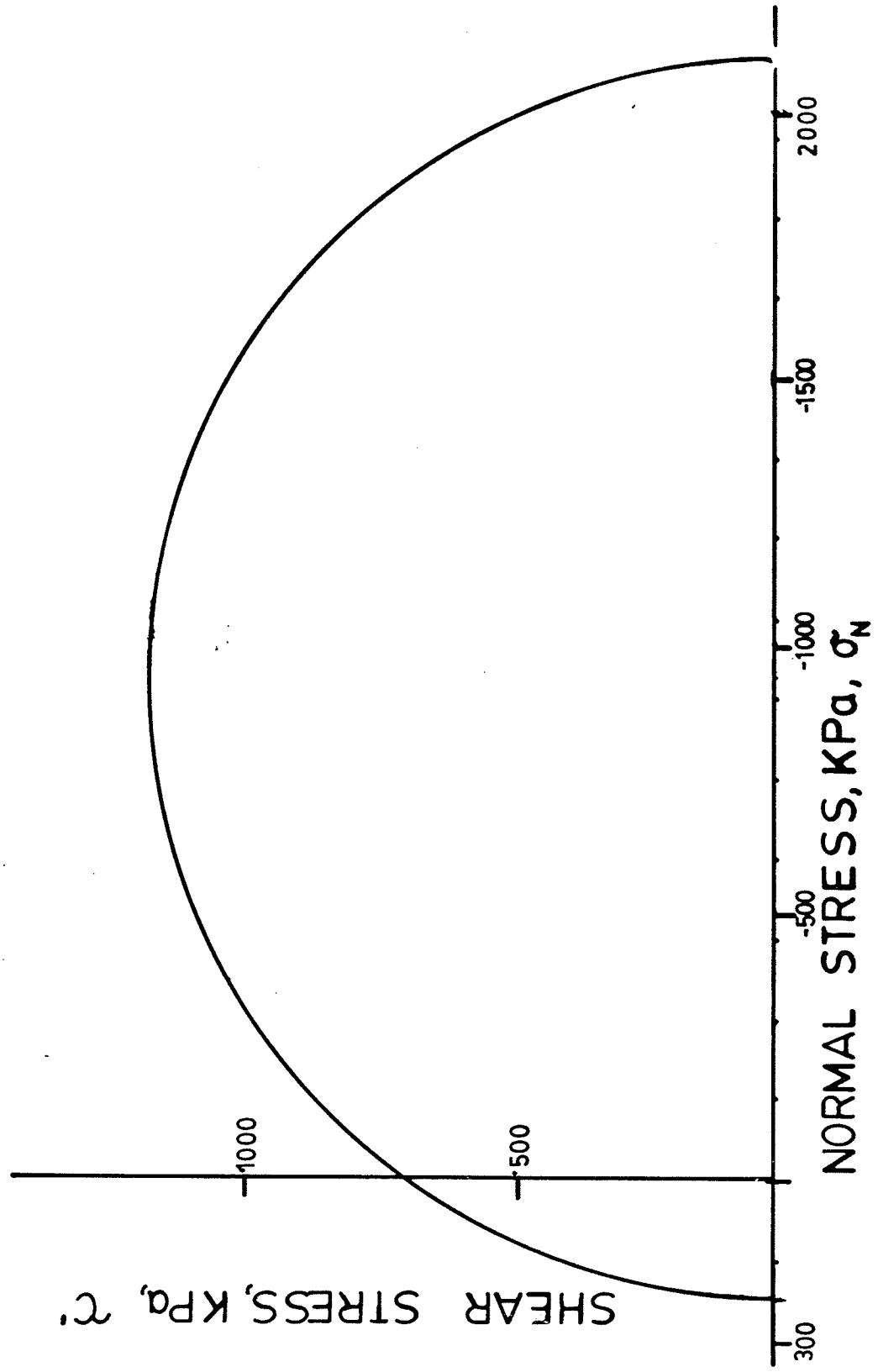

Fig. 5.2 Mohr Circle for a typical oil sand specimen tested at the University of Manitoba

5.3) Results of the Fracture Toughness Measurements

Because the DCDT had to be readjusted in each experiment, interpretation of the the plots from the X-Y plotter was very complicated. (See Figure A.II.8) Complete digital reconstruction was performed on only one test (1/13/1/86). Partial reconstruction was used promptly after each test to determine the failure load. These results are summarized in Table A.II.7.

The event 1/JAN/13/86 was converted into a full set of digitized data. This was done by hand. The raw data was input into a computer and processed to create a second set of data in the appropriate units eg.: Pa, N., mm.. It was then plotted using a special routine to produce Figure 5.3.

Two features of note on Fig. 5.3 are the two sharp drops in load at the time of the DCDT resets and is the two smaller drops that mark the "Load at Failure".

These two minor drops, at loads of 4.5 N., were chosen as the critical load (P_c) values for the fracture toughness calculations because they are the first indications of loss of load-carrying capacity in the specimen, that is, they are the first sign indicating that a crack was initiated at the tip of the notch and was starting to advance.

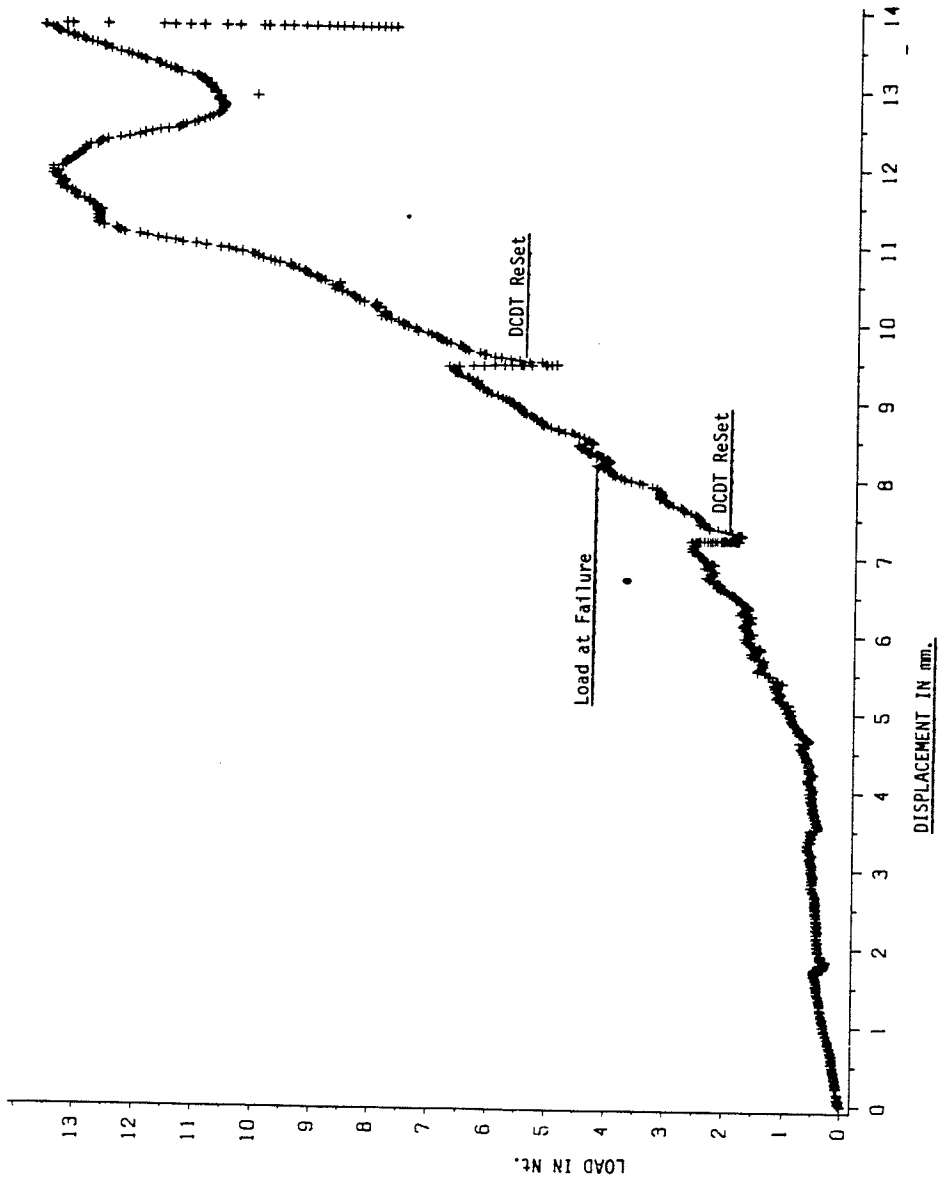

Fig. 5.3 Test # 5 Fracture Toughness Measurement (Jan 13, 1986)

The increases in loading thereafter may be the result of increased friction, change in crack geometry, or the onset of specimen crushing. The peak load of about 12.5 nt. was achieved in pushing the specimen apart. After this the load increased very quickly, indicating a pure crushing motion, suggestive of the bottom of the braille interacting with the specimen.

The data gathered can be summarized in the following Table 5.4

5.4) Discussion of the Results of the Fracture Toughness Measurements

The results from the five tests indicated that the fracture toughness of oil sands is close to 30 kPa$\sqrt{m}$.

The curious loss of force during DCDT reset was distressing. It reflected the slow plastic deformation in the oil sands. Another set of tests, with a longer reaching DCDT may be desirable. However, it is a marginal proposition as the other tests encountered less severe problems with DCDT reset.

The questions that arose from the differences between the experimental design and the hidden assumptions in ASTM-E-399 will be discussed in the next chapter.

Table 5.4 Summary of Results of the

Fracture Toughness Measurement

Test #	Load Vert. Nt.	Load* Horz. Nt.	A/W	ASTM Pa√m
1	3.95	11.41	0.486	26513
2	4.00	10.40	0.581	34921
3	4.50	11.98	0.596	31533
4	4.51	10.51	0.545	23348
5	4.52	10.26	0.560	25165
6	5.50	13.82	0.406	21527
Average	4.497	11.40	0.529	27168

* in horizontal direction used for all calculations

Chapter 6

Discussion II

The Compliance Function

6.1) Problem Definition

Fracture toughness, as used in this thesis, is a value which reflects a material's resistance to Mode I (opening or parting mode) fracture. It reflects the breaking of the individual mechanical joints between sand grains that occurs at the crack tip. It can thus be regarded as a material property.

Consequently it is reasonable that the fracture toughness, like the Young's moduli and the tensile strength of oil sands, will change with confining pressure and strain rate. It is likely that the compliance function, which relates the fracture toughness and the applied load, would also change with the specific circumstances of the experiment.

Because of the lack of tensile strength (σ(Ultimate Tensile)) and stiffness ($\pounds_T$) data for oil sands at confining pressures other than 2100 kPa, the author can only suspect that the tensile properties of oil sands are sensitive to confining pressure. It is therefore realistic to attempt to develop a crack advance criteria at any other confining pressure.

There were only three sets of data available for the tensile properties of oil sands, measured at confining pressures of 2100, 90, and 0 kPa. Of these only the data at 2100 kPa includes the ratio of tensile and compressive Young's moduli. Because of this it is impossible to develop more than one set of estimates for load at failure.

A set of estimates of P_c was prepared for typical ranges values of a/w and $\pounds_c/\pounds_T$ on the WLCT specimen used in experimentation (See Figure 4.3).

In conventional fracture toughness measurements of WLCT specimens made of metallic materials, the standard formula described in the ASTM-E-399-CT [23] can be used [30, 27].In the present research however, a new function had to be developed due to the unique characteristics of oil sands, and the presence of a confining pressure.

The function developed, which varies inversely as the load, is used only for the analysis of the failure of the specimens under the confining pressure used. The author cannot accept any liability for the use of these equations in any other application.

6.2) Finite Element Analysis of a WLCT Specimen

Finite element analysis of a WLCT specimen was done using the SandFrac Code, [31]. This package had been modified to accommodate both the different compressive and tensile Young's moduli observed in oil sands. This was achieved by putting the tensile value in the properties of an element stiffness matrix if the maximum stress in that element was positive.

A finite element mesh was developed to generate a data base from which the compliance function could be computed. This mesh could be easily modified to give various a/w ratios.

The numbered (Nodes & Elements) drawing of the master mesh is shown in Figures A.II.9 to A.II.11. An unnumbered drawing is shown as Figure 6.1

The master mesh is almost twice the size required to model any 'specimen' based on a 28 mm cube. To form a specimen with particular a/w ratio, the first and last regions were trimmed so that the total 'height' (w) was 28 mm. For convenience, each row of nodes in the 'top' and 'bottom' region was located about 1.4 mm or 5% of 28 mm. apart.

A force at 20° to the horizontal was applied to the top of the numerical specimen. A modified Sandfrac program was run to determine the maximum stress developed in every element. When the maximum tensile stress just reached 225 kPa the corresponding applied load was recorded as P_c for the "Specimen". See Table A.II.13 and A.II.14 for the values of P_c results.

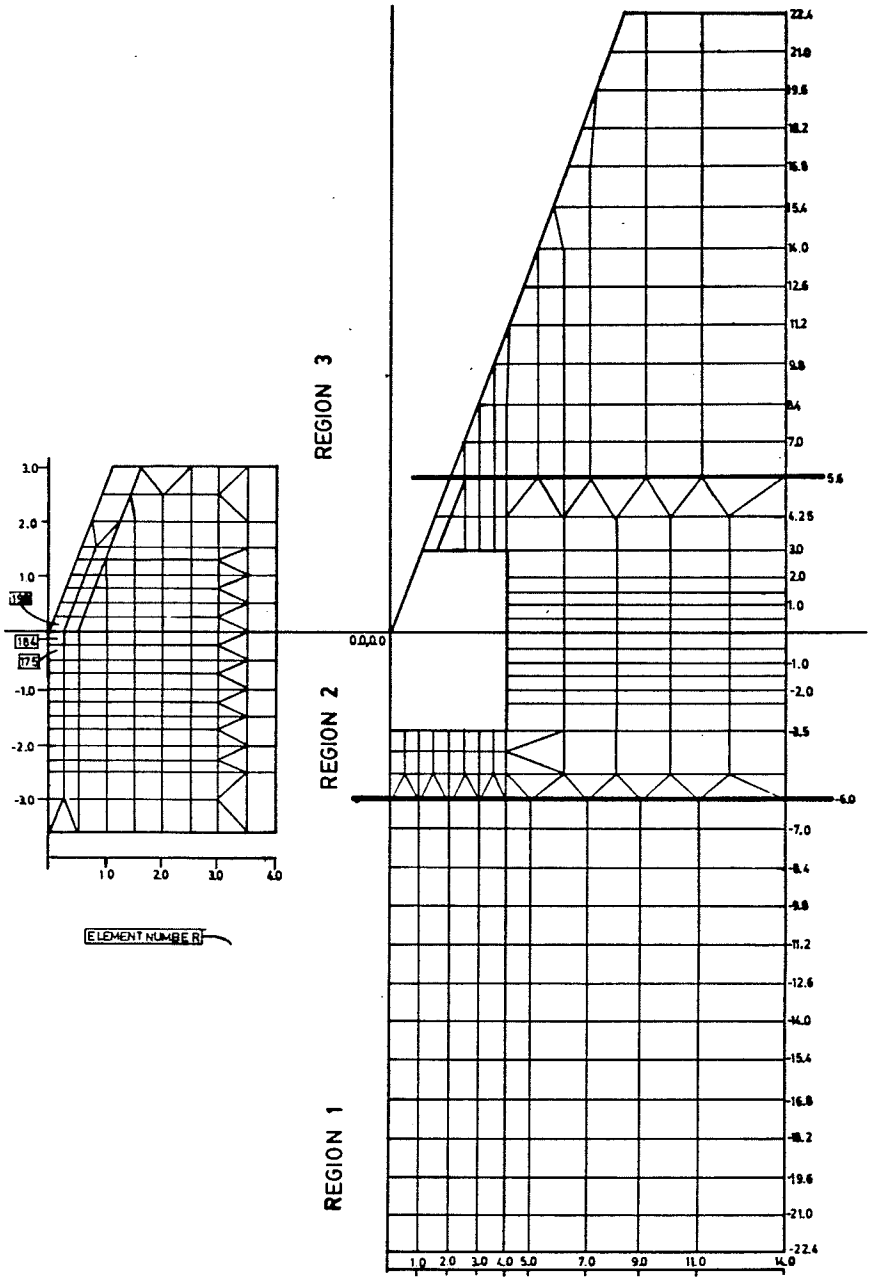

Scale 7.3728:1 Scale 3.6864:1

Fig. 6.1 Finite Element UnNumbered Master Mesh
With detail of mesh at critical point

When $\varepsilon_c/\varepsilon_T < 1.50$ then Element # 198 Fails
When $\varepsilon_c/\varepsilon_T > 1.50$ then Element # 184 Fails

The reason for this choice of failure criteria, rather than a more elaborate type of criterion such as a "J-Integral" [32] are:

1) Simplicity of Use. This study involves the determination of 85 P_c's. Each data point required a minimum of 5 computer runs, and some as many as 18, a complex analysis would have greatly slowed the work.

2) Quality of Input The extent of scatter in the results from experimentation, $\varepsilon_c/\varepsilon_T$ ranging between 2.00 and 3.00, and the variation of σ(Ultimate Tensile) by a similar factor.

3) The Handling of $\varepsilon_c/\varepsilon_T$ by the finite element program which caused massive numerical instability, and left a number of elements largely with the wrong stiffness.

For these reasons the author did not feel justified at the time in using anything but the simplest analysis. Hence the use of σ(Ultimate Tensile) in one element as the "crack advance" criterion.

The modification to accommodate ratios of other than 1.ØØ proved to be numerically unstable. The modification divided the stiffness matrix of those elements in tension by the $\varepsilon_C/\varepsilon_T$ ratio. The cause of the numeric instability was the elements around the border of the tensile zone which were only partly in tension.

The small tensile stress in the next iteration softened the element and resulted in the formerly tensile element adjacent going into compression, and the formerly compressive element opposite going into tension. As the iterations progressed the model became increasingly unstable.

A similar approach was adopted to permit this first examination of the validity of the ASTM-E-399-Compact Tension Specimen compliance function to the experimental design.

This approach did not allow the numeric instability to develop. It also did not modify the mesh to insure that all of each element was in either tension or compression. The result of this is that the tensile volume is too large, and the load at failure is probably underestimated.

This approach considered the specimen to be two materials, one with the tensile £ and the other (most of the specimen) with the compressive £. The first run of the model permitted the designation of selected elements as having the tensile moduli.

This procedure allowed the author to control which elements were "tensile" from one run to another, and through most of the a/w range tested. The record of the "tensile elements" is recorded in Table A.II.4.

No attempt was made to develop a program that controlled the numeric instability, as this represents a major programming effort of the same order of magnitude as the experimental part of this thesis.

6.3) Results

Calculations were done for meshes with a/w ratios that ranged from .2 to .8 at increments of .Ø5, with $£_C/£_T$ ratios of 1.Ø, 2.Ø, 2.5, and 3.Ø. This series of calculations, the results of which are listed in table A.II.13 gave a broad picture of the behavior of the load, and with it the compliance function.

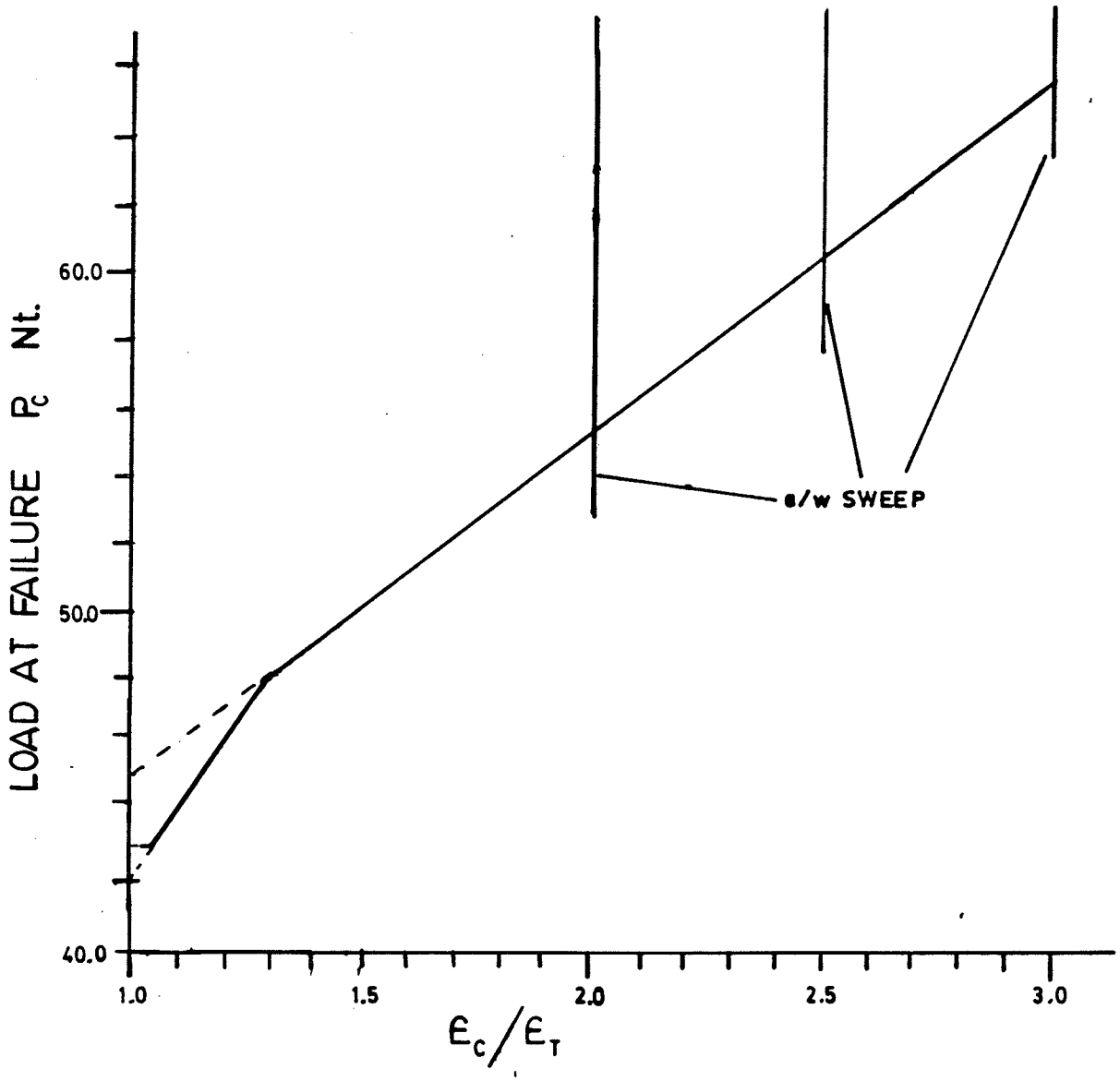

Fig. 6.2 Load @ a/w = 0.50 with $\varepsilon_c/\varepsilon_T$

Additional calculations were done with an a/w ratio of .5Ø and values of $\varepsilon_c/\varepsilon_T$ ratios varying between 1.Ø and 3.Ø by varying amounts up to a maximum step of Ø.Ø1. The results of these calculations are listed in table A.II.14. This gave a clear indication of the effect of varying $\varepsilon_c/\varepsilon_T$ ratio on the load and compliance function.

Table A.II.14 shows the effect that varying $\varepsilon_c/\varepsilon_T$ has on P_c. Figure 6.2 shows how $\varepsilon_c/\varepsilon_T$ affects P_c as it varies from 1.Ø to 3.Ø.

Above 1.5Ø the plot is linear. The author extended the plot of P_c to the $\varepsilon_c/\varepsilon_T = 1.ØØØ$ axis where it intercepted at 45.Ø45 (not 42.ØØØ N. found by the finite element analysis program). This was done because of the movement of the failing element, and the belief that there may be a significant change in behavior taking place extremely close to the point where $\varepsilon_c/\varepsilon_T = 1.ØØ$. Further work is needed to clarify the behavior of P_c near this point. This work should wait for the availability of a program that effectively allows for $\varepsilon_c/\varepsilon_T \geq 1.ØØ$.

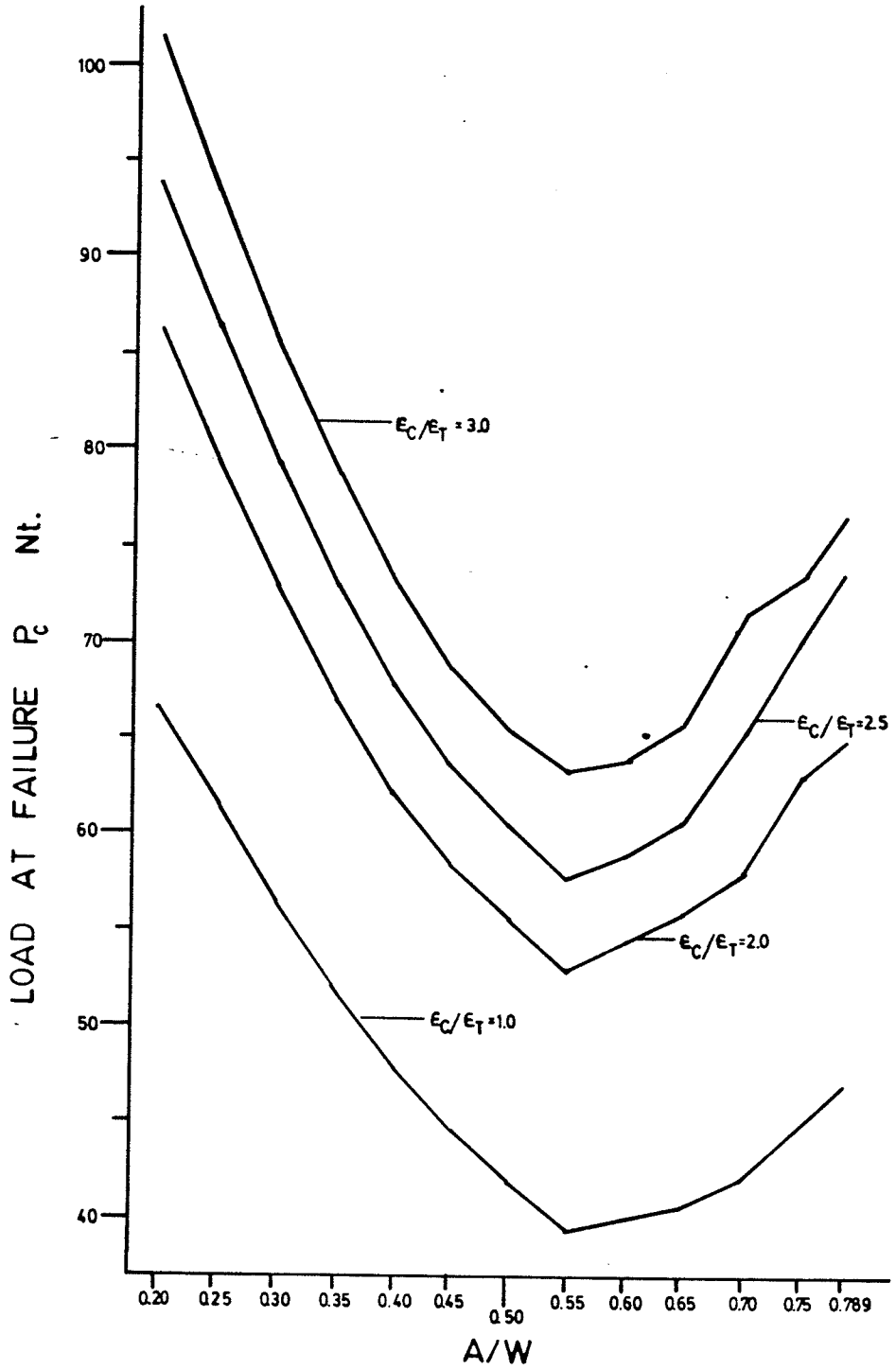

Fig. 6.3 Load vs. A/W Curve
with $\varepsilon_c/\varepsilon_T$ Ratios of 1.0, 2.0, 2.5, 3.0

The element undergoing failure changes from #184 to #198 at or near $\varepsilon_c/\varepsilon_T$=1.75 also. The author does not care to speculate whether this is a real phenomenon, or a numerical artifact.

Fig. 6.3 shows the load vs. the a/w. More points are desirable for the development of a compliance function which is valid throughout the range of $0.2 \leq a/w \leq 0.8$. This is particularly true of the region $0.4 \geq a/w \geq 0.6$. The author did however find an acceptable compliance function for the range $0.20 \leq a/w \leq 0.45$.

A compliance function can be approximately obtained by taking the inverse of the load as it varies with a/w. In this particular case the author chose to plot the values of $100*2\pi$/Load. The 2π comes from the surface tension/energy analysis of fracture first developed by A. A. Griffiths [re- referenced from 22-27]. The factor of 100 was added solely to give f(a/w) values similar to those used in the ASTM-E-399-CT compliance function.

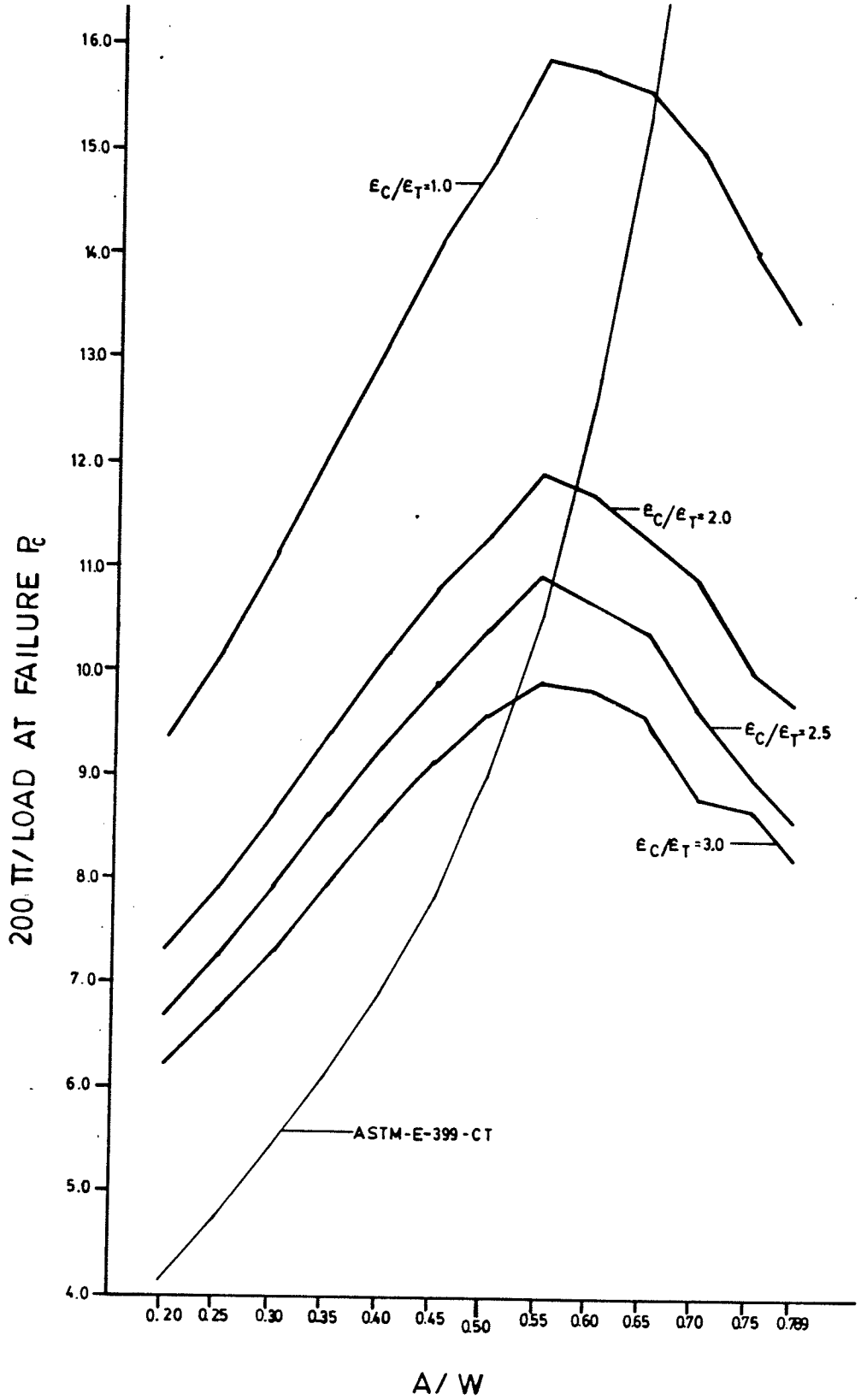

Fig. 6.4 100 * 2π/Load versus a/w and
$\varepsilon_C/\varepsilon_T$ ratios of 1.0, 2.0, 2.5, 3.0
With the ASTM-E-399-CT compliance function.

The plot of any group of these values between a/w = 0.20 - 0.45 is a straight line. Hence the relative compliance function is:

$f(a/w, \varepsilon_c/\varepsilon_T = 1.0, CP=2.1\ MPa) = 18.70 * (a/w) + 5.61$

$f(a/w, \varepsilon_c/\varepsilon_T = 2.0, CP=2.1\ MPa) = 12.63 * (a/w) + 4.74$

$f(a/w, \varepsilon_c/\varepsilon_T = 2.5, CP=2.1\ MPa) = 12.06 * (a/w) + 4.38$

$f(a/w, \varepsilon_c/\varepsilon_T = 3.0, CP=2.1\ MPa) = 10.64 * (a/w) + 4.21$

CP≡ Confining Pressure

These functions result in values that are consistent with those found in the study to within 1%.

6.4) Discussion of the Results of the Computer Modelling of the Compliance Function

These numerical results deviate significantly from the ASTM-E-399-CT compliance function. This suggests that the phenomenon under study is radically different from that discussed by ASTM-E-399! It is highly probable that these numerically derived compliance functions are also strongly affected by the confining pressure.

These difficulties suggest that the problem examined in this thesis is significantly beyond the developed theory of fracture mechanics. It is clear that a major research effort to better understand the implications of the effects of the $\varepsilon_C/\varepsilon_T$ ratio not equaling one and confining pressure on the fracture toughness of oil sands and similar materials is needed.

From Figure 6.5 it is also clear that something, very possibly a numeric artifact, occurs in the range $1.4 \leq \varepsilon_C/\varepsilon_T \leq 1.5$. It is in this range that the element undergoing failure shifts from 198 (above the notch), to element 184 (below the notch).

The author has extended the high range $\varepsilon_C/\varepsilon_T \geq 1.50$ to $\varepsilon_C/\varepsilon_T=1.00$. It joins at 13.66. ASTM evaluates this point as 9.02 (the horizontal axis), and the finite element program gave a result of 14.96.

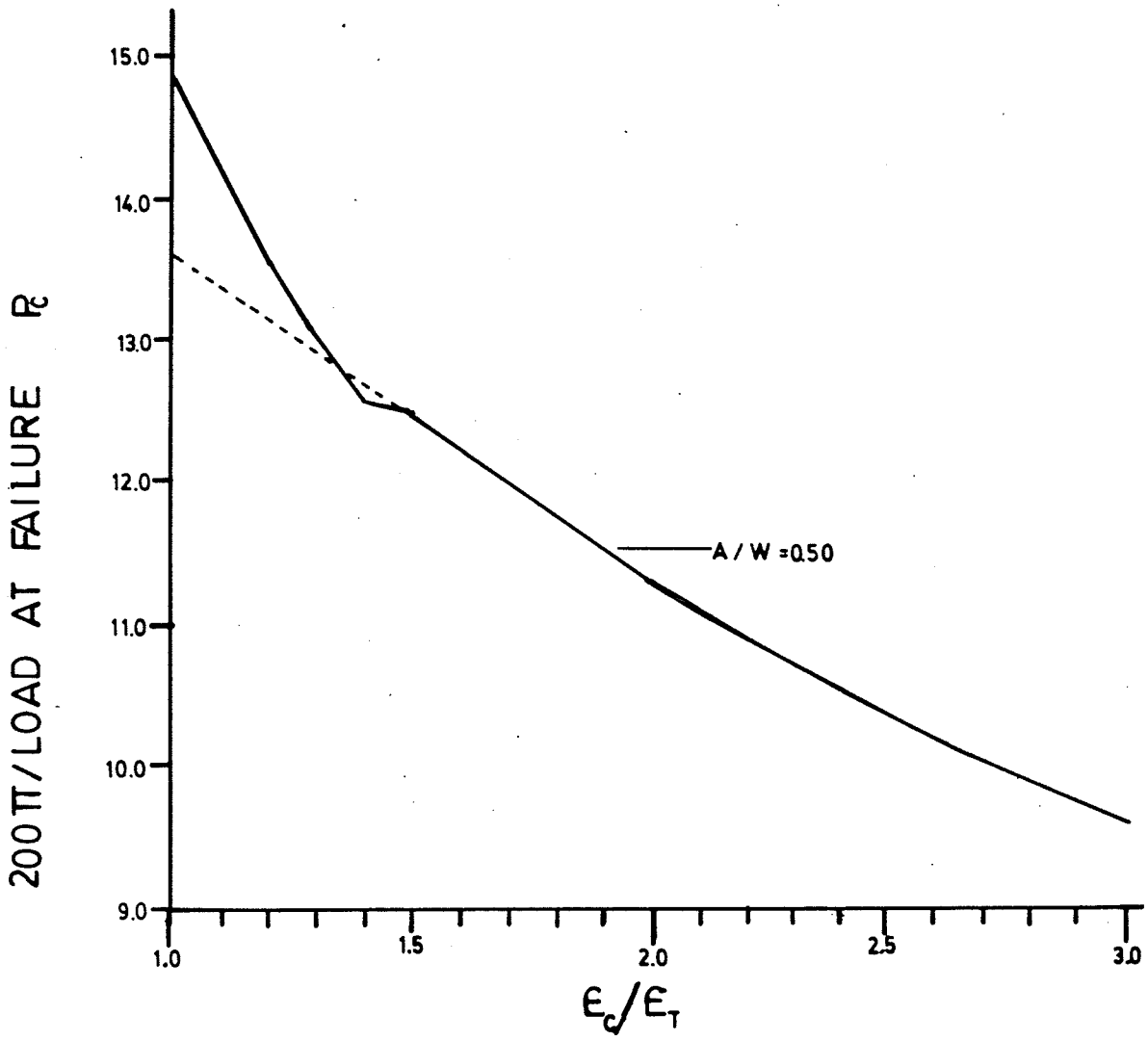

Fig. 6.5 100*(2*π/Load) versus $\varepsilon_c/\varepsilon_T$ and a/w ratio of 0.50

Given the results of the fracture testing with these new compliance functions Table 5.4 can be rewritten as Table 6.6. The values of $K_{IC\ THESIS}$ are potentially 1% of the average value of $K_{IC\ ASTM}$. The cause of the difference lies in both the phenomenon of fracture of oil sands and other geomaterials and the absence of an adequate theory describing it.

The much higher values of loading that are found in the finite element modelling (Table A.II.13 & 14) than are found in the experimental results (Table A.II.7) are possibly the consequence of the different local strain rates at the tensile point of failure. The rate of strain in the fracture toughness specimen was much lower than that in the tensile specimen that was used to establish the failure criteria for the finite element analysis of the fracture toughness of oil sands.

Table 6.6 Fracture Toughness Summary # 2 with the Compliance Function from this Thesis

Test #	Load* Horz. Nt.	A/W	Compliance** $\varepsilon_c/\varepsilon_T$= 2.5	K_{Ic} Thesis Pa$\sqrt{m}$	K_{Ic} ASTM Pa$\sqrt{m}$
1	11.41	0.486	10.22	29,280	26,513
2	10.40	0.581	11.36	31,303	34,921
3	11.98	0.596	11.54	27,125	31,533
4	10.51	0.545	10.94	22,833	23,348
5	10.26	0.560	11.12	23,750	25,165
6	13.86	0.406	9.26	26,961	21,527
Average Values:	11.40	0.529	1.757	26,559	27,168
Engineering Values				25,000	30,000
				2 ½	3 x 10^4

$$K_{Ic} = \frac{P_c * f(a/w, \varepsilon_c/\varepsilon_T=2.5)}{b\sqrt{w}}$$

$$= \frac{P_c * [12.06*(a/w)+4.38]}{b\sqrt{w}}$$

* In all applications only the horizontal load is used to calculate the value of K_{Ic}

** Taken from Figure 6.4 and by liner interpolation from Table A.II.15

CHAPTER 7

Conclusions & Recommendations

7.1) Conclusions

The most important conclusions that can be drawn from this research are as follows:

Under a confining pressure of 2.1 MPa, the oil sands have the following properties for engineering purposes:

Tensile Strength	225	kPa.
$\varepsilon_c/\varepsilon_t$ Ratio	2.5	
Fracture Toughness	30	kPa$\sqrt{m}$ (ASTM)

These values are expected to vary with confining pressure and strain rate.

The above value for $\varepsilon_c/\varepsilon_t$ ratio is the only available measured value for oil sands to the best of the author's knowledge.

The ASTM compliance function is not suitable for application in conditions where there is confining pressure and/or where $\varepsilon_c/\varepsilon_t$ Ratio is not equal to one (1.0). The load at failure is very sensitive to both strain rate and confining pressure and somewhat less sensitive to the $\varepsilon_c/\varepsilon_t$ ratio.

7.2) Further Research

More work will be required to directly extend the research carried out in this thesis to other confining pressures. Specifically the tensile strength and Young's modulus testing of oil sands under 1 MPa, 3 MPa, 4 MPa, and 5 MPa of confining pressure should be undertaken. These experiments must be conducted at a variety of controlled strain rates. Further, to link strength and stiffness to fracture toughness test results there should be an effort made to link strain rates at the notch tip to crack opening displacement rates.

Before further theoretical work can be carried out it will be necessary to develop a numerically stable, geometrically flexible element, finite element analysis program which accommodates $\dot{\varepsilon}_c/\dot{\varepsilon}_T$ ratios other than 1.00. The preparation of a finite element code that accommodates the $\dot{\varepsilon}_c/\dot{\varepsilon}_t$ ratio will be a very complex task that should be begun at once.

When such a code is in hand it will then be worthwhile doing a parametric study of a WLCT fracture, using a much larger "specimen" to define a four dimensional space in which the variables are critical load (P_c), a/w ratio, $\varepsilon_c/\varepsilon_T$ ratio, and confining pressure (σ_3). From this space it will be possible to develop more adequate formulae.

The development of an understanding of the effects of the $\varepsilon_c/\varepsilon_t$ ratio and confining pressure on the compliance function will require extensive testing on a number of materials with different $\varepsilon_c/\varepsilon_t$ ratios, each at a number of confining pressures. The effect of $\varepsilon_c/\varepsilon_t \rightarrow 1.000$ on the Mohr Circle must also be evaluated.

REFERENCES

1 Newton, John W., Asst. Mgr. Economics Dept.,
ERCB Submission to House of Commons:
Stand.Comm. on Energy, Mines, & Resources.
June 3, 1986

2 Dusseault, Maurice B.
Geotechnical Characteristics of Athabasca Oil Sands
Ph.D Thesis, U. of A. 1977.
Page 27.

3 Ibid: P 235

4 Ibid: P. 41, after Carrigy'67

5 Ibid; P. 9

6 Ibid

7 Ibid P. 142

8 Hsu, T.-R; Piziey, G.S.
Sandfrac Code for Computer Modeling of In Situ
Fracture of Oil Sands Formation
U. of Man.,Dept. of Mech. Eng., Report # 84-1-80,
July 23, 1984, pp. 124.

9 Hsu,T.-R.; Chen,G.G. ; Gong,Z.L.
A Technique for the Measurement of Dynamic
Mechanical Properties of Oil Sands
The Journal of Canadian Petroleum Tech., Vol. 24,
No. 3,June 1985 pp. 63 - 69

10 Plewis,H.; Scott, J.D.
Triaxial Testing of Syncrude Oil Sand Low Pressure
Triaxial Testing.
Private Communication paper to T.-R. Hsu,1985.
See Reference 18

11 Dusseault, op. cit., Page 202-203

12 Siever, R.
Petrology and Geochemistry of Silica Cementation
in some Pennsylvania Sandstones
Silica in Sediments. Soc. Econ. Paleontologists and
Min. Spec. Pub. No. 7, pp. 55-79.

13 Dapples, E.C.
The Behavior of Silica in Diagenesis.
Silica in Sediments. Soc. Econ. Paleontologists and
Min. Spec. Pub. No. 7, pp. 36-54

14 Dusseault, reference # 1, Page 227

15 Ibid p. 235

16 Plewis, H; Scott, J.D.; Hsu, T.-R.
Dynamic Fracture of Oil Sands
HO & OS Tech. Symp. Proc, U.of.C., Feb. 1985

17 Hsu, T.-R.; Scott, J.D.;
Personal Communication.

18 Plewis, H.
Undrained Properties of McMurray
Formation Oil Sands
M. Sc., U. of A., 1987.

19 Hsu, T.-R.; Scott, J.D.
Measurement of the Thermophysical and Mechanical
Properties of Oil Sands
Department of Energy / Western Research Institute
Tar sands Symposium, Jackson's Hole, Wyoming,
July 1-6, 1986

20 Broek, David
Elementary Engineering Fracture Mechanics
Noordhoff International Publishing, Leyden,1974, pp.408

A note in text shows a 3 rd Ed. pub. in 1982 not seen.

21 Dawes, M.G.: G.G. Chell ed.
Developments in Fracture Mechanics --1
Applied Science Publishers Ltd., Ripple Rd.,
Barking, Essex, England, pp. 1-28.

22 American Society for Testing Materials
Standard Test Method for Plane-Strain Fracture
Toughness of Metallic Materials.
Specification E-399, 1983.

23 Gross, B.; Srawley, J.E.,
Stress-Intensity Factors by Boundary Collocation
for Single-Edge-Notch Specimens Subject to
Splitting Forces
NASA Tech Note # TN D-3295,NASA Feb. 1966.

24 Srawley, J.E.; Jones, M.H.; Gross, B.,
Experimental Determination of the Dependence of Crack Extension Force on Crack Length for a Single-Edge-Notch Tension Specimen.
NASA Tech Note # TN D-2396,NASA Aug. 1964.

25 Srawley, J.E.; Gross, B.,
Stress Intensity Factors for Cracked Line Loaded Edge Crack Specimens
NASA Tech Note # TN D-2396,NASA Aug. 1964.

26 Tobler, R.L; Carpenter, W.G.
A Numerical and Experimental Verification of Compliance Functions for Compact Specimens.
Engin. Fract. Mech.; Vol. 21, No. 3; pp. 563-571, Pergamon Press, 1985.

27 Klepaczko, J.R.; Bassim, M.N.; Hsu, T.-R.
Fracture Toughness of Coal Under Quasi-Static and Impact Loading.
Eng. Fract. Mech.; Vol. 19, No. 2, pp. 305-316, 1984

28 Op. Cit #16

29 Au,K.-S.
The Strength-Deformation Properties of Alberta Oil Sands
Draft M. Eng. Practicum, U. of Alta. April, 1984.

30 Hsu, T.-R.
A comment on previous draft of this thesis.

31 Hsu, T.-R.; Piziey, G.S.
Sandfrac Code for Computer Modelling of In-situ Fracture of Oil Sand Formations.
U. Of M., Dept. of Mech. Eng. Report #84-1-80, July 23, 1984. pp 124.

32 Hsu, T.-R.;Chen,G.G.;Gong,Z.L.;Sun,N.S.
On Thermofracture Behavior of Leaking Thin Wall Pipes
Int. J. Pres. Ves. & Piping 24(1986) 269-281

Appendix I

Membrane Fabrication

Initial attempts were made with existing commercially available membranes to achieve a water tight seal around a WLCT specimen. The results were not satisfactory as the membranes were not very flexible, and they leaked.

A series of film packaging experiments, both in a loose fit and tight shrink fit, were tried with similar disappointing results.

Two gallons (US) of the liquid latex used in the manufacturing of the commercially available membranes was then acquired. The manufacturer indicated that ordinary dish washing liquid would serve as a parting liquid. For this application a quantity of Palmolive liquid was acquired.

A metal mandrel was fabricated in the shape of a 32 mm cube specimen. For the first attempt it was covered in dish washing liquid and then dipped. The latex ran off the mandrel before it set. A number of attempts were made using a variety of turning strategies to cause the liquid latex to flow back onto the mandrel.

A small amount of latex was put into a container and allowed to partly cure. When thickened it was applied to the mandrel using a palate knife. The results were lumpy, stiff, but did hold water.

The preliminary test of a completed membrane was to fill it with water and observe it on a dry surface for 5 minutes. It was taken as sound if there was no stain.

A number of other attempts were made using slightly thinned mixtures of the thickened latex. The results were not uniform, frequently very thick, and didn't always hold water.

On one thinning a rather large amount of water was added resulting in a very thin mixture. It was decided to apply this as a wash over a thin layer of parting compound. The result was a surface to which latex would adhere, and that formed part of the membrane. A number of subsequent coats were applied.

The use of a brush, and the availability of both thick and thin material allowed the development of a two-coat system. The first coat was applied to a damp mandrel with a thinned latex.

The second coat went over the first, with thick latex. This coat was worked with the brush until it was almost set. The results were repeatable, however there was a system of brush marks all over the membrane and the membrane was still too thick.

The size of the specimen was changed at this point in the process. It was therefore decided to make new mandrels. These were made out of wood, and covered with a layer of epoxy glue to give them a smooth uniform outside surface finish. They also had a base which measured 38 mm dia. and were 30-35 mm tall.

These mandrels were fabricated with a notch form with a side height that was deliberately larger than the specimen's expected geometry. This allowed extra space for the material to move during crack advance, and also provided easier mounting of the specimen.

Further attempts were made to get uniform membranes by the painting process using these mandrels.

It was then decided to attempt to reduce the effect of the parting compound by thinning it with water and then allowing the coating to dry overnight. This resulted in a very easy application of the first coat that was very uniform. The results of the first series of attempts using various consistencies of latex were generally too thick. They were however otherwise satisfactory.

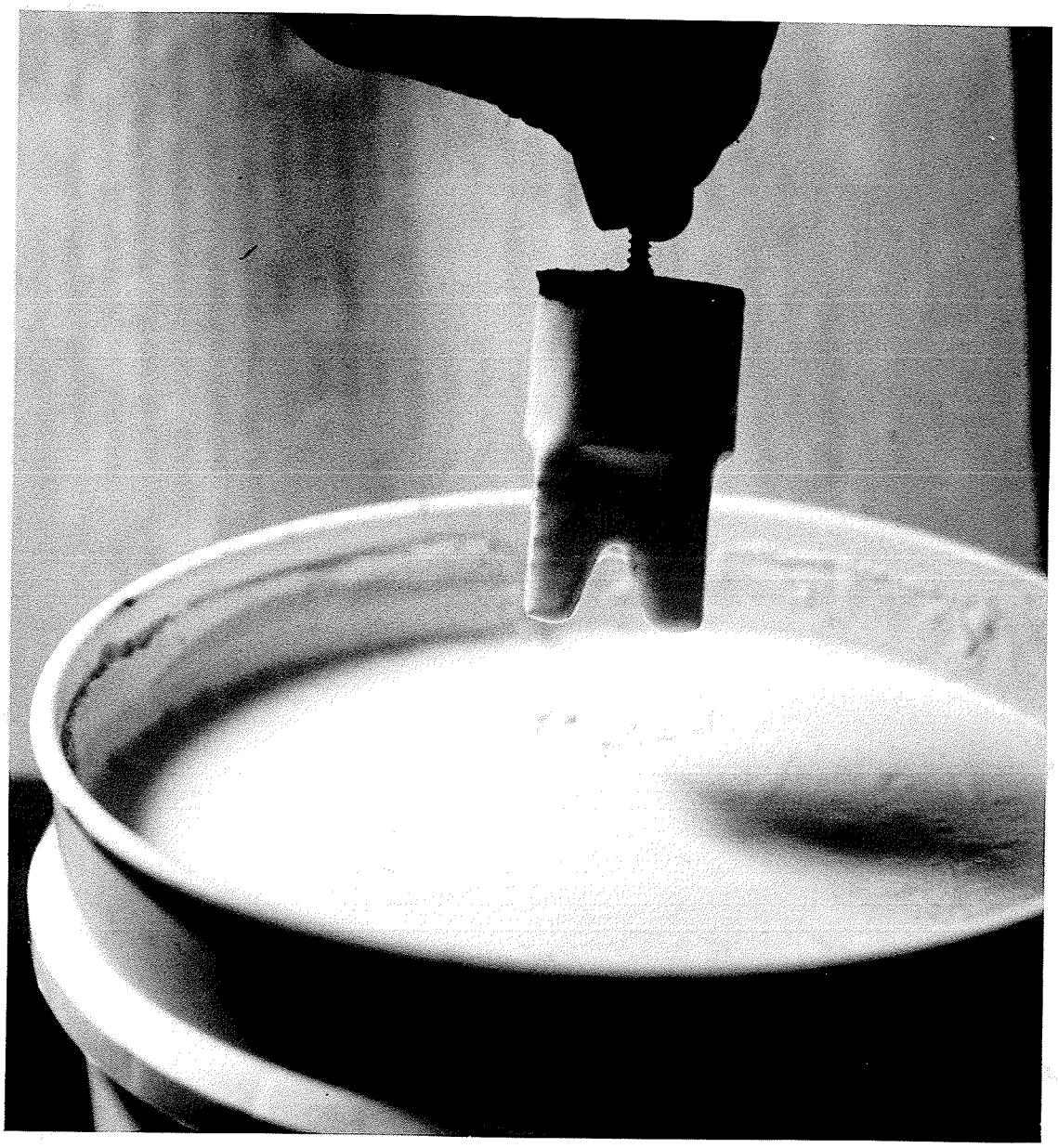

Fig. A.I.1 The Mandrel Is Dipped and Spun
Photographed by D. Kuss

A trial was made to apply the remains of the original material onto a dry mandrel. The result was lumpy and had drips on the bottom, which could be simply cut off.

The final procedure consisted of:

1: Coating the mandrel in a 50/50 mixture of dish washing liquid and water using a paint brush, followed by the removal of any excess liquid.

2: Drying overnight. This was done by suspending the mandrel upside down to ensure a good parting on the complex specimen portion.

3: Dipping into latex. This was done in such a manner so as to reduce the probability of the formation of bubbles.

4: Spinning and shaking the mandrel to remove any excess material that would form droplets on the top of the membrane that would not fall off. Care was taken to ensure that the tip of the notch was as well wetted and drained as possible.

5: Being sure to break any bubbles that might form from insertion or afterwards. These, if left in, the liquid would form weak spots and leak. This was particularly important in the tip of the notch. This was done with the tip of a palette knife.

6: When no longer dripping, set the mandrel upright to allow latex to cure.

7: Coat the sharp edges of the specimen portion with additional latex to reinforce these surfaces. This was done on the exterior right angles only. There was no reinforcing of the notch tip zone.

8: The second partial layer was allowed to cure.

9: Beginning at the bottom a thin palette knife was inserted under the latex. Water was injected into the space created and a little more force applied to lift off the membrane. When the space between the mandrel and the membrane had received as much water as it could conveniently hold the palette knife was worked gingerly around the base of the mandrel in the space between the membrane and the mandrel.

10: The palette knife was then advanced up the sides and ends of the specimen portion. Water was added to the space as needed. When the knife had passed below the rest of the membrane, and if there were no apparent weak spots, the edges of the notch would be lifted. If weak spots became apparent or the blunt ended knife came through the top of the specimen section, additional latex would be applied.

11: The membrane was grasped on the specimen section and slowly pulled off the mandrel without reversing it.

12: If the tops seemed too thin a small amount of latex could be poured in to reinforce the top surfaces of the specimen portion. As these areas were not expected to experience any relative motion this would not affect the result.

13: The membrane was coated inside and out with parting compound to prevent self adhesion during storage. A number of early thin membranes had become inseparable lumps of latex while lying in the laboratory.

14: Before use any droplets at the bottom were cut off, and the membrane washed, dryed overnight and the shims applied. See Chapter 4.2

Fig. A.I.2 Edging the Membrane Photo
Photographed by D. Kuss

APPENDIX II
EXPERIMENTAL DATA

A.II.1) Tensile Data

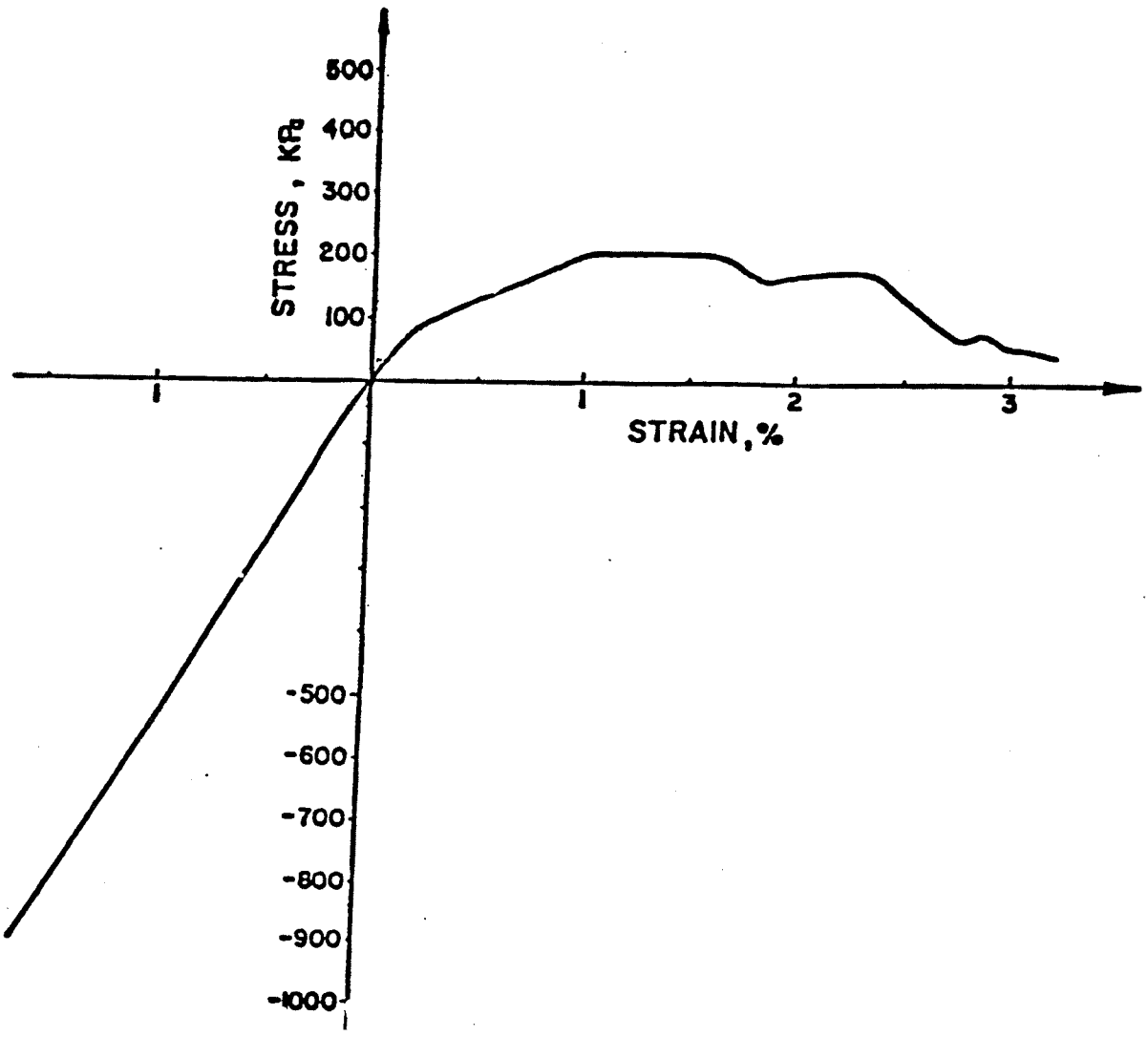

Fig. A.II.1 August 29, 1985 (01/29/08/85)

Diameter: 31.48 mm
Length: 64.25 mm
Confining Pressure
± 1% ε

$\varepsilon_c/\varepsilon_t$ = 2.64
$\sigma_{ult\ ten}$ =200 KPa
= 2.1 MPa
├ 100 kPa σ

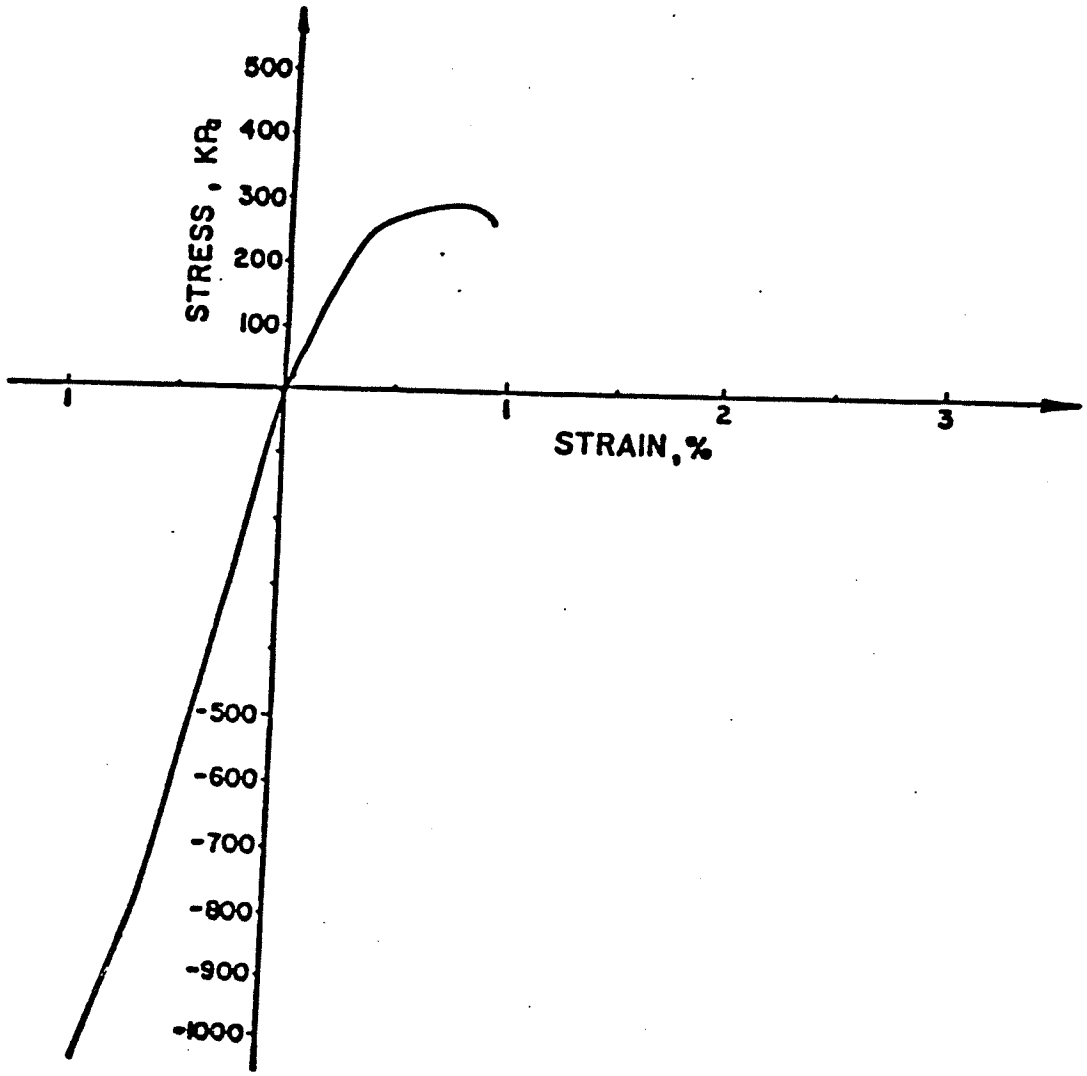

Fig. A.II.2 September 9, 1985 (01/09/09/85)

Diameter: 30.95 mm
Length: 62.00 mm
Confining Pressure
⊥ 1% ε

$\varepsilon_c/\varepsilon_t$ = 2.41
$\sigma_{ult\ ten}$ =266 KPa
= 2.1 MPa
├ 100 kPa σ

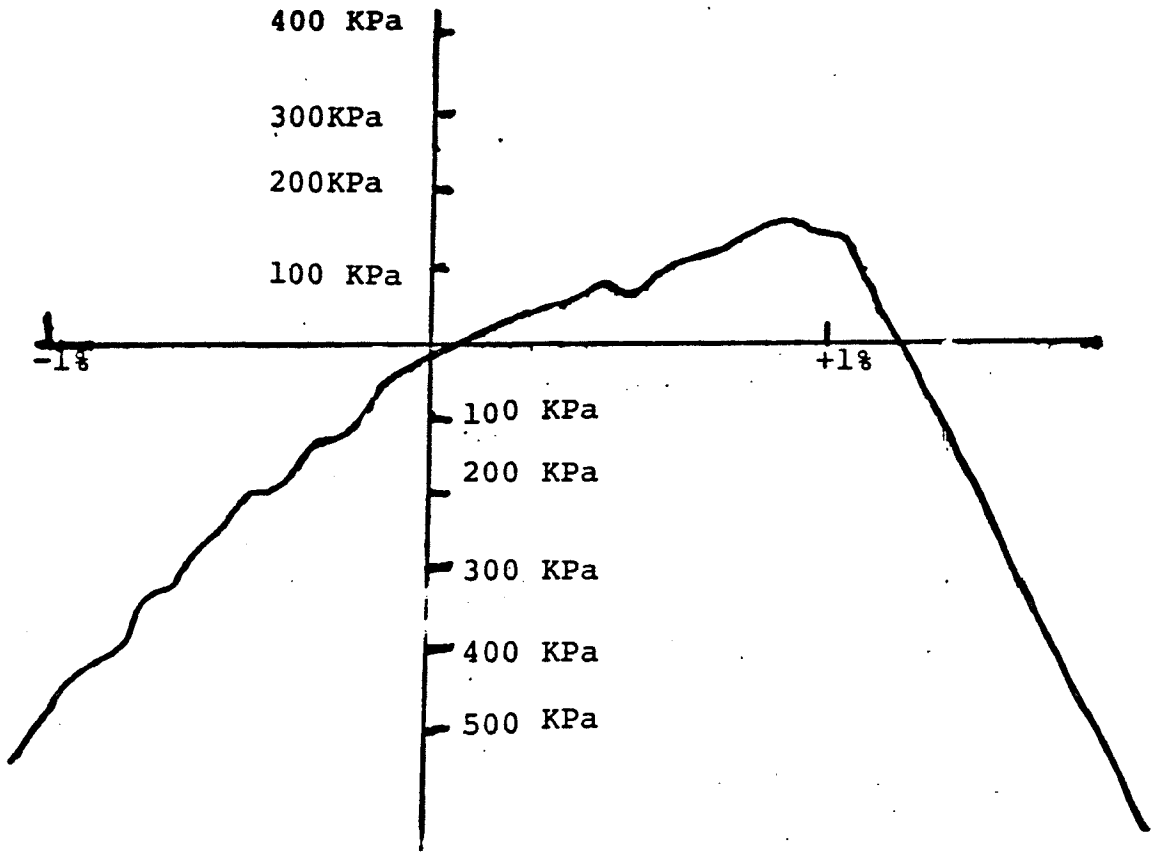

Fig. A.II.3 March 10, 1986 (01/10/03/86)

Diameter: 31.22 mm
Length: 44.48 mm
Confining Pressure
⊥ 1% ε

E_c/E_t = 3.0
$\sigma_{ult\ ten}$ =177 KPa
= 2.1 MPa
├ 100 kPa σ

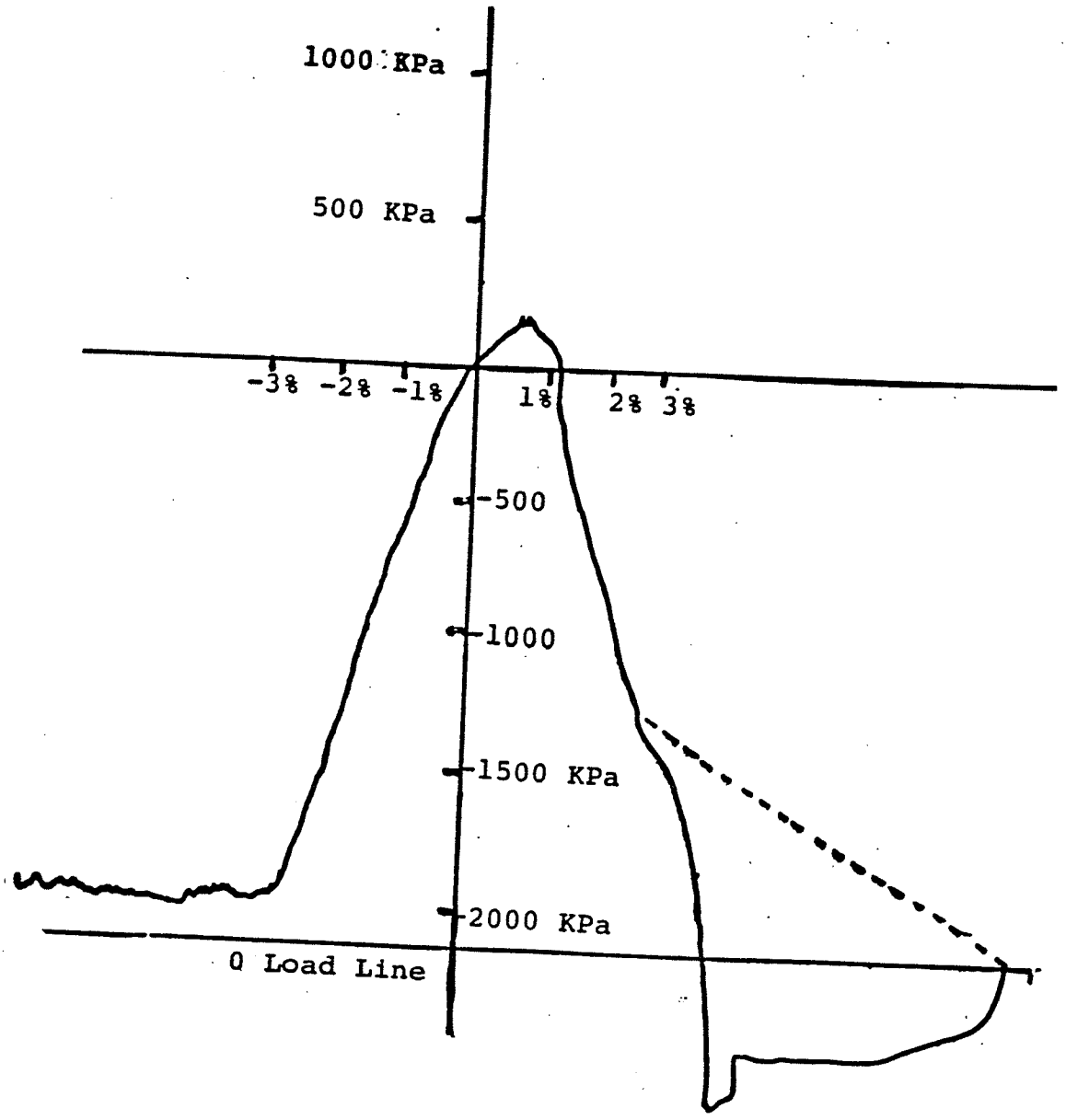

Fig. A.II.4 March 13, 1986 (01/13/03/86)

Diameter: 31.31 mm
Length: 56.24 mm
Confining Pressure
⊥ 1% ε

$\varepsilon_c/\varepsilon_t$ = 2.7
$\sigma_{ult\ ten}$ =227 KPa
= 2.1 MPa
⊢ 500 kPa σ

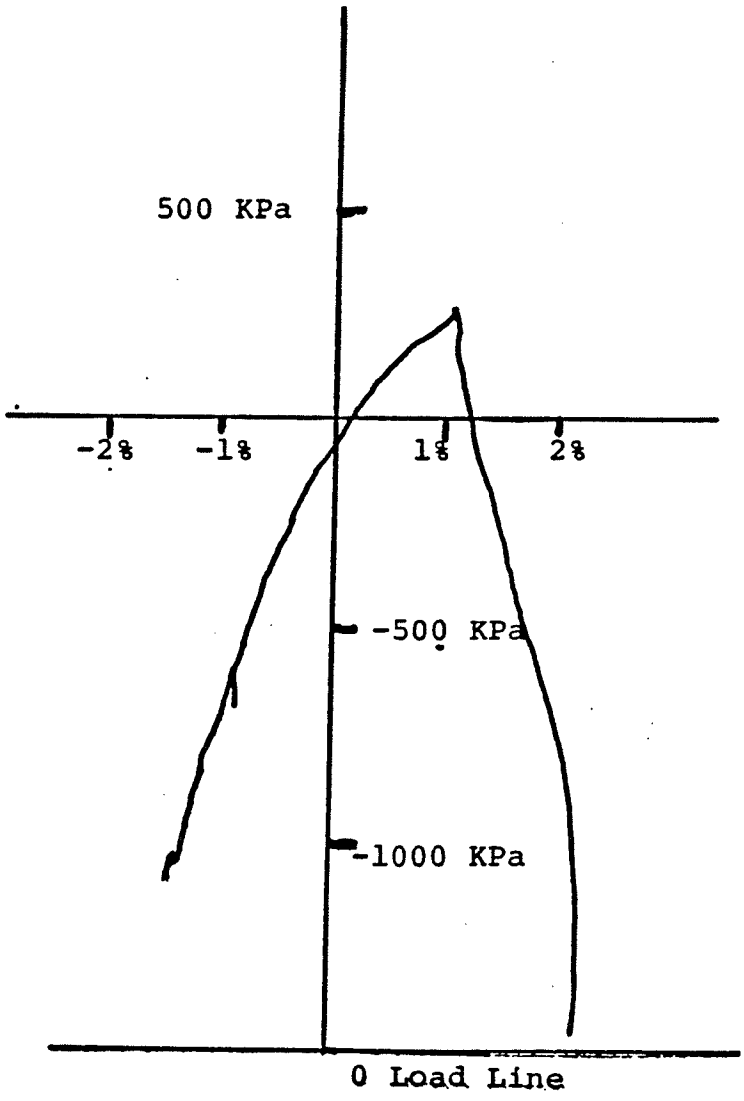

Fig. A.II.5 March 14, 1986 (Ø1/14/Ø3/86)

Diameter: 31.32 mm
Length: 56.24 mm
Confining Pressure
⊥ 1% ε

$\varepsilon_c/\varepsilon_t$ = 2.5
$\sigma_{ult\ ten}$ =22Ø KPa
= 2.1 MPa
├ 5ØØ kPa σ

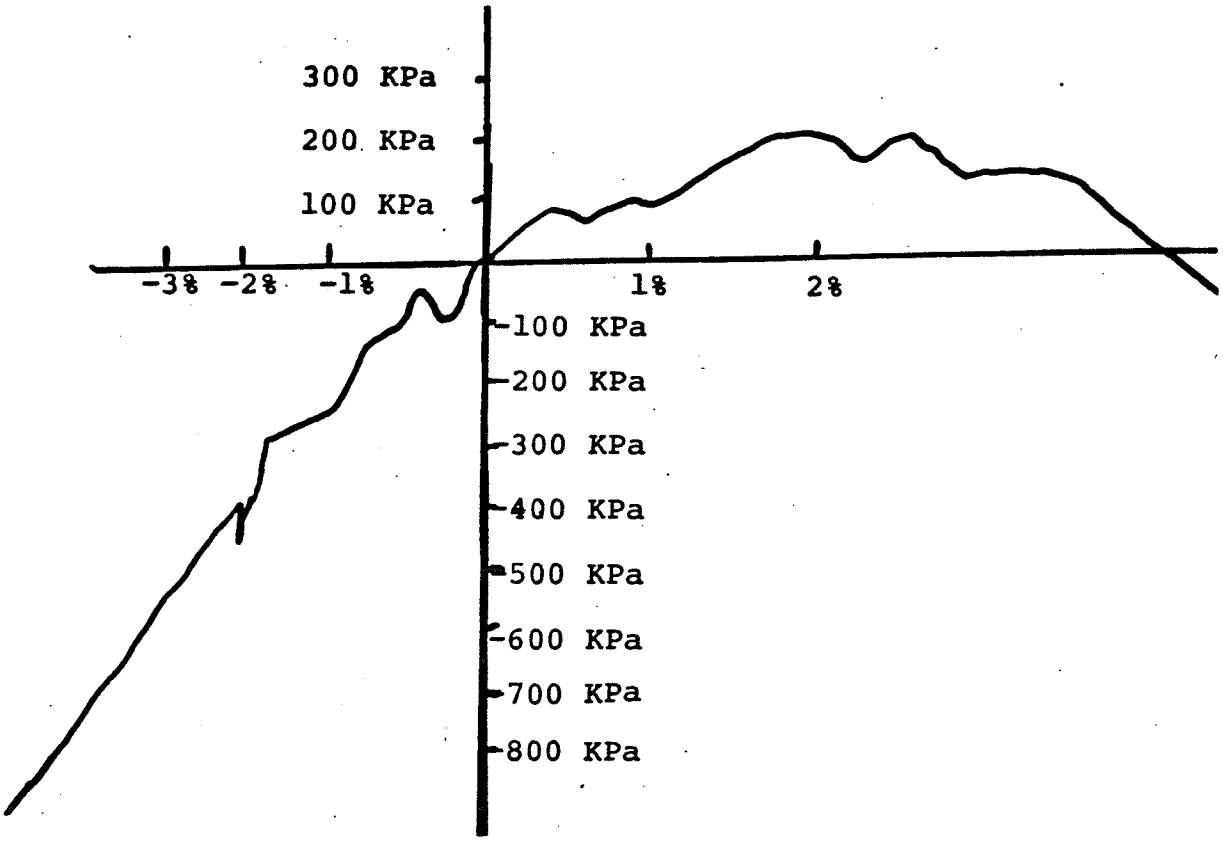

Fig. A.II.6 March 15, 1986 (01/15/03/86)

Diameter: 31.57
Length: 70.18
Confining Pressure
⊥ 1% ε

$\varepsilon_c/\varepsilon_t$ = 2.1
$\sigma_{ult\ ten}$ =192 KPa
= 2.1 MPa
⊢ 100 kPa σ

A.II.2) Fracture Data

Fracture Toughness Data

Test #	1	2	3	4	5	6
Date	Dec 23	Jan 6	Jan 6	Jan 7	Jan 13	Jan 24
	Raw Data In Inches * 1000					
Length # 1	1040	1210	1010	1150	1127	1185
Length # 2	1029	1127	1017	1170	1152	1215
Length # 3	1027	1195	1047	1191	1147	1205
Avg Length	1032	1177	1025	1170	1142	1202
Hight # 1	1060	1112	1193	1148	1062	1175
Hight # 2	1036	1059	1197	1156	1082	1152
Hight # 3	1001	1025	1170	1157	1098	1133
Hight # 4	1024	1050	1205	1146	1109	1107
Hight # 5	1065	1057	1207	1239	1100	1111
Hight # 6	1072	1055	1230	1254	1086	1120
Avg Hight	1043	1060	1200	1183	1090	1133
Thick' # 1	986	901	1210	1133	1132	1052
Thick' # 2	972	916	1150	1143	1140	1095
Thick' # 3	952	900	1136	1153	1140	1124
Avg Thick'	970	906	1165	1143	1137	1090
Web #1	510	417	472	551	472	693
Web # 2	562	472	472	525	486	653
Avg. Web	536	445	472	538	479	673
Avg "a"	507	615	728	645	611	460
Gap # 1	348	455	522	552	551	349
Gap # 2	336	465	535	559	541	356
Gap # 3	369	500	510	551	521	405
Avg Gap	351	473	522	554	538	370
Radians						
Angle #1	0.6322	0.6602	0.6894	0.8674	0.8441	0.7429
Angle #2	0.6806	0.7770	0.7043	0.7794	0.8397	0.7192
Avg. Angle	0.6564	0.7186	0.6968	0.8234	0.8419	0.7310
Angle Avg	0.6665	0.7345	0.6886	0.8109	0.8296	0.7648
Degrees						
Angle #1	36.22	37.83	39.50	49.70	48.37	42.56
Angle #2	38.99	44.52	40.35	44.66	48.11	41.20
Avg. Angle	37.61	41.17	39.92	47.18	48.24	41.88
Angle Avg	38.19	42.09	39.45	46.46	47.53	43.82

Fig. A.II.7a Fracture Data Summary: Raw Data
As Measured Specimen Geometries
in 1000th's of an inch

Processed Data

Test #	1	2	3	4	5	6
Date	Dec 23	Jan 6	Jan 6	Jan 7	Jan 13	Jan 24
			Raw Data In MilliMeters			
Length # 1	26.42	30.73	25.65	29.21	28.63	30.10
Length # 2	26.14	28.63	25.83	29.72	29.26	30.86
Length # 3	26.09	30.35	26.59	30.25	29.13	30.61
Avg Length	26.21	29.90	26.03	29.73	29.01	30.52
Hight # 1	26.92	28.24	30.30	29.16	26.97	29.85
Hight # 2	26.31	26.90	30.40	29.36	27.48	29.26
Hight # 3	25.43	26.04	29.72	29.39	27.89	28.78
Hight # 4	26.01	26.67	30.61	29.11	28.17	28.12
Hight # 5	27.05	26.85	30.66	31.47	27.94	28.22
Hight # 6	27.23	26.80	31.24	31.85	27.58	28.45
Avg Hight	26.49	26.92	30.49	30.06	27.67	28.78
Thick' # 1	25.04	22.89	30.73	28.78	28.75	26.72
Thick' # 2	24.69	23.27	29.21	29.03	28.96	27.81
Thick' # 3	24.18	22.86	28.85	29.29	28.96	28.55
Avg Thick'	24.64	23.00	29.60	29.03	28.89	27.69
AVG CUBE	25.96	26.68	29.15	29.72	28.31	28.94
Web #1	12.95	10.59	11.99	14.00	11.99	17.60
Web # 2	14.27	11.99	11.99	13.33	12.34	16.59
Avg. Web	13.61	11.29	11.99	13.67	12.17	17.09
Avg "a"	12.88	15.63	18.50	16.39	15.51	11.68
Gap # 1	8.84	11.56	13.26	14.02	14.00	8.86
Gap # 2	8.53	11.81	13.59	14.20	13.74	9.04
Gap # 3	9.37	12.70	12.95	14.00	13.23	10.29
Avg Gap	8.92	12.02	13.27	14.07	13.66	9.40
Varriances	RMS(X-XBAR, OR DELCLARED VALUE					
Length	0.1452	0.9173	0.4076	0.4252	0.2744	0.3168
Hight	0.6382	0.6610	0.6415	1.1442	0.3863	0.6094
Thickness	0.3544	0.1859	0.8153	0.2074	0.0958	0.7513
Gap	0.3464	0.4901	0.2593	0.0904	0.3168	0.6328
On Avg. mes.	0.7913	2.1982	1.6651	0.8149	0.6144	1.0169
On Cube 28mm	1.9368	2.4757	1.9406	1.6964	0.6707	1.3044
Overall varriance on cube			1.7642 mm			
E2 (28mm)	2.0514					
E3 (28 mm)	-1.4962					

Fig. A.II.7b Fracture Data Summary:Processed Data
Specimen Geometries in mm
Variance Study by specimen and against 28 mm cube
E2 = $\sqrt{}$sum($(x_i-28)(x_i-28)/(n-1)$)
E3 = $\sqrt[3]{}$sum($(x_i-28)(x_i-28)(x_i-28)/(n-2)$)

RESULTS

Test #	1	2	3	4	5	6
Date	Dec 23	Jan 6	Jan 6	Jan 7	Jan 13	Jan 24
Avg Length (L)	26.21	29.90	26.03	29.73	29.01	30.52
Avg Thick (B)	24.64	23.00	29.60	29.03	28.89	27.69
Avg Hight (W)mm	26.49	26.92	30.49	30.06	27.67	28.78
Avg Hight (W) M	0.0265	0.0269	0.0305	0.0301	0.0277	0.0288
Root Hight	0.1628	0.1641	0.1746	0.1734	0.1664	0.1696
a	12.88	15.63	18.50	16.39	15.51	11.68
a/w	0.4861	0.5805	0.6068	0.5454	0.5603	0.4060
Angle Rad	0.67	0.73	0.69	0.81	0.83	0.76
angle deg	38.19	42.09	39.45	46.46	47.53	43.82
Vertical Load	3.95	4.00	4.50	4.45	4.25	6.50
Horizontal Load	11.41	10.40	12.55	10.37	9.65	16.16
ASTM E 399 CT Compliance Function						
F1=[2+a/w]	2.49	2.58	2.61	2.55	2.56	2.41
F2=0.886+4.64a/w	3.14	3.58	3.70	3.42	3.49	2.77
F3=-13.32(a/w)2	-3.15	-4.49	-4.90	-3.96	-4.18	-2.20
F4=+14.72(a/w)3	1.69	2.88	3.29	2.39	2.59	0.99
F5=-5.6(a/w)4]	-0.31	-0.64	-0.76	-0.50	-0.55	-0.15
F6=[1-a/w]3/2	0.37	0.27	0.25	0.31	0.29	0.46
CF=F1*F[2+3+4+5] / F6	9.26	12.68	14.03	11.18	11.78	7.40
F.T.= Hz.Ld.*CF / B*SQRT(W)	26349	34921	34055	23038	23662	25441
Thesis developed Compliance Function						
Interpolation from 2 pi 100/load from Table Â.II.15						
CF(E/E=1.0,+a/w)	14.14	15.93	15.78	14.96	15.93	13.18
CF(E/E=1.0,-a/w)	14.96	15.78	15.63	15.93	15.78	14.14
CF(E/E=1.0)	14.73	15.84	15.76	15.84	15.90	13.30
CF(E/E=2.0,+a/w)	10.80	11.91	11.72	11.32	11.91	10.14
CF(E/E=2.0,-a/w)	11.32	11.72	11.31	11.91	11.72	10.80
CF(E/E=2.0)	11.18	11.79	11.66	11.86	11.87	10.22
CF(E/E=2.5,+a/w)	9.90	10.91	10.68	10.38	10.91	9.30
CF(E/E=2.5,-a/w)	10.38	10.68	10.39	10.91	10.68	9.90
CF(E/E=2.5)	10.25	10.77	10.64	10.86	10.86	9.37
CF(E/E=3.0,+a/w)	9.15	9.91	9.86	9.59	9.91	8.60
CF(E/E=3.0,-a/w)	9.59	9.86	9.58	9.91	9.86	9.15
CF(E/E=3.0)	9.47	9.88	9.82	9.88	9.90	8.67
F.T=f(E/E=1.0)	41920	43634	38267	32626	31931	45737
F.T=f(E/E=2.0)	31800	32492	28323	24419	23840	35155
F.T=f(E/E=2.5)	29157	29670	25837	22370	21815	32241
F.T=f(E/E=3.0)	26941	27217	23849	20351	19882	29812

Fig. A.II.7c Fracture Data Summary: Results
ASTM function is built up in steps
Thesis results interpolated as function valid only where $0.2 \leq a/w \leq 0.45$

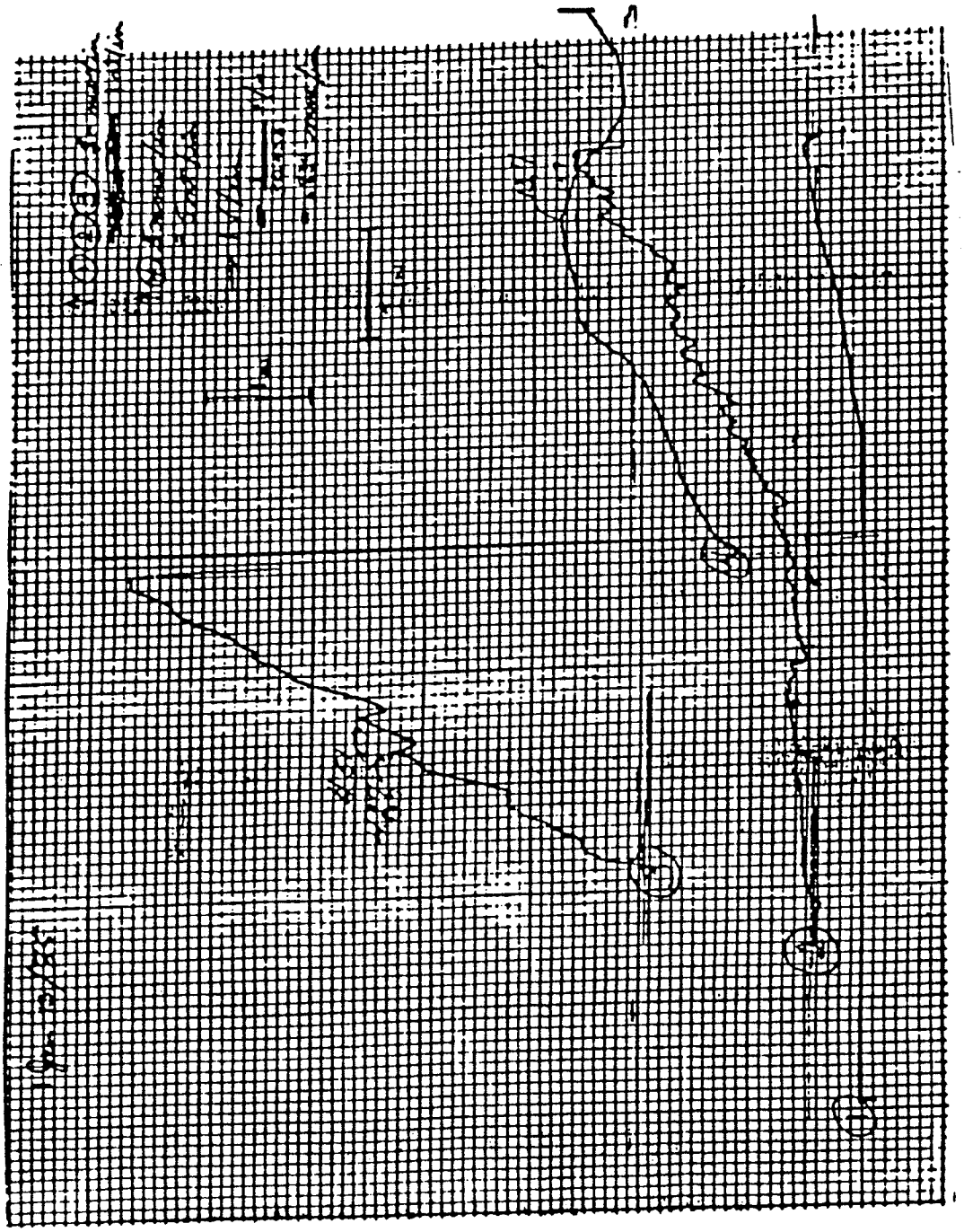

Fig. A.II.8 Result Plot From the X-Y Plotter
Fracture Test #1 January 13, 1986 (1/13/1/86)

A.II.3) Compliance Study Mesh

Region #2

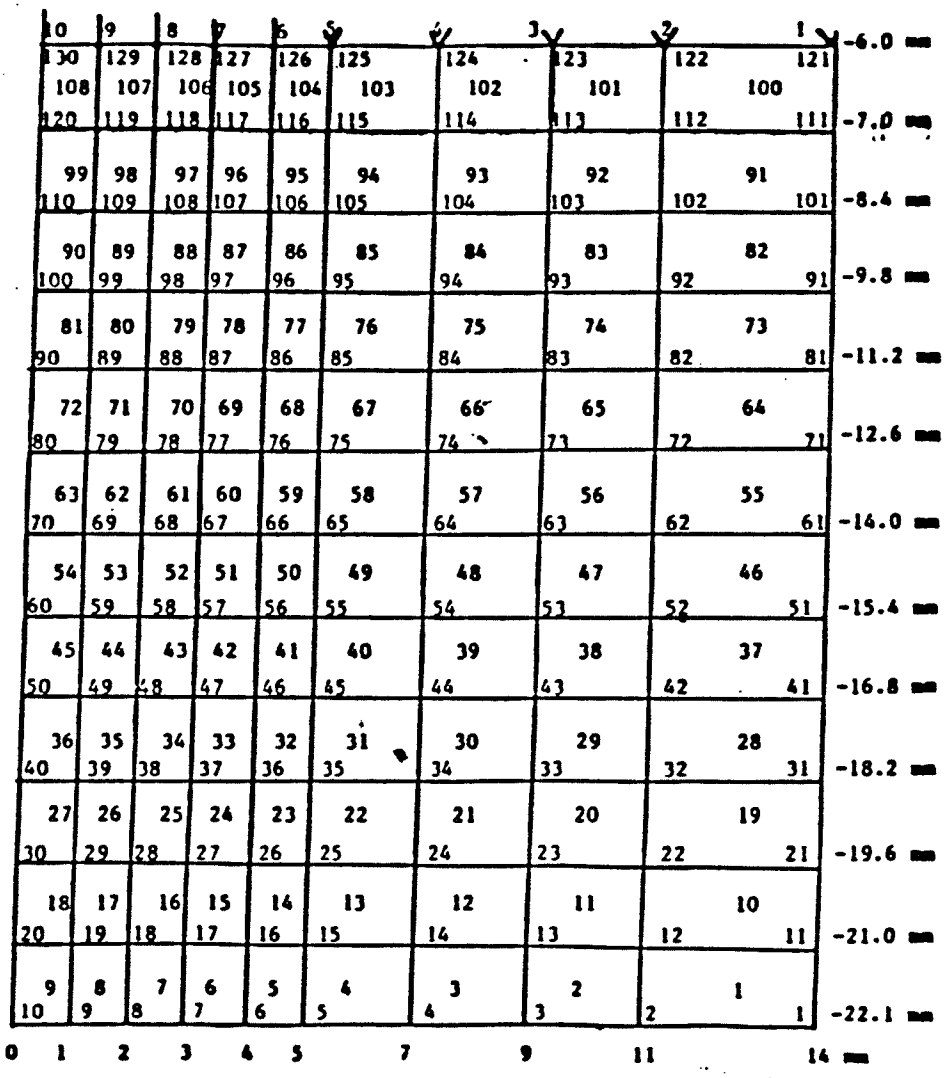

Fig. A.II.9 Mesh Region 1 Full Extent
The base of the specimen.

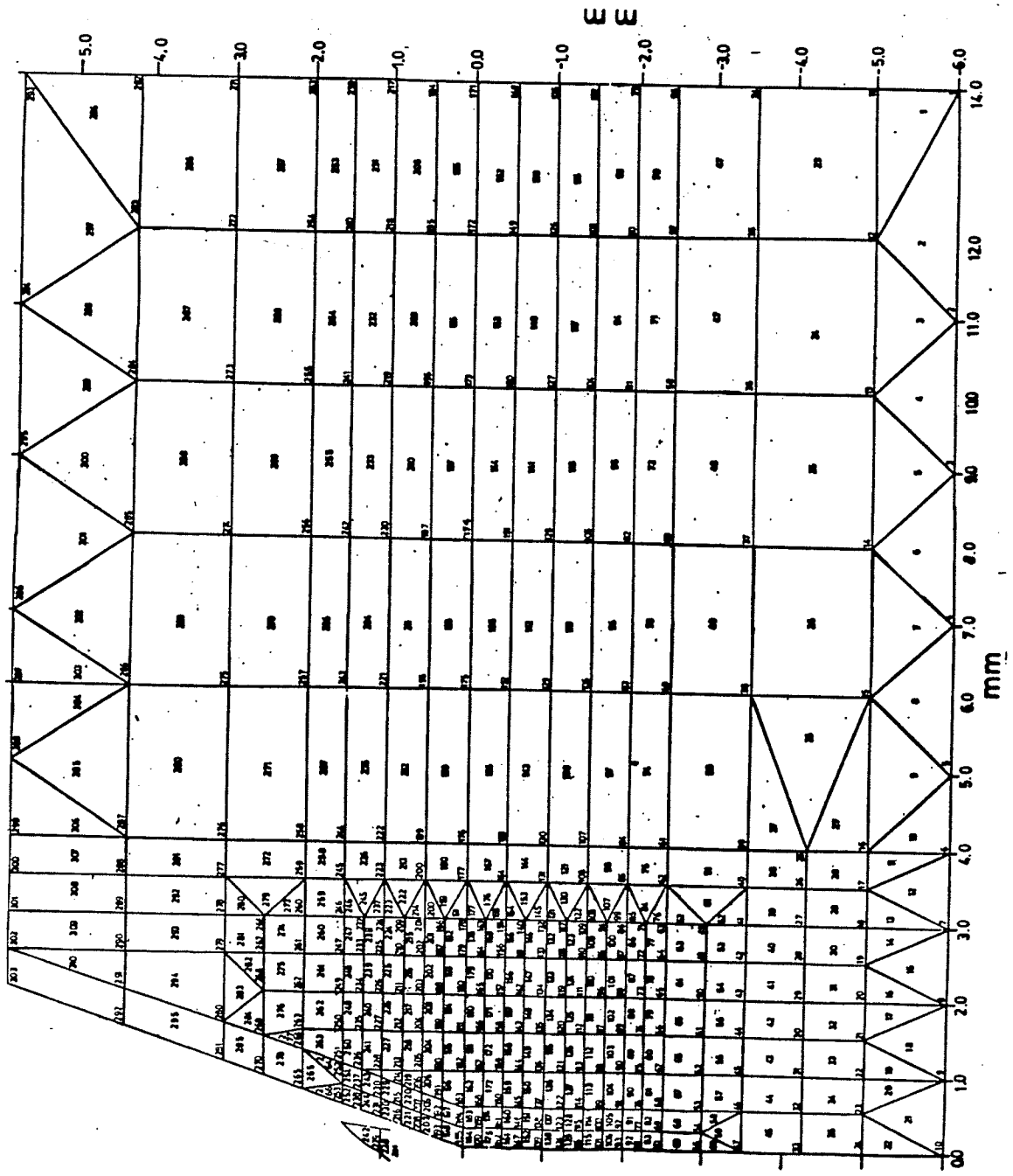

Fig. A.II.10 Mesh Region 2

This part of the mesh is in all cycles.

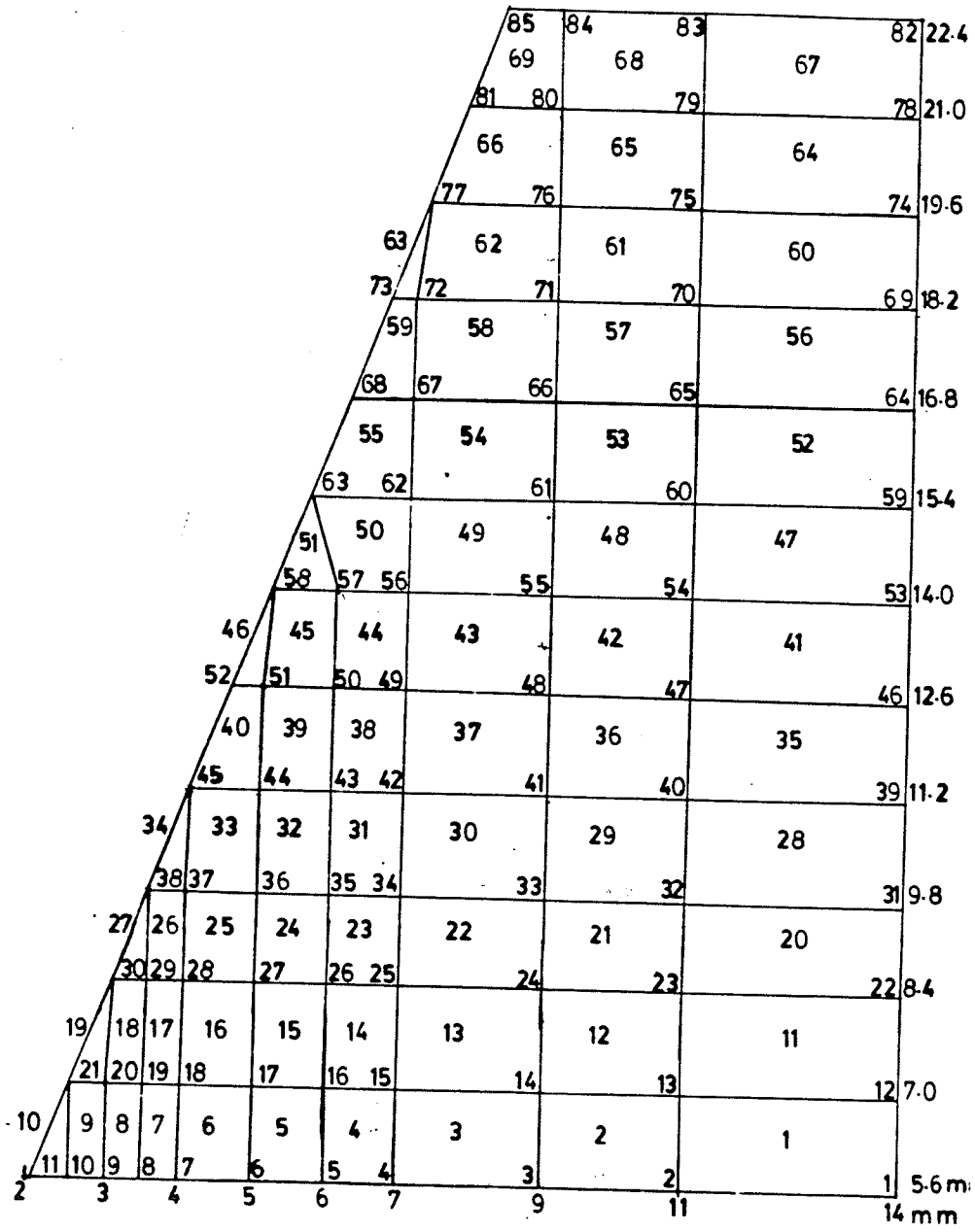

Fig. A.II.11 Mesh Region 3
The top of the specimen.

A.II.4 Compliance Study results

Table A.II. 12 Tensile Elements

	$\pounds_C$ / $\pounds_T$	$\pounds_C$ / $\pounds_T$	$\pounds_C$ / $\pounds_T$	$\pounds_C$ / $\pounds_T$
A/W	1.0	2.0	2.5	3.0
0.20	184,198*	-175,184*,-198	-175,184*,-198	-175,184*,-198
0.25	184,198*	-175,184*,-198	-175,184*,-198	-175,184*,-198
0.30	184,198*	-175,184*,-198	-175,184*,-198	-175,184*,-198
0.35	184,198*	-175,184*,-198	-175,184*,-198	-175,184*,-198
0.40	184,198*	-175,184*,-198	-175,184*,-198	-175,184*,-198
0.45	184,198*	-175,184*,-198	-175,184*,-198	-175,184*,-198
0.50	184,198*	-175,184*,-198	-175,184*,-198	-175,184*,-198
0.55	184,198*	-175,184*,-198	-175,184*,-198	-175,184*,-198
0.60	184,198*	-175,184*,-198	-175,184*,-198	-175,184*,-198
0.65	184,198*	-175,184*,-198	-175,184*,-198	-175,184*,-198
0.70	184,198*	-175,-184,198*	-175,-184,198*	-159,-175,-184,198*
			-183,-197	-160,-174,-183,-197
0.75	184,198*	-175,-184,198*	-175,-184,198*	-175,-184,198*
		-197	-174,-183,-197	-161,-174,-183,-197
				-173,-182,-196
0.80	198*	-175,-184,198*	-175,-184,198*	-175,-184,198*
		-174,-183 -197	-174,-183,-197	-161,-174,-183,-197
				-173,-182,-196

* Failed Element (lowest Value that yielded 225 kPa)

- Element with Material #2 (Lower £) but with

Negative stress

Table A.II. 13 Compliance Study P_c Main Table

Critical horizontal load (Newtons) causing cleavage crack propagation in a WLCT specimen made of tar sands under a confining pressure of 2.1 MPa

	$\varepsilon_c/\varepsilon_T$			
a/w	1.0	2.0	2.5	3.0
0.20	66.699	86.206	93.804	101.464
0.25	61.749	79.194	86.349	93.394
0.30	56.474	72.598	79.161	85.615
0.35	51.669	66.789	72.827	78.786
0.40	47.669	61.973	67.585	73.114
0.45	44.419	58.178	63.464	68.666
0.50	42.000	55.487	60.547	65.526
0.55	39.451	52.755	57.592	63.355
0.60	39.801	53.581	58.817	63.702
0.65	40.215	55.539	60.489	65.556
0.70	41.841	57.779	65.003	71.277
0.75	44.613	62.969	70.077	72.246
0.80	46.859	64.724	73.180	76.564

Table A.II. 14 Compliance Study P_{∞} $\varepsilon_c/\varepsilon_T$ Sweep

$\varepsilon_c/\varepsilon_T$ a/w	0.45	0.50	0.55
1.000	44.419	42.000	39.451
1.025		42.970	
1.050		43.090	
1.075		43.629	
1.100		44.167	
1.150		45.237	
1.200		46.292	
1.300	50.461	48.087	45.486
1.400		49.186	
1.500	52.729	50.266	47.464
1.600		51.331	
1.700		52.384	
1.800	56.025	53.427	50.786
1.900		54.462	
2.000	58.178	55.487	52.755
2.100		56.506	
2.200		57.522	
2.300	61.323	58.535	55.672
2.400		59.544	
2.500	63.464	60.547	57.592
2.600		61.545	
2.700		62.544	
2.800	66.588	63.540	60.461
2.900		64.536	
3.000	68.666	65.526	63.355

Table A.II.15 Compliance Study Table of F(a/w)

$$F(a/w) = (2 * \pi * 100)/P_{\varepsilon_C/\varepsilon_T}$$

a/w	ASTM*	1.0	2.0	2.5	3.0
0.20	4.16	9.38	7.29	6.70	6.20
0.25	4.76	10.17	7.94	7.28	6.73
0.30	5.41	11.12	8.65	7.94	7.34
0.35	6.11	12.16	9.41	8.63	7.97
0.40	6.91	13.18	10.14	9.30	8.60
0.45	7.85	14.14	10.80	9.90	9.15
0.50	9.02	14.96	11.32	10.38	9.59
0.55	10.53	15.93	11.91	10.91	9.91
0.60	12.54	15.78	11.72	10.68	9.86
0.65	15.36	15.63	11.31	10.39	9.58
0.70	19.48	15.02	10.88	9.66	8.82
0.75	25.89	14.08	9.98	8.97	8.69
0.80	36.69	13.41	9.71	8.58	8.21

* Values of the ASTM-E-399-Compact Tension Compliance Function Eq. 1.2

A.II.16 Table Compliance Study $F(a/w)\varepsilon_c/\varepsilon_t$ Sweep

	A/W		
$\varepsilon_c/\varepsilon_T$	0.45	0.50	0.55
1.000	14.14	14.96	15.93
1.025		14.62	
1.050		14.58	
1.075		14.40	
1.100		14.22	
1.150		13.89	
1.200		13.57	
1.300	12.45	13.07	13.81
1.400		12.59	
1.500	11.91	12.49	13.24
1.600		12.24	
1.700		11.99	
1.800	10.80	11.76	12.37
1.900		11.54	
2.000	10.07	10.73	11.28
2.100		11.12	
2.200		10.92	
2.300	10.24	10.73	11.28
2.400		10.55	
2.500	9.90	10.38	10.91
2.600		10.21	
2.700		10.05	
2.800	9.44	9.89	10.39
2.900		9.74	